Title
Hydrodynamics and Salt Dispersion in Intermittently Closed Bar-Built Estuaries

Author
Williams, Megan

Publication Date
2014

Peer reviewed|Thesis/dissertation

Hydrodynamics and Salt Dispersion in Intermittently Closed Bar-Built Estuaries

by

Megan E. Williams

A dissertation submitted in partial satisfaction of the

requirements for the degree of

Doctor of Philosophy

in

Engineering - Civil and Environmental Engineering

in the

Graduate Division

of the

University of California, Berkeley

Committee in charge:

Professor Mark T. Stacey, Chair
Associate Professor Fotini Katapodes Chow
Professor John L. Largier
Assistant Professor Stephanie M. Carlson

Fall 2014

Hydrodynamics and Salt Dispersion in Intermittently Closed Bar-Built Estuaries

Abstract

Hydrodynamics and Salt Dispersion in Intermittently Closed Bar-Built Estuaries

by

Megan E. Williams

Doctor of Philosophy in Engineering - Civil and Environmental Engineering

University of California, Berkeley

Professor Mark T. Stacey, Chair

Shallow, bar-built estuaries on wave-dominated coasts in Mediterranean climates experience an intermittent connection to the ocean. Their inlets may completely close as a result of nearshore sand transport, but even the open condition these inlets remain constricted. Extensive field measurements in the highly salt-stratified Pescadero estuary in Northern California were made to elucidate hydrodynamic processes in these ecologically important yet understudied systems. Here we present unique detailed observations and a framework for understanding dynamics in small, shallow bar-built estuaries.

While closed, ocean water from waves overtopping the sand barrier and freshwater from two creeks maintain stratified conditions within the Pescadero estuary. Wind may cause hydraulic setup of the two-layer lagoon and induce mixing, but does not fully mix the water column. The transition from closed to open mouth states occurs when the sand barrier is breached and the lagoon drains and erodes this sand barrier. Fast drains are associated with full mixing of the water column, and a slow fall of the lagoon water level is associated with incomplete vertical mixing.

Observations show that in the open state, the shallow mouth causes these estuaries to experience discontinuous tidal forcing. While the ocean and estuary are fully connected with near equal water levels, tidal velocities are slow but infragravity motions in the nearshore cause large velocity oscillations. As the ocean tide falls, infragravity forcing is cut off because the estuarine mouth is perched above the low tide ocean water level, and ebbing velocities are set by bed friction. Observations reveal this oscillation between ocean-forced conditions and frictionally-controlled conditions characterizes and sets the hydrodynamics and salt dynamics in these estuaries. Additional wave setup of the lagoon water level emphasizes the dependence of these estuaries on nearshore ocean conditions, but the diurnal or semidiurnal retreat of the ocean below the mouth cuts off this nearshore influence. The salt field responds to this discontinuous forcing, being transported upstream on the flood and becoming trapped in deep pools of the estuary on ebb.

Longitudinal salt dispersion within the Pescadero estuary is calculated using velocity and salinity records. Dispersion of high salinity water was found to be an order of magnitude

lower than dispersion of low salinity water. Vertical salinity measurements indicate that on the large ebb tide, high surface salinities rapidly relax, and a second pulse of salty water follows the relaxation. This pulse may induce vertical mixing in the fresher upper water column, and incites the high dispersion seen among low salinities. Upstream processes are implicated in trapping lower salinity water, while higher salinity water is bathymetrically restricted from marsh or shallow channel trapping.

Finally, observations were being made in the Pescadero estuary in March 2011 when the tsunami generated by the Tohokū earthquake arrived to the California coast. Measurements show that the presence of a tsunami-period signature in this shallow, bar-built estuary was modulated by tidal stage and that the tsunami-induced rise and fall of the ocean water level modulated the velocities seen within the estuary. The initial arrival of waves due to the tsunami caused some flushing of the estuary. Later, high velocities induced more mixing than typically seen in this estuary. After several days sand transport nearly choked closed the mouth of the estuary. These observations point to mechanisms which were likely important during the 2011 Tohoku tsunami in many Eastern Pacific estuaries.

Contents

List of Figures

List of Tables

Acknowledgments

My research advisor, Mark Stacey, suggested I pursue research in a beautiful estuary, supported and trusted my trial and error approach to field measurements, and continually encouraged my development as a scientist. I was lucky to have a brilliant and gracious advisor, and I will remain indebted for his guidance and mentoring throughout my studies.

My committee, Tina Chow, John Largier, Stephanie Carlson, and Jim Hunt, were excellent teachers and mentors, kept me on my toes by asking oral exam questions that were the opposite of those for which I prepared, and provided helpful feedback on this dissertation.

I was lucky to be surrounded by brilliant colleagues and wonderful friends in the environmental fluid mechanics group. Among them, Susan Willis, Rusty Holleman, Wayne Wagner, Ian Tse, Audric Collignon, Lauren Goodfriend, Bowen Zhou, Maureen Downing-Kunz, Margaret Byron, Cristina Poindexter, Dave Wiersema, Maddie Foster-Martinez, and Rachel Allen were there help figure out what it means to be a graduate student. Whether through long hours of field work, grappling with the physical meaning behind a strange piece of data, or the consumption of ample coffee and beer, the community in O'Brien Hall created an invaluable environment in which to pursue doctoral research. Furthermore, Daniella Rempe and Case van Genuchten were instrumental in my survival of our Masters year.

Measurements in the Pescadero estuary would not have been possible with out field assistance from a long list of people. Along with my promises of a day at the beach, Mother Nature often delivered cold water, wind, and rain. I am especially thankful for those people who spent hours digging in the sand below cold water to free buried moorings. For this help and more, I thank Cristina Poindexter, Audric Collignon, Andreas Brand (without whom I may still be trying to figure out how to build and deploy moorings), Susan Willis, Rusty Holleman, Wayne Wagner, Rocky Geyer, Jordon Hemingway, Kevin Hsu, Rudi Schuech, Ian Tse, Mark Stacey, Felix Sturm, Bowen Zhou, Lauren Goodfriend, Andy Torkelson, Jason Simon, Dave Weirsema, DJ Gaker, Eric Huber, Dane Behrens, Nate Butler, Justin Jasper, Gabrielle Boisrame, Arthur Wiedmer, Gabriele Bellani, Hugh Wagner, Julia Schoen, Ryan Sanders, and those friends and colleagues whose assistance I failed to write down in my field notebook. California State Parks provided permits for fieldwork in the Pescadero estuary.

The Hillegass-Parker Cooperative house introduced me to great minds and great friends, and I thank all of the residents there from 2009 - 2013, especially Matt Tucker-Simmons, Katie Adamides, and Tim Ruckle, for being my family and making the house into my home. The Berkeley Art Studio, and members and instructors in the ceramics studio there also contributed to my graduate school education.

Finally, I want to thank my parents, Arlene and Earl, and my sisters, Emily and Lauren, for valuing education, for encouraging my varied pursuits, and for being role models and friends.

This research was supported by a National Science Foundation Graduate Research Fellowship (DGE 1106400).

Chapter 1

Introduction and motivation

Along the world's coastlines, rivers and streams drain water from all the planet's land area through estuaries. In many cases estuaries contain unique, productive ecosystems at this confluence of fresh and ocean water. The natural harbor character of many estuaries has also brought large human population centers, international shipping, and industry, leading to contamination, the introduction of invasive species, and the loss of peripheral wetlands.

An understanding of the dynamics of estuaries is necessary to protect, restore, or limit the negative impacts of human development. Estuarine hydrodynamics are slowly driven by the large density difference between freshwater and ocean water and complicated by tidal forcing, changing riverine discharge, wind, and in large estuaries the effects of Earth's rotation. A complete understanding of these processes and interactions can inform conditions felt by estuarine flora and fauna and transport of contaminants or nutrients, yet, this complete understanding is elusive.

Within the state of California on North America's west coast, the San Francisco Bay drains the Sacramento-San Joaquin watershed, consisting of the California Central Valley and western slope of the Sierra Nevada. California's Coastal Range lies west of the Central Valley, and these coastal watersheds drain the western side of California through small bar-built estuaries. Like larger estuaries, these small systems are historically beneficial environments for aquatic species, host migratory water birds, and provide human recreation space. Coho salmon and steelhead trout pass through California's small estuaries en route to spawn in the headwaters, and those fish who spend time in lagoons perched behind sand barriers grow faster and are more likely to survive in the Pacific Ocean (Hayes et al. 2008; Bond et al. 2008).

Bar-built estuaries are formed when ocean processes form a sand bar at the downstream end of drowned river valleys (Nielsen 2009). In California, these estuaries are small and have an intermittent connection to the ocean. The sandy inlet of these estuaries may close for days, seasonally, or may only temporarily open with large flood events.

Intermittently closed estuaries exist worldwide, primarily on wave-dominated coasts with seasonal rainfall. Those in South Africa, where they are named temporary open/closed estuaries (TOCE), and Australia, where they are called intermittently closed/open lakes

and lagoons (ICOLL), have received the most scientific attention. Estuaries with temporarily closed inlets also exist in Chile (Dussaillant et al. 2009), Brazil (Suzuki et al. 1998), Spain (Moreno et al. 2010), Portugal (Fortunato et al. 2014), New Zealand (Schallenberg et al. 2010), India and Sri Lanka (Ranasinghe and Pattiaratchi 2003), and likely elsewhere. In this dissertation, the terms intermittently closed and intermittently open are used nearly interchangeably, emphasizing estuaries that are more often open to tides as "intermittently closed" and those that more often cut off from the ocean by a sand barrier as "intermittently open." Estuarine processes important in intermittently closed estuaries may also be relevant to small bar-built estuaries that do not experience inlet closure.

Traditional estuarine hydrodynamics research has focused on much larger estuaries, so despite the prevalence of small, intermittently closed estuaries, they remain understudied. Several factors may play into this. These small estuaries are not often navigable by large ships, limiting their economic importance. Estuarine physics research is usually within the realm of physical oceanography or environmental engineering, and the small size of intermittently closed estuaries contrasts with the scales typically studied by physical oceanographers. Furthermore, some research on these small estuaries has been performed in the sphere of coastal management and consulting engineering where reports on findings may not be readily accessible or widely distributed.

Some important work on intermittently closed estuaries is highlighted below. Many studies focus on inlet morphodynamics, especially on closure mechanisms, though the ability to predict mouth closure is still elusive. Some work has examined hydrodynamic processes. A brief description of our current understanding follows. When possible, examples from California are cited.

Inlet morphodynamics

We provide a short summary of sand transport in inlets, highlighting elements important to this dissertation research. Research on morphodynamics tends to focus on inlet closing and conditions setting this closure. A small set of papers addresses how the sand berm grows after inlet closing, and at least a few experimental papers have addressed how the sand berm is eroded upon breach. Much literature analyzes inlet migration and sediment transport in non-closing inlets, and while these processes may also be relevant to closing inlets, their contributions are not important to research contained within this dissertation.

Ranasinghe and Pattiaratchi (2003) define two mechanisms for the sand transport required for inlet closure: (1) by longshore currents, or (2) by cross-shore currents causing sandbars to migrate on shore. Either of these mechanisms interacts with tidal and riverine flow at the mouth. Both tidal and riverine flow act opposite infilling of the inlet. The mechanism responsible for mouth closure may be seasonally varying for the same estuary. Examining a dataset of over 60 years of mouth state records, Behrens et al. (2013) found closure of the Northern California Russian River mouth likely to be due to cross-shore transport during the summer and early fall, but due to longshore transport during other seasons.

Within California, some examples of conditions for mouth closure have been described. In a tidal marsh in San Francisco's Crissy Field, located inside of the Golden Gate on the San Francisco Bay, the sandy inlet closes either after a period of large waves (typically from the northwest), but also was seen to close under a small wave climate with long period swell from the south or southwest (Hanes et al. 2011). During low flow conditions characteristic of summer Mediterranean climates, the probability of inlet closure increased with ocean wave height at the Russian River mouth, and streamflow determined the length of closure (Behrens et al. 2013). Modeling morphodynamics coupled with hydrology on the Carmel River inlet in Central California, Rich and Keller found an exponential decrease in closure probability as freshwater streamflow increased (2013). Perhaps these studies are best summarized by saying that given enough freshwater flow, the inlet will remain open, and in the absence of enough riverine flow, it might not.

After the estuary inlet has closed, swash overwash is responsible for berm development (Baldock et al. 2008). Two modes have been proposed to grow the berm: vertical berm growth due to wave overtopping the sand berm during spring tides and horizontal berm growth toward the ocean as a smaller berm is formed at the base of the larger berm during neap tides (Weir et al. 2006).

In many cases, the breaching of the sand barrier at the mouth is artificial, where the inlet is opened by human intervention (e.g. Fortunato et al. 2014; Behrens et al. 2013). Stretch and Parkinson (2006) investigated breach dynamics by building an experimental lagoon, cutting a small outlet, and observing the resulting outflow, finding a relationship between outflowing volume and breach width. Further work in their experimental lagoon characterized timescales of sand berm breach in relation to outflow volume, hydraulic head, and the breadth of the sand barrier (Parkinson and Stretch 2007).

Intermittently open estuarine hydrodynamics

Historically, hydrodynamic observations made in South African then Australian intermittently open estuaries set the framework for understanding general salt dynamics and circulation within these estuaries. Work in the small, South African Palmiet estuary defined the general circulation: salt water enters the estuary as a tidal intrusion front owing to the constricted, sill-like inlet, flows upstream as a density current, and is removed by shear entrainment into fresher (outflowing) surface waters (Largier et al. 1992). Field measurements in Wilson Inlet in southwestern Australia show a similar salinity intrusion and trapped salt water in the open state (Ranasinghe and Pattiaratchi 1999). Wilson Inlet is a large coastal lagoon that experiences wind forced circulation and the effects of Coriolis, but salinity intrusion similarities suggest that the constricted mouth of small and large intermittently open estuaries allows some processes to remain similar across length scales.

In the closed-mouth state of intermittently open estuaries, stratification and circulation are most often studied in the context of degraded water quality often accompanying the closed state. Cousins et al. (2010) explored seasonal hydrodynamics in Rodeo Lagoon, a eutrophic, infrequently open estuary north of San Francisco, California. The typically closed condition

of Rodeo Lagoon means that tidal forcing is cut off so wind forcing drives circulation and mixing. Wave overwash provides a salt water source to the lagoon, and resulting density stratification damps turbulence in lower waters. In the summer, wave overwash is rare and wind-mixing converts the lagoon to a well-mixed, brackish state.

Measurements or numerical modeling of the hydrodynamics of the transition from an open to closed state (sand bar breach) are essentially non-existent. In the case of a well-mixed lagoon, one would expect the lagoon draining to start as surface flow out and progress quickly to vertically homogeneous outflow. In the case of a highly stratified lagoon, stratification could impede uniform flow out. In the case of a fish mortality event triggered by an artificial mouth opening in the Australian Surrey estuary, it was hypothesized that oxygenated (fresh) surface waters flowed out of the estuary during the breach and hypoxic or anoxic higher salinity water was left behind (Becker et al. 2009). No velocity measurements were made, leaving this hypothesis unconfirmed.

Pescadero Estuary

Morphodynamics of intermittently open estuaries are generally described in terms of wave conditions and freshwater flow, but the influence of the energetic coastal wave environment on estuarine hydrodynamics is not commonly discussed. Salt transport within the open state of intermittently open estuaries has been described in terms of estuarine circulation on tidal timescales. However, work to understand mixing and dispersion commonly quantified in larger estuaries is lacking, owing in part to advancement of the estuarine physics field since measurements were made in the Palmiet estuary in South Africa in the 1980s.

To attempt to fill in gaps in scientific estuarine knowledge, observations in the Pescadero estuary in Northern California were made during several field campaigns over the years 2010 - 2012. Measurements occurred during the open state, the closed state, and the transitions between these more stable conditions. The Pescadero estuary is just one of many California bar-built estuaries, but one that has been plagued by mortality of federally threatened steelhead trout (*Oncorhynchus mykiss*). One of the goals of this project was to characterize the Pescadero estuary to inform management decisions.

Coupled with the current state of understanding, field measurements and analyses were aimed at understanding several processes: dynamics of the estuary breach, high frequency forcing, and salt transport and mixing within the estuary. Furthermore, chance observations during the tsunami generated by the 2011 Tohokū earthquake provided a rare glimse of how small estuaries respond to small tsunamis.

This thesis will attempt to answer four research questions spanning mouth states, timescales, and forcing:

Research questions:

1. How does the Pescadero estuary function during open, closed, and transitioning mouth states?

2. What are the drivers of hydrodynamics in the open state of a small intermittently closed bar-built estuary?

3. What processes set salt dispersion in a strongly stratified bar-built estuary?

4. How did the tsunami generated by the 2011 Tohokū earthquake alter flow in a California bar built estuary?

To address these general questions, the dissertation will follow the outline described below. The entire dissertation addresses question 1, chapters 3 and 4 focus on question 2, chapter 4 is more detailed and specific to question 3, and chapter 5 describes forcing relevant to question 4.

Dissertation outline

This dissertation presents findings from observations and analysis of a bar-built estuary in Northern California, and hopes to push forward understanding of hydrodynamics in intermittently open estuaries while promoting these systems as having many still unanswered and interesting science questions.

Chapter 2 focuses specifically on the Pescadero estuary. This chapter describes the estuary, field methods relevant to the work in general, and the conditions affecting dynamics in the system. These descriptions are followed by an observational discussion of closed state hydrodynamics and a look at how the Pescadero estuary responds to the opening of the closed mouth. This chapter aims to provide insight to land managers through insight into the general functioning of the Pescadero estuary.

Chapter 3 examines open-state forcing and hydrodynamics. The connection between waves and nearshore sand transport is well established, but this chapter will look at observed high velocity oscillations caused by this wave forcing as an energetically important variable in California's bar-built estuaries. The influence of the shallow mouth perched above low water in the ocean is shown to modulate nearshore forcing and alter tidal flow. The influence of this discontinuous forcing on salt transport is then described.

Chapters 3 and 4 address salt transport in the open state, first as general movement into and out of the open estuary in Chapter 3, and then in Chapter 4 looking at dispersion of the salt field during the tidal cycle, which varies at different salinities, probably due to interaction with the marsh surrounding the Pescadero estuary.

Chapter 5 describes the response of the Pescadero estuary to the arrival of waves from the tsunami generated by the 2011 Tohokū earthquake. Early tsunami waves induced high velocity flows within the estuary. As tsunami conditions lingered, the resultant waves raised and lowered the ocean water level, modulating estuarine forcing like short period tides.

Finally, chapter 6 gives a summary of the content of this dissertation.

Chapter 2

The Pescadero estuary

The Pescadero estuary is located at the confluence of Pescadero Creek and Butano Creek in southern San Mateo County on the California coast (Figure 2.1). The estuary drains a watershed of 210 km^2 located in the Santa Cruz mountains in California's coastal range. The coastal range is rainfall dominated, and freshwater streamflow on the creeks is flashy. California's Mediterranean climate is characterized by distinct wet and dry season, though large variation in interannual winter rainfall exists. The mouth of the estuary closes by sand transport during dry months and opens with the seasonal increase of freshwater flow.

A history of the Pescadero marsh was compiled as the M.A. dissertation work of Viollis (1979). Historically, the marsh was bigger, and it has a history of being farmed, drained, and leveed. Large changes in the 20th century included impacts from the construction of levees and roads, logging, increased agriculture in the watershed, and increased water use. The marsh underwent further alterations in the 1990s when the Highway 1 bridge was replaced and culverts were installed between the Pescadero creek and channel to the North Pond in an attempt to create habitat for threatened and endangered species (ESA 2004).

California's intermittently closed estuaries play an important role in the life cycle of juvenile salmonids. Studies in Central California's Scott Creek showed that steelhead reared in the estuary and lagoon habitat exhibited much faster growth rates than those that reared primarily in upper reaches of the estuary (Hayes et al. 2008). Subsequent survival in the ocean of the larger fish also increases (Bond et al. 2008). A similar nutrient rich environment should exist in the Pescadero estuary and be beneficial to the threatened steelhead trout. Unfortunately, massive fish mortality has been observed with the opening of the mouth of the Pescadero estuary in late fall in many recent years. This problem has led to scientific study (Sloan 2006; Smith 2009) as well as lawsuits (Scheck 2012), but to date a conclusive explanation for the triggers of fish mortality has not been defined.

Work to understand hydrodynamic and salt transport processes in intermittently closed estuaries in general and in the Pescadero estuary in specific aims to develop a framework for understanding these understudied systems. This chapter outlines observation methods from field studies in the Pescadero estuary, describes the forcing seen to be dominant in the system, and finally describes hydrodynamics and salt transport in the closed state and

Figure 2.1: Photograph of the Pescadero Beach and Natural Marsh Preserve. The Highway 1 bridge crosses the shallow inlet of the estuary. Butano Creek arrives to the confluence of two creeks from the right of the image through wetlands. Pescadero Creek is more wooded and channelized. Photograph taken Sept. 25, 2010. In 2010 the inlet closed in October.

during the rapid transition from closed to open.

2.1 Measurements made in the Pescadero estuary

Measurements were made over the course of three years to quantify dominant forcing during the open and closed states of the estuary. A description of measurement methods precedes a description of general observations and functioning of this estuary.

Field measurements were made in the Pescadero estuary during four field deployments:

1. March - May 2010
2. September 2010

3. November 2010 - May 2011

4. August 2011 - June 2012

Measurements were not always continuous because instrument sometimes failed, were damaged, or buried by sediment. Later deployments utilized more instruments and so had better resolution in space. The frequency of measurements was also increased in later deployments.

Bathymetry

Bathymetry measurements were made using the bottom track feature of an acoustic Doppler current profiler (ADCP; RDI Workhorse Monitor 1200kHz) pulled on a raft behind a canoe on 17 November, 2010 while the estuarine inlet was closed. The bathymetry map (Figure 2.2) shows that the lower embayment of the estuary is shallow and becomes deep in the narrow channel upstream of the lagoonal area. The mouth was not measured because measurements were made in the closed-mouth state. While open, the geometry of the mouth is constantly changing. Bedrock sits below the mouth, setting a minimum elevation for the mouth, but the bedrock is usually covered with sand.

Sensors were located according to bathymetry. Early attempts to collect measurements in the inlet resulted in buried and broken instruments, even after short 24-hour deployments, so long term measurements were limited to regions of the estuary with less rapid sand transport.

Depth

Depth measurements were made using the pressure transducer on conductivity, temperature, depth (CTD) sensors attached to weighted milk crates (RBR XR-420 CTD, Figure 2.3). The pressure values on the instruments were adjusted to changing atmospheric pressure using air pressure measurements from the Half Moon Bay airport (KHAF). An approximate density of $\rho = 1021$ kg m^{-3} is used with the hydrostatic pressure equation $p = \rho g h$, slightly overestimating the depth when the estuary is fresh and density is lower than this value. Error in the pressure measurement using this assumption may be up to 2.5%. Further error is introduced comparing pressure measurements in a quiescent water column to a quickly moving flow. Stagnation pressure p is given by $p = \rho\ g\ h\ +\ 0.5\ \rho\ v^2$, where h is water depth above the reference location, v is velocity, g is gravity and ρ is water density (Young 2004). Under quiescent flow, pressure values measured are hydrostatic pressure, so under small velocities, error in this assumption is small. If flow reaches 1 m s^{-1} in a 1 m water column, the pressure reading will increase by 5% therefore depth calculated from these measurements not accounting for dynamic pressure will be slightly overestimated.

A staff gauge on the Highway 1 bridge has been surveyed as recording 2.87 ft (or 0.875 m) above the North American Vertical Datum (NAVD88) (C. Hammersmark, *pers. comm.*). Mean low low water (MLLW) is 0.0303 m above NAVD88 on the coast by the Pescadero estuary. We observe error in comparison of recorded water level (according to the staff gauge

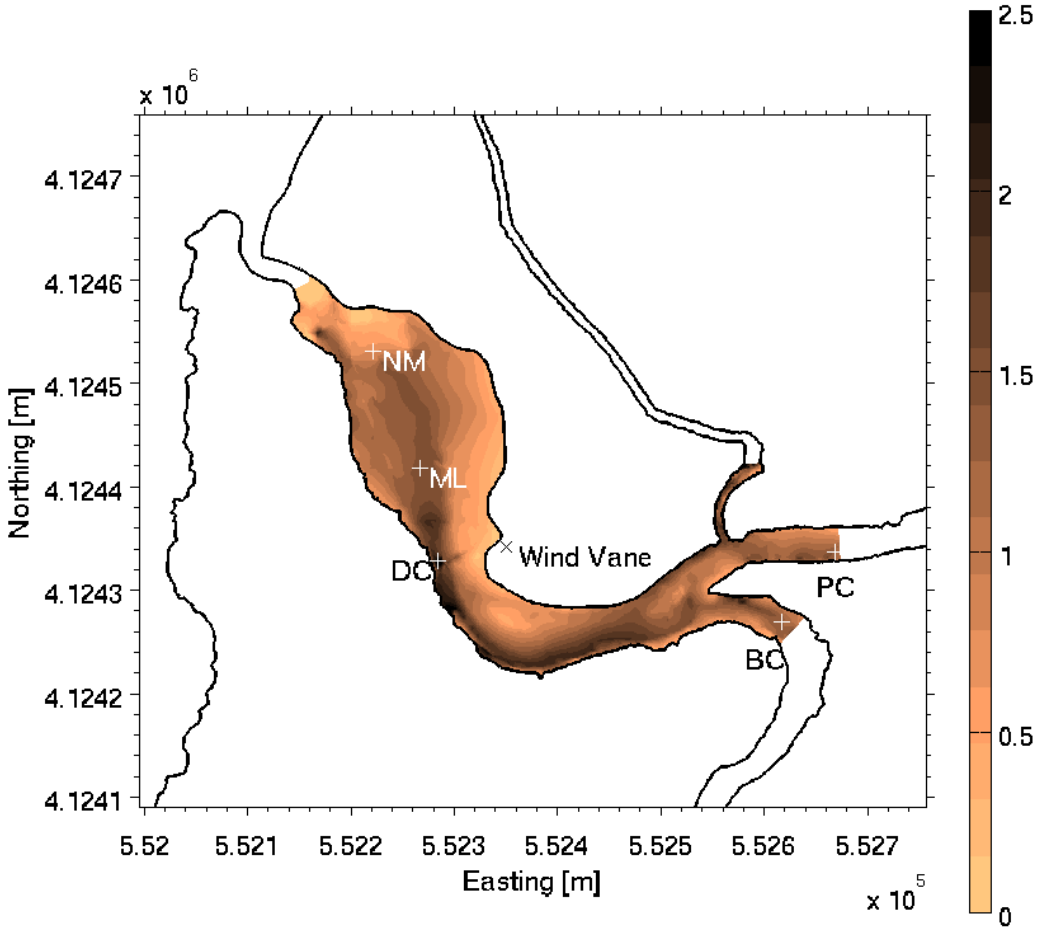

Figure 2.2: Bathymetry map of the Pescadero estuary. Locations of moorings from September 2011 - June 2012 are shown on this map. Mooring locations for November 2010 - May 2011 deployments are shown in Chapter 5. In the 2010-2011 deployment, DC and DS are in approximately the same location, and an upstream (US) station was located about 70 m upstream from DC/DS.

on the highway 1 bridge) while the estuary is draining in February and March 2012 and expect this error to be due to dynamic pressure readings. Thus, to set the water level in the estuary to a NAVD88 or MLLW datum, we use measurements taken during the closed water state when available and assume quiescent flow. Further error is introduced as moorings were weighted to the ground but not fastened in place and some movement of the bed or mooring

Figure 2.3: A mooring consisting of several CTDs and buoys attached to a weighted milk crate. Bed CTDs were attached 0.2 m above the bottom of the milk crate.

may have occurred.

Salinity and Temperature

Salinity and temperature were also measured by moored CTDs. The instruments were attached to weighted milk crates, floating lines, and floating buoys (Figure 2.3). In some cases, subsurface buoys maintained taut lines. Shorter, taut lines seemed to be more prone to being dragged away from their original location so later deployments allowed sensors to be more free floating. Salinity data presented is matched with its depth measurement.

Velocity

Velocity measurements were made with moored ADCPs as well as with moored acoustic Doppler velocimeters (ADV; Nortek Vector, Figure 2.4). ADCPs were attached to flat plates and placed on the bed of the estuary. The ADCPs are designed for use in deeper flow, and were not always successful in measuring velocities. Some data dropouts are attributed to interference by reflection from the surface. The ADVs, usually attached downward facing from a sawhorse frame (Figure 2.4), were consistently able to measure velocity, but instruments fixed near the mouth were susceptible to damage by floating debris. In one instance, the titanium probe of an ADV was bent after being deployed only eight hours, probably by a car wheel found the next day in the intertidal zone floating on quickly moving infragravity bores

Figure 2.4: Photographs of downward facing ADVs and an upward facing ADCP used in field deployments.

(cf chapters 3 and 5). Driftwood logs are also ubiquitous along the shores of the Pescadero estuary.

ADCP measurements presented in this chapter are from the DC location. ADV data presented in chapters 3 and 4 are from the near mouth (NM) station.

Wind measurements

Wind measurements were made using an anemometer installed during the Fall 2011 - Spring 2012 field deployment (Model #05106, RM Young). The wind vane was mounted approximately 3 m above the water level in the marsh adjacent to the estuary (See location on figure 2.2). Measurements show that wind direction through the marsh is almost entirely bi-directional (Figures 2.6 and 2.7). Wind direction of between 300 and 360 degrees is blowing from the ocean and wind blowing from 100 to 170 degrees is land-sourced wind. This constrained directionality is attributed to topography of the marsh. The inlet is protected by bluffs to the south and historical sand dunes reinforced for the Highway 1 bridge to the north. The marsh itself is located in a low valley, further constricting wind flow paths. Wind speeds from the ocean are higher than those from the land (Figures 2.6 and 2.7).

2.2 Climatic conditions and external forcing

The years 2010-2012 encompassed El Niño and La Niña years, and drought conditions in California were present for much of the study. Increased storm activity in the Pacific Ocean with El Niño years has been attributed to an increased wave climate seen on the coast of California (Seymour et al. 1984). Freshwater flow in water year 2010 (1 October, 2009 to 30

Figure 2.5: An anemometer made wind measurements approximately 3 m above the water level in the Pescadero estuary.

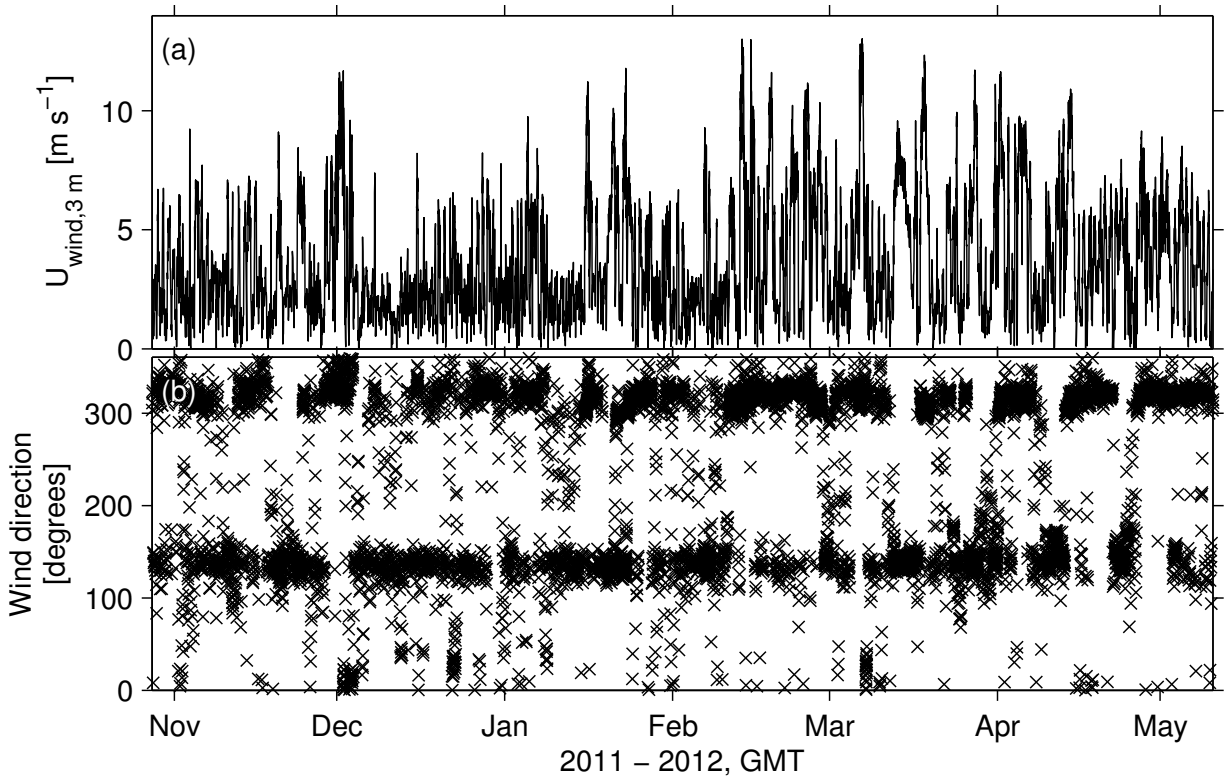

Figure 2.6: Wind measurements made in the Pescadero marsh. (a) is wind speed [m s^{-1}] at 3 m above the water surface. (b) is wind direction in degrees.

September, 2010) was above the 61 year median, at least after April 2010, and flow in water year 2012 was below the 61 year median.

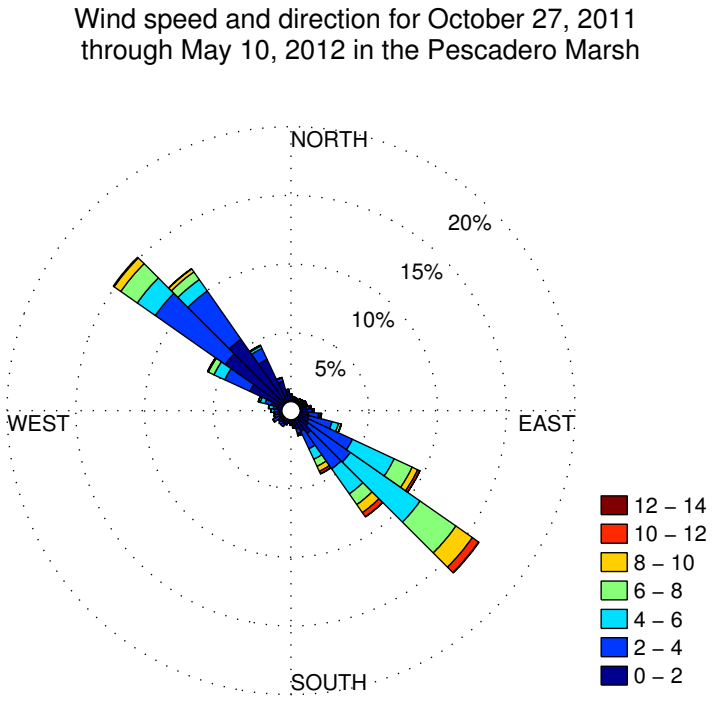

Figure 2.7: A wind measurement histogram shows that wind blows in two directions and faster velocity wind comes from the ocean direction (blowing SE).

Freshwater

Freshwater streamflow into the Pescadero estuary is estimated based on a United States Geological Survey (USGS) gauge located on Pescadero Creek 8.5 km upstream from the mouth of the estuary (USGS 11162500). The gauge is downstream of 57 % of the watershed, so to estimate freshwater flow into the estuary the gauged discharge measurement is multiplied by a scaling factor ($Q_R = 1.76 Q_{R,G}$). Unaccounted for freshwater diversions are thought to exist downstream of the gauge which likely reduce actual freshwater flow into the estuary. We do not have a way to quantify these diversions and thus will report freshwater flow as if they do not exist. Flow into the Pescadero estuary was highest in the early part of the calendar year. The highest flow recorded at the USGS Pescadero gauge during our field deployments was $Q_{R,G} = 169$ m^3 s^{-1} in March 2011, and freshwater flows under 0.1 m^3 s^{-1} were common for late summer and early autumn (Figure 2.8a).

The Mediterranean climate of California is highlighted by seasonal precipitation. Freshwater flow in the rainfall-dominated Pescadero Creek watershed follows this trend. Figure 2.9 shows median gauged creek flow at the USGS Pescadero gauge including data from 1951 to 2012 and the freshwater discharge curves for the water years of our study.

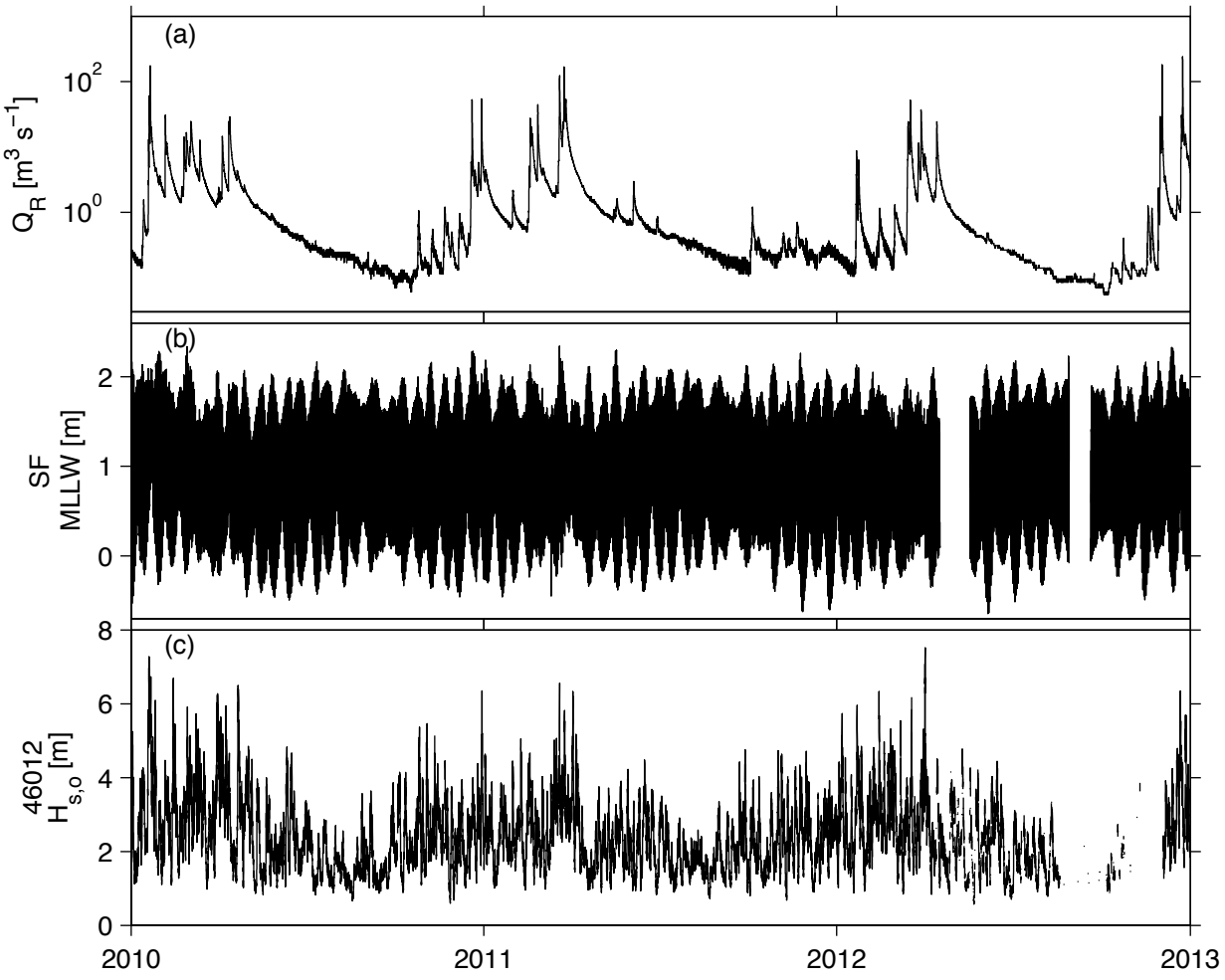

Figure 2.8: External conditions relevant to Pescadero estuarine dynamics include estimated freshwater discharge into the Pescadero estuary (a), tidal water level at San Francisco's Crissy Field (b), and ocean significant wave height (c). These values are given for calendar years 2010, 2011, and 2012.

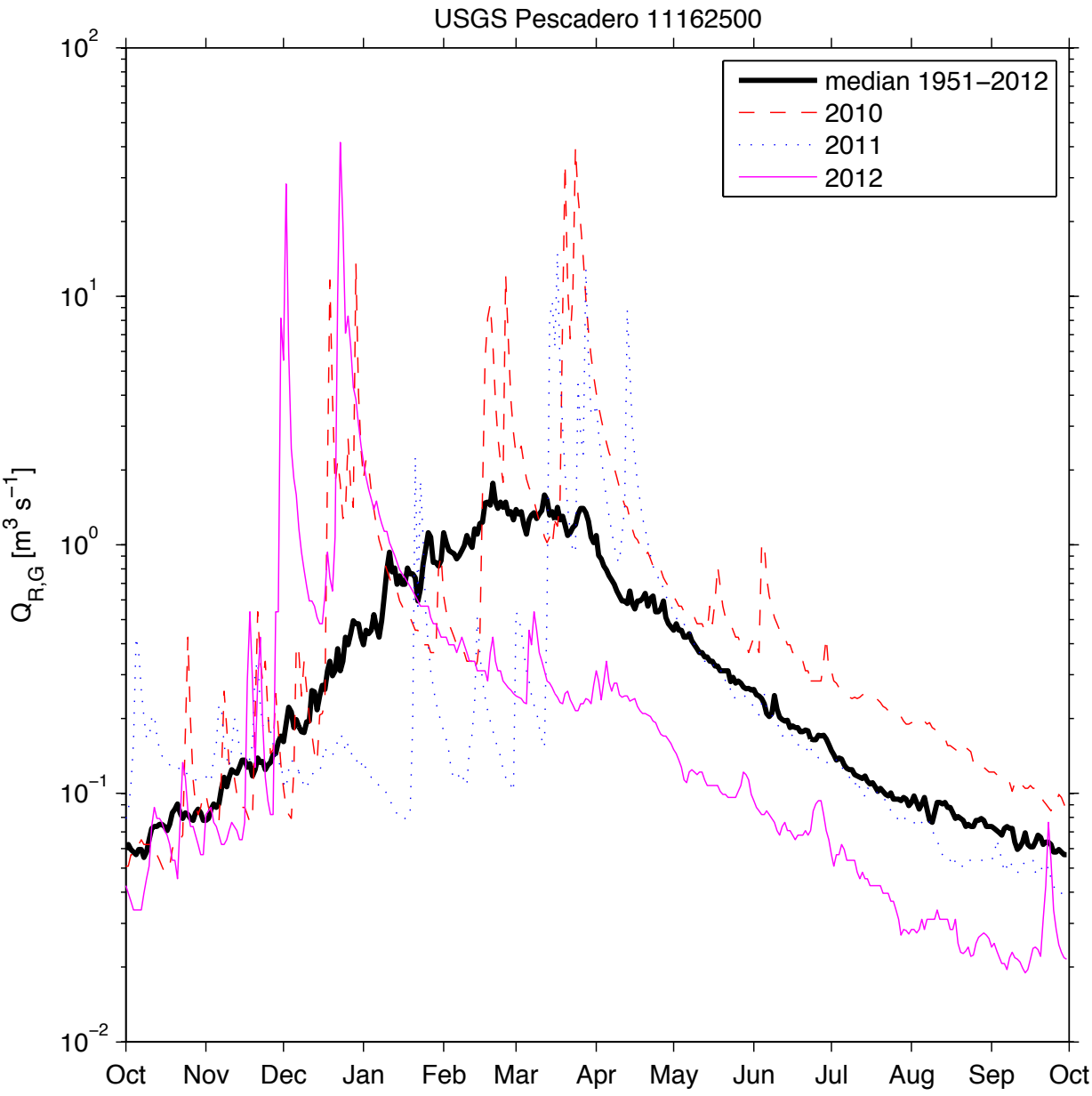

Figure 2.9: Gauged freshwater discharge at the USGS Pescadero gauge (11162500) for the years of data collection compared to the median freshwater flow for water years 1951 - 2012.

Tides

The nearest ocean tide gauges to the Pescadero estuary are operated by the National Oceanic and Atmospheric Administration (NOAA) at Crissy Field in San Francisco, California (Station 9414290) and in Monterey Harbor in Monterey, California (Station 9413450). Water level in both locations is recorded every six minutes, and one minute tsunami-capable unverified data is also recorded. The Northern Californian coast experiences a semidiurnal tide with a neap tide range of under 1 m and a spring tide range up to almost 3 m (Figure 2.8b). High and low tide levels in San Francisco during the deployment years were 2.34 m and -0.64 m MLLW, respectively.

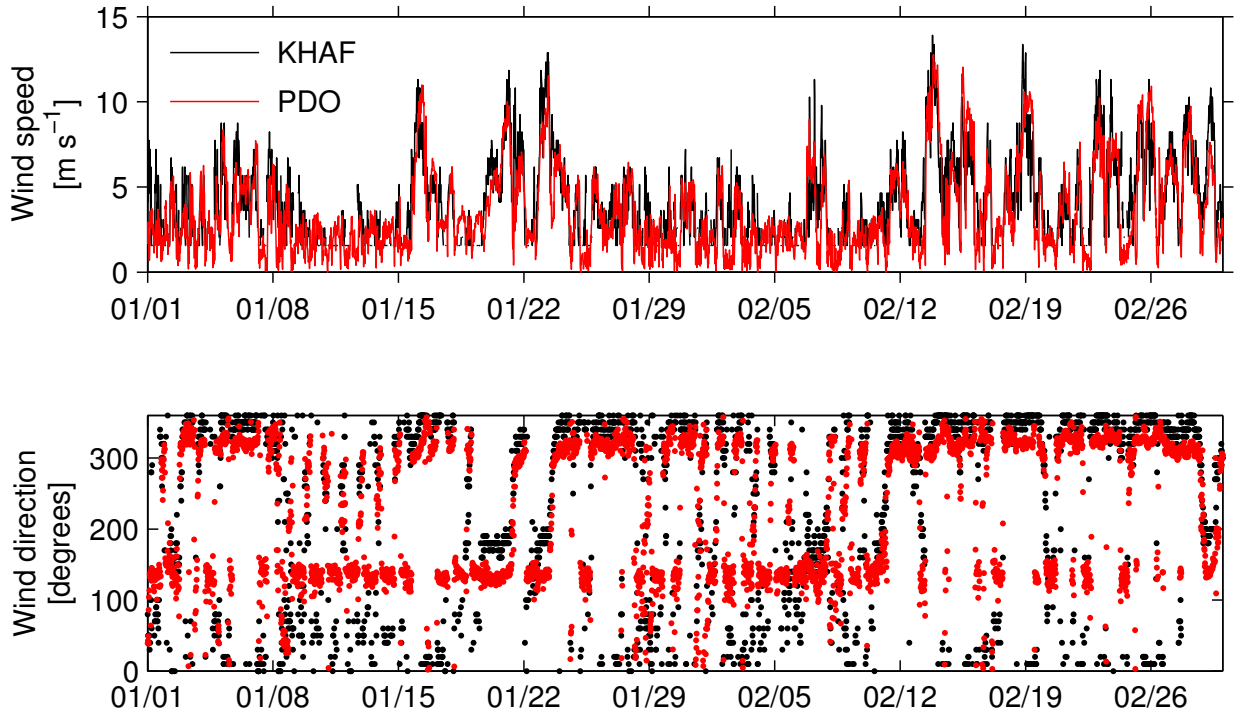

Figure 2.10: Wind measurements in Half Moon Bay (black) and in Pescadero (red). Wind from the northwest blows off the ocean and agreement is better between KHAF and Pescadero measurements. High wind speeds show good agreement regardless of the direction.

Ocean wave climate

Ocean wave conditions are obtained through the NOAA National Data Buoy Center (NDBC). NDBC buoy 46012 is located approximately 40 km WNW of the Pescadero estuary at 208.8 m depth. This buoy reports ocean significant wave height every hour. Deep water wave heights are larger than wave heights experienced at the coast, but larger waves 40 km from

shore will cause larger waves at the coast thus we use this value as a proxy for coastal ocean conditions. Maximum wave heights in the ocean from 2010 - 2012 were over 7 m, and minimum were under 1 m (Figure 2.8c). Ocean wave heights also follow a seasonal trend with smaller waves in the summer months transitioning to larger wave climates in the fall, winter and spring months when storms on the Pacific Ocean generate large swell.

Wind

Wind conditions are approximated by measurements at the Half Moon Bay airport (KHAF) during periods before the wind anemometer was installed in the Pescadero estuary. There is good agreement in wind speed and direction between KHAF and our measurement (Figure 2.10). Wind direction measurements agree better when wind speeds are high.

Tsunami

The 2011 Tohoku earthquake generated a Pacific Ocean-wide tsunami. A description of the ocean state and the response of the Pescadero estuary to the forcing of the small amplitude tsunami that reached California is found in chapter 5.

2.3 Estuarine state as determined by the condition of the inlet

Two inlet conditions exist for the Pescadero estuary: open and closed (Figure 2.11 and 2.13). These conditions set the hydrodynamic state of the estuary. The inlet continuously expands and contracts as nearshore sand transport competes with freshwater and ebb tidal scour. An open estuary is characterized by any period in which the estuarine water level falls with the outgoing tide (Figure 2.12, prior to 23 August), and a closed estuarine state is highlighted by the lack of outflowing water thus no falling depth (Figure 2.12, prior to 23 August). Within the open state, tides in the estuary may be an attenuated version of the ocean tides (Figure 2.12, prior to 20 August), and this state we will consider to be fully open. An extensive description of relevant hydrodynamic and salt transport processes in the fully open state is found in chapters 3 and 4.

Because the estuarine inlet is in a constantly unstable condition, an intermediate state between fully open and closed is also common in the Pescadero estuary. In this state, the sandy inlet is constricted. Here, the estuarine water level rises and falls in response to ocean tides, but may only fill with the diurnal high high tide (Figure 2.12, 20-23 August) or be severely attenuated. We consider this condition to be a highly-constricted open state. The open state of the estuary is a continuum. Sand moves in and out of the inlet with tidal flow and waves. High freshwater discharge will scour the mouth.

Figure 2.11: The mouth of the Pescadero estuary in the open state on 15 April, 2010. The photograph was taken from a camera attached to a kite, and the kite string is visible in the image. Photograph credit: Rusty Holleman

The closed state of the estuary is characterized by tidal depth oscillations being shut off. This does not mean that the ocean tides cease to influence water level in the estuary but just that water is not flowing through the channel.

Some discussion of mouth closure in the Pescadero estuary following the 2011 Tohoku tsunami is found in chapter 5, but the subject is largely untreated here. Work in the Russian River (Behrens 2012; Behrens et al. 2013) as well as in the Carmel Lagoon (Rich and Keller 2013), both California estuaries, discuss processes for mouth closure relevant to the Pescadero estuary. The specific north facing geometry of the mouth of the Pescadero inlet may affect the direction from which waves must arrive to cause nearshore sand transport to close the mouth in comparison to other California estuaries, but this is a topic for further research.

The transition from the closed state to open state in the Pescadero estuary naturally occurs when increased freshwater streamflow overtops the sand bar at the mouth and may artificially occur with human intervention.

A description of estuarine dynamics during the closed and transitioning states follows in this chapter, with the description of dynamics in the open state to follow in chapters 3-5.

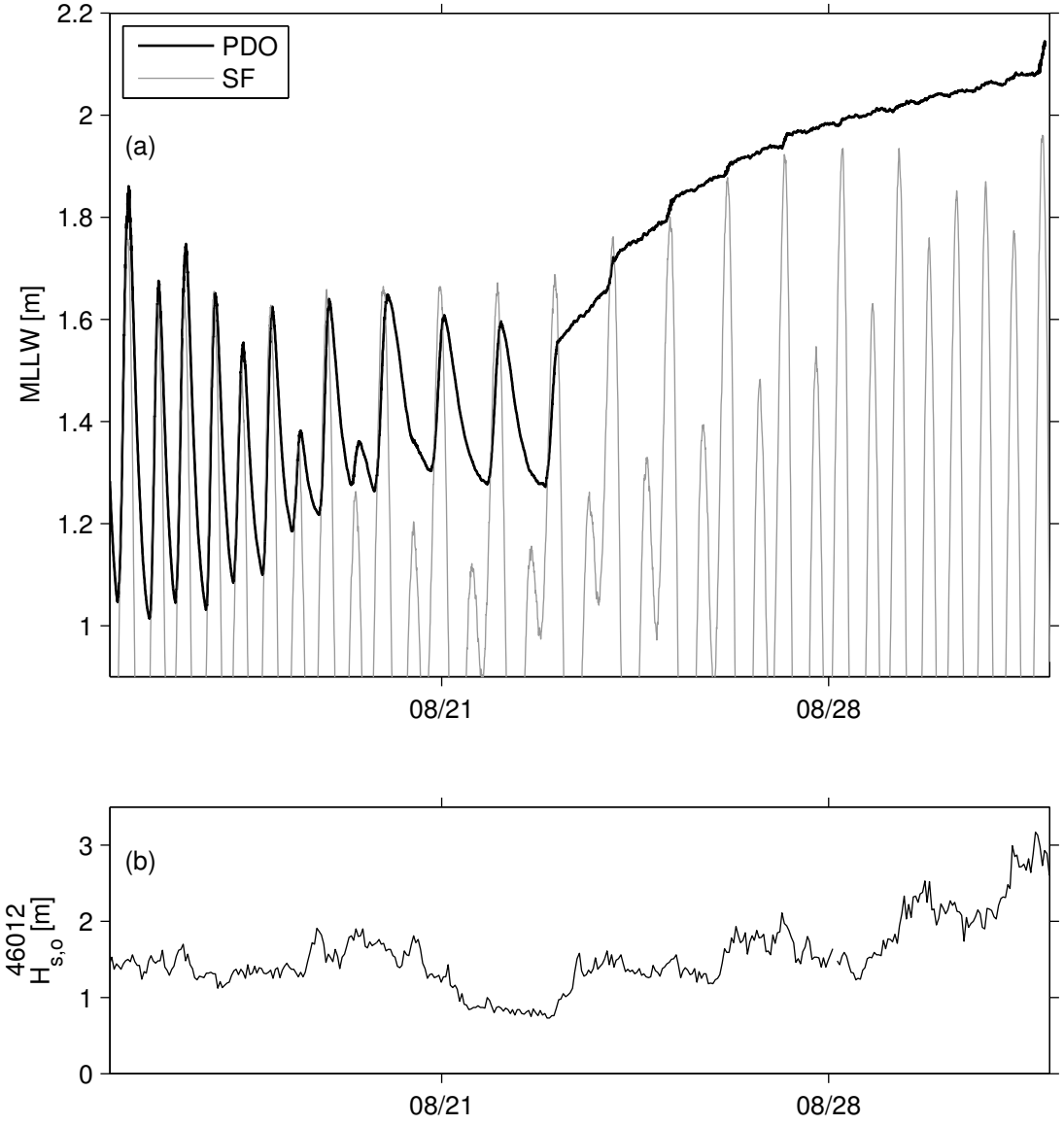

Figure 2.12: Water surface elevation in the Pescadero estuary in August 2011 (a) and significant wave height in the ocean (b). This graphic shows fully open, partially open, and closed mouth estuarine water levels. Early increases in lagoon depth are rapid and attributed to high high ocean tide wave overwash. More gradual depth increases are attributed to freshwater flow into the lagoon. The large water level increase on 31 August is from wave overwashing over the length of Pescadero Beach forming a salt water river running into the estuary while ocean wave conditions are large (See figures 2.15).

2.3.1 Closed State

The dominant forcing in open estuaries is due to tidally driven flows. When the mouth of intermittently closed estuaries chokes closed, tidal momentum and buoyancy fluxes are cut off. Thus, we look to other estuarine processes to set hydrodynamics within the closed Pescadero estuary.

Figure 2.13: The mouth of the Pescadero estuary in the closed state on 11 November, 2010. Photograph credit: Rusty Holleman

Closed estuarine water levels

Immediately after closure, the mouth of the Pescadero estuary is still low in elevation (Figure 2.14). Throughout the closed period, we expect the height of the sand berm to be equal to or slightly above the height of the estuary water surface. Initial lagoon infilling occurs primarily by ocean water overtopping the low sand berm. Figure 2.12 shows the estuarine water level and ocean water level for the nine days following the mouth closure on August 23, 2011. Water levels in the estuary rapidly increase at high tide for the days immediately after mouth closure.

There are at least two mechanisms by which ocean water enters the Pescadero estuary during the closed mouth state to cause rapid lagoon filling: (1) waves overtop the sand berm

Figure 2.14: Photograph of the mouth of the recently-closed Pescadero estuary on August 25, 2011.

directly into the estuary, and (2) waves overtop the crest of the steep bermed beach, and gravity causes salt water to flow down the beach and into the estuary in a river of sea water (Figure 2.15). The second mechanism is less frequent, but more dramatic, with the one event observed corresponding with a rapid increase in lagoon water level on 31 August, 2011, just before instruments were pulled out to be redeployed (Figure 2.12).

Wave overwash carries salt water into the estuary and grows the sand berm. A study on the Belongil Beach and Belongil Creek inlet in New South Wales, Australia showed fast berm growth can be attributed to swash overwash (Baldock et al. 2008). Our observations suggest that wave overtopping in the Pescadero estuary occurs on an infragravity timescale, consistent with forcing seen in the open state of the estuary (cf chapter 3).

Due to the hypsometry of the marsh, initial wave overwash is most relevant to raising the water level in the closed lagoon. After a certain point, the surface of the lagoon begins to spill across the marsh and lagoon filling becomes much more gradual. Because nearshore forcing is primarily responsible for sand transport causing accretion of the sand berm at the mouth of the estuary, it is unlikely that a condition exists where the mouth becomes high enough that ocean water cannot enter.

Figure 2.15: Photographs of sea water flowing into the closed Pescadero estuary as waves overtop the entire beach. (a) Ocean water flowed into the Pescadero estuary on 31 August, 2011 both through waves overtopping the closed mouth and through waves overtopping the steep beach and traveling as a river of salt water down the beach and into the closed estuary. (b) Looking north up the Pescadero beach on 31 August, 2011 after the tide retreated, it is apparent that water flowed into the Pescadero estuary traveling as a river of salt water down the beach and into the closed estuary. Highway 1 is to the right of the photograph, the Pacific Ocean is to the left and the mouth of the estuary is behind the photographer.

Closed estuary density structure

With an episodic flux of salt water from the ocean into the Pescadero estuary and a flux of freshwater into the estuary from the creeks, conditions are set to allow the estuary to remain stratified in the closed state (Figures 2.16 and 2.17). The density is set by salinity of the water column, and a fresh or well-mixed brackish state was never observed in our closed-state measurements. The density structure is maintained by freshwater slowly increasing the thickness of the fresh surface mixed layer, and by episodic inputs of salt water coupled with limited mixing allowing the stratification to persist.

Temperature response to stratification

Since salinity sets stratification in the Pescadero estuary, the temperature structure observed is a product of that stratification as opposed to its driver as is common in lakes and oceans. Observations show that after the estuary has closed and a freshwater layer is present, water temperature in the mixed surface waters follow a diurnal trend of warming and cooling in accordance with solar heating (Figure 2.18). The salt-stratified lower layer of the estuary does not feel the diurnal heating, and may be much warmer than the surface water.

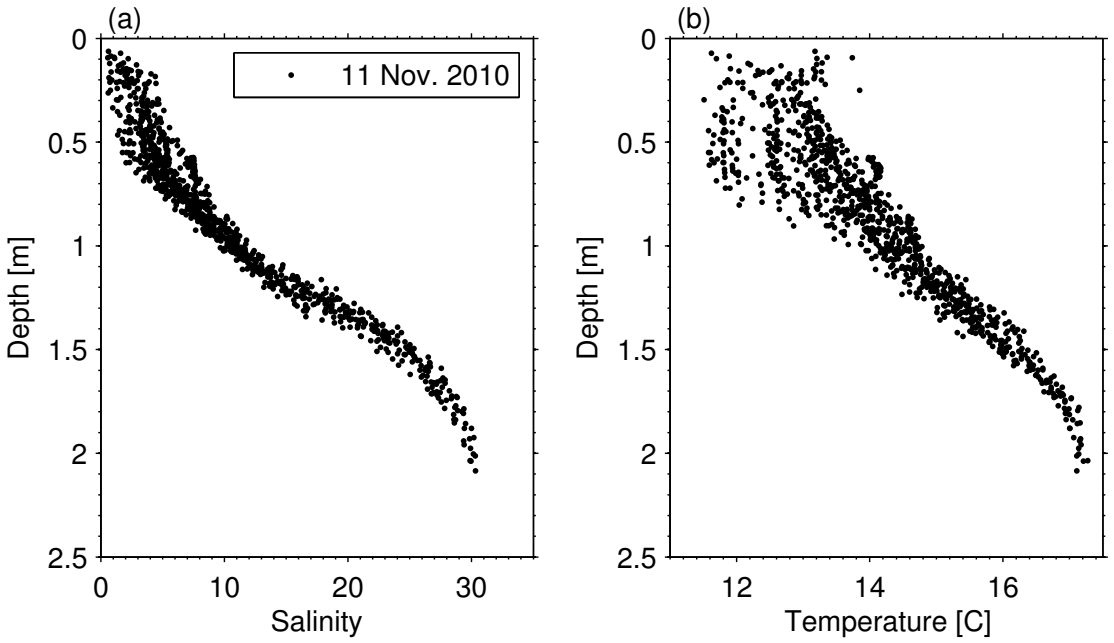

Figure 2.16: November 2010, (a) Salinity, (b) Temperature profiles with CTD depth. Measurements were made with a profiling CTD at many locations within the closed estuary.

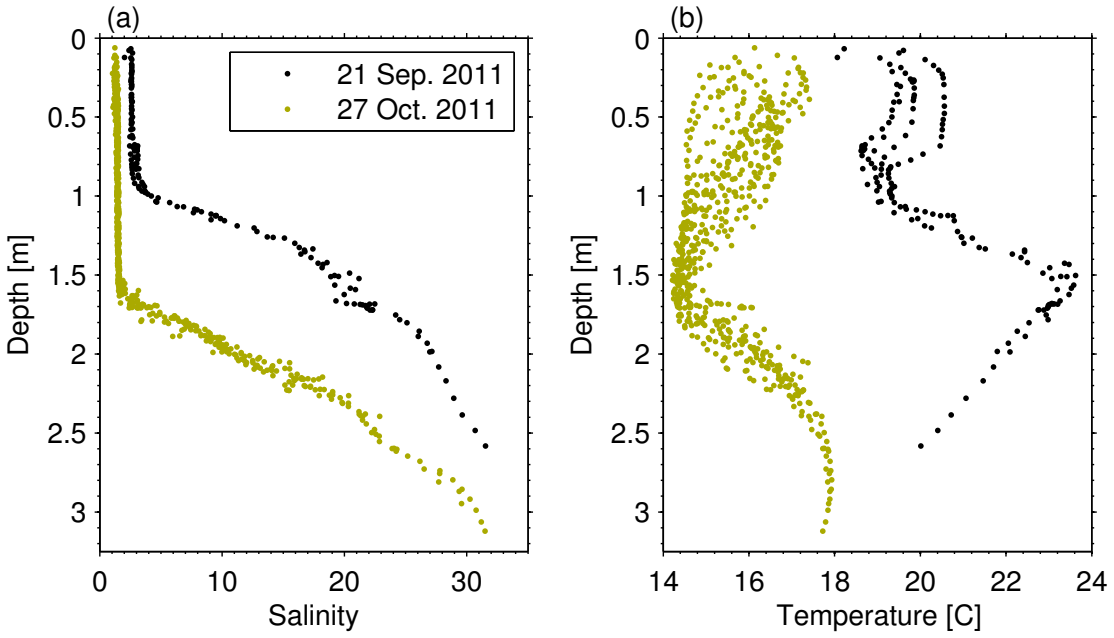

Figure 2.17: Fall 2011, (a) Salinity, (b) Temperature profiles with CTD depth. Measurements were made with a profiling CTD at many locations within the closed estuary.

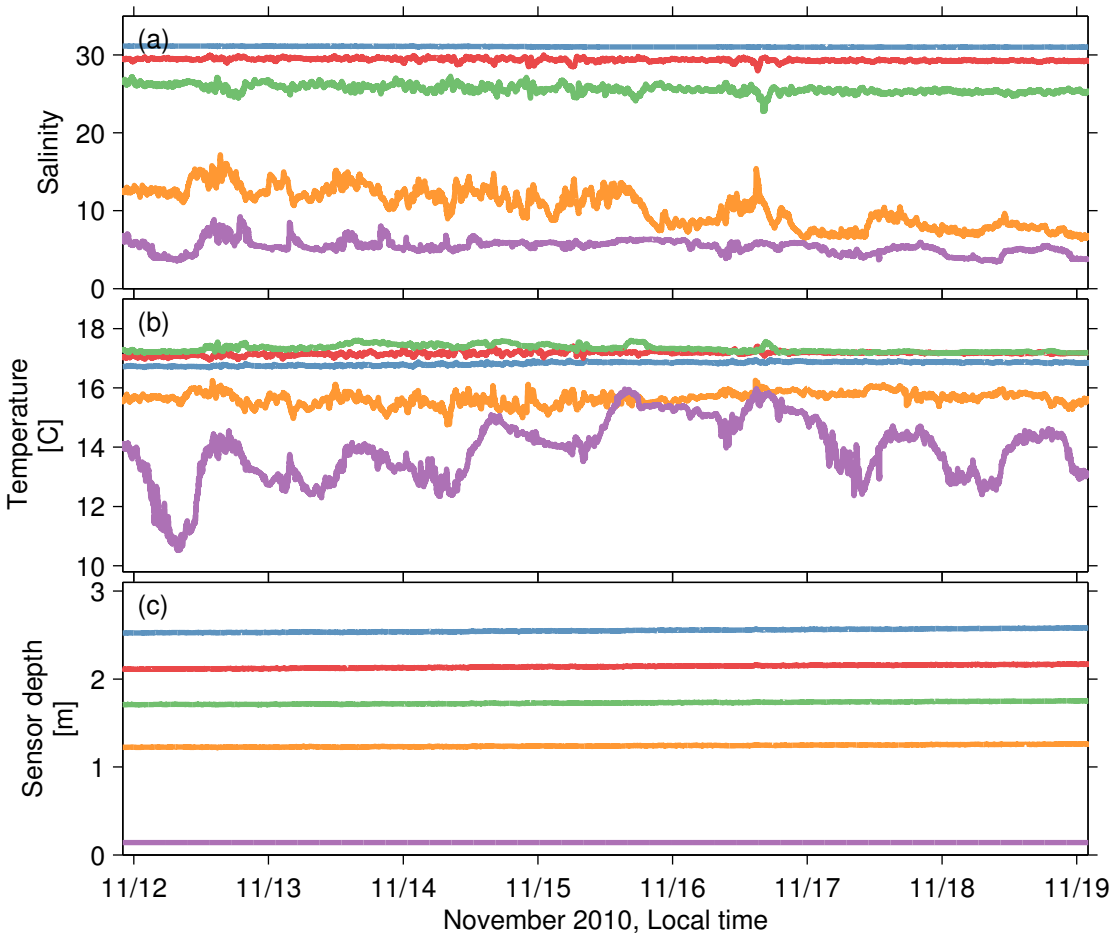

Figure 2.18: Sensors vertically distributed during the closed state in November 2010 show that the fresh upper water column (purple lines) responds to solar heating while the lower, stratified water column (blue, green, red lines) does not.

Closed estuary velocity description

While the estuary is open to tidal influence, tides are the main driver of flow (in the absence of very large freshwater discharge). After the inlet closes, tidal forcing is cut off. Velocity measurements show that flow within the closed lagoon is driven by wind forcing. The stratified water column reacts to surface wind stress from gentle wind forcing with two or three layer flow, and with upwelling in the presence of strong sustained winds. Large wind events which trigger upwelling of the saline lower waters in the closed Pescadero estuary cause some vertical mixing. A description of one such event follows.

Wind driven flow

An observed example wind setup and mixing in the Pescadero estuary occurred just prior to the sand bar breach on November 24, 2010 (Figure 2.19). In situ velocity and salinity measurements combined with wind measurements at Half Moon Bay airport are used to understand this event: On November 23, wind forcing was seaward, small surface velocities in the Pescadero estuary were consistent with this forcing, and the water column was vertically stratified. Three layer flow is apparent which may be related both to the vertical stratification and the influence of shallow bathymetry between the ADCP and closed mouth. Wind shear drives surface flow downstream, and the lower water column will respond by flowing upstream. At the deep DC sensors, a third recirculation region may exist (Figure 2.20).

From this point, the wind direction slowly shifted to become landward, and on November 23 at 18:20 GMT, the wind picked up to above 7 m s^{-1}. The water column responded immediately to this increased wind stress with surface flow in line with the wind and the deeper water column compensating with flow in the other direction (Figure 2.21). Three-layer flow may not be seen because the upper estuary is deeper and the leeward end of the estuary has a steep wall compared to the shallow lagoonal embayment, or because upwelling occurred rapidly. Salinity measurements suggest that the strong wind forcing caused upwelling of saltier water at the DS mooring (Figure 2.19e,f solid line), and downwelling of fresher water at US (Figure 2.19e,f dashed line) as the deeper sensor there went from measuring 18 PSU to less than 5 PSU in 13 hours while the sensors remained vertically fixed.

Around 06:00 on November 24, wind speeds slowed to under 5 m s^{-1} and the water column relaxed, as evidence by flow reversal. ADCP measurements suggest that the surface mixed layer at the instrument is shallower because the depth of highest shear (where flow reverses) at the setup event is deeper than at the start of relaxation. Salinity measurements agree. Whether this is evidence of vertical mixing or longitudinal or lateral movement of water masses is not necessarily distinguishable from this data. Mid-column sensors do become fresher as the relaxation occurs, suggesting mixing.

Large, wind-forced mixing events where persistent high wind upwells the halocline occur with some frequency. These events are significant as a mechanism of destratifying the water column, although observations suggest that at best the mid-column or deep water becomes a few PSU fresher.

It is upon this more well-mixed water column that the mouth bar is breached in November 2010, an event possibly induced by the relaxation of wind and subsequent slosh back of setup waters.

2.3.2 Closed inlet breach and rapid transition

Our measurements can shed some light on the hydrodynamic response of the lower estuary to the inlet opening. Breach events occurred on the following days within our measurement period:

- 24 November, 2010

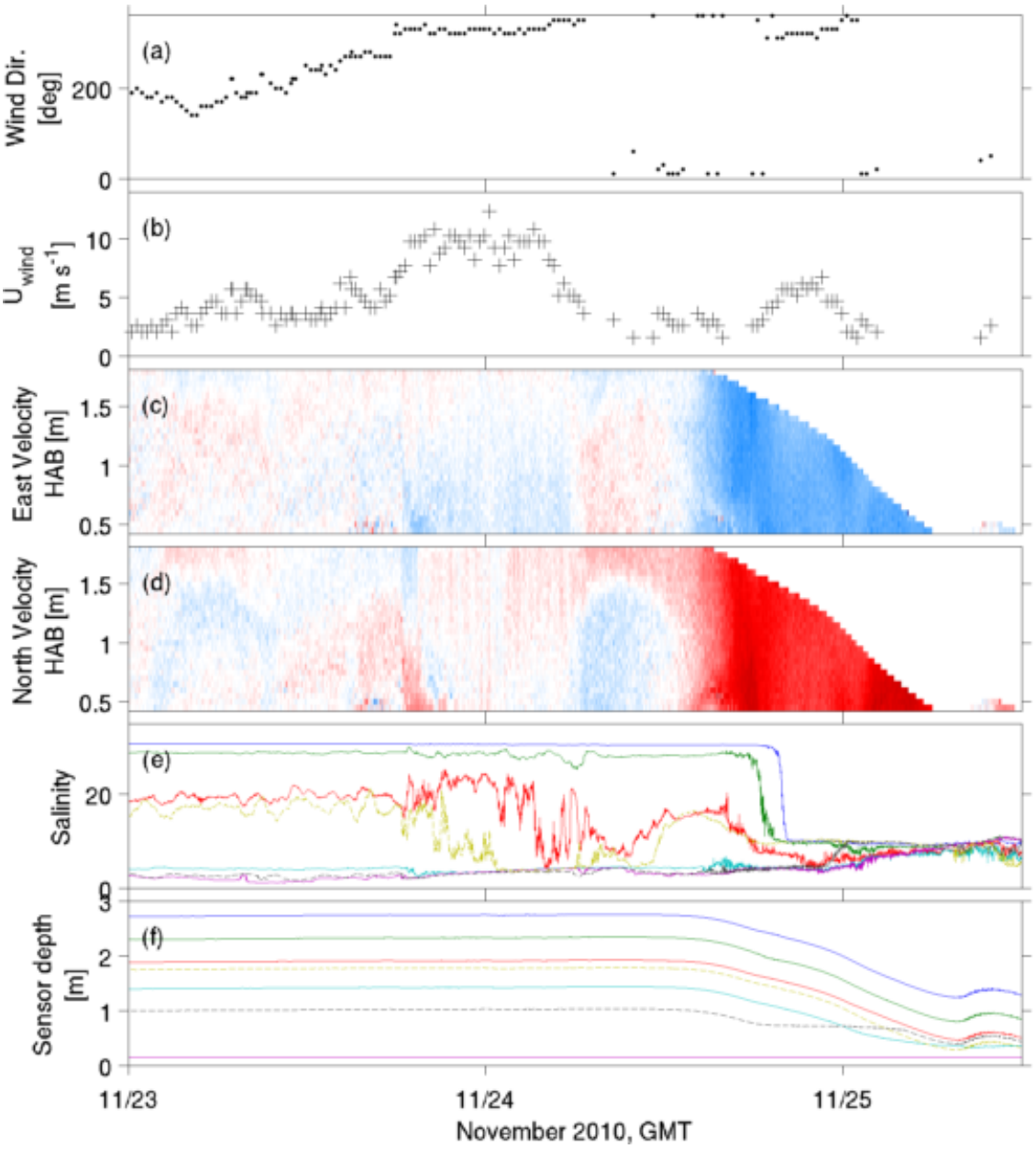

Figure 2.19: Observations of wind setup and the inlet breach on 24-25 November, 2010. Plotted are wind measurements at KHAF (a) and (b), ADCP velocity measurements [color range ± 0.5 m s^{-1} with red positive and blue negative] (c) and (d) and the DS (solid line) and US (dashed line) CTD mooring measurements (e) and (f). Solid lines in (e) and (f) represent CTDs at the DS mooring and dashed lines represent CTDs at the US mooring. Colors match for the salinity (e) time series and the instrument depth (f), indicating where in the water column each sensor was located. Observations show a wind setup event on 23 November, and a rapid draining of the estuary which resulted in full mixing of the water column at the DS and US moorings.

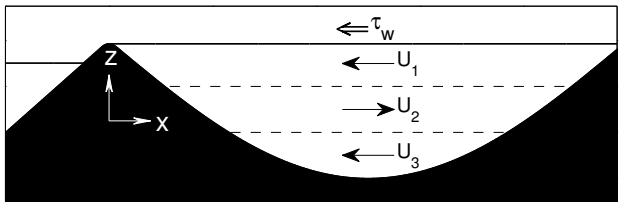

Figure 2.20: Three layer flow may occur with wind stress on the surface of the closed lagoon coupled with the effects of stratification and bathymetry.

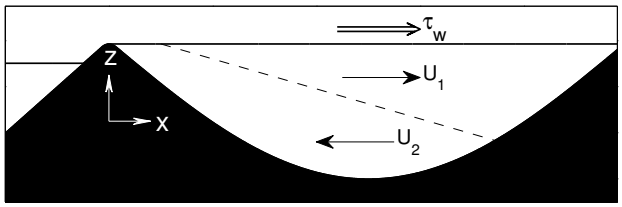

Figure 2.21: High, persistent winds push surface waters and may upwell the more dense bottom waters.

- 10-11 November, 2011
- 20-21 January, 2012
- 20-21 Feburary, 2012
- 3-4 March, 2012

The mouth remained in an open state after the November 2010 breach until August 2011, although a short period of near-closure occurred after the March 2011 tsunami (see Chapter 5). Following the November 2011 inlet opening, the mouth again closed and continued to oscillate between an open and closed state until March 2012 at which point it remained open for the duration of our field deployment which ended on June 5, 2012. Of the events measured, 20 February, 2012 is known to be an artificial breach, triggered by the mouth being manually excavated. Whether other bar breaches were instigated by natural or artificial means is not known, although the data inform speculations that the November 2011 breach was also trigged by human intervention. We made measurements of flow in the lower estuary, but do not have measurements on top of the submerged wetlands or many measurements in the creeks upstream of the confluence.

Two salt responses to inlet opening

In general, there appear to be two manifestations of breach dynamics in the Pescadero estuary. In one, the water column freshens and destratifies (Figures 2.19, 2.24, and 2.25). In a second formation, the water column does not freshen, and salt water is retained in the

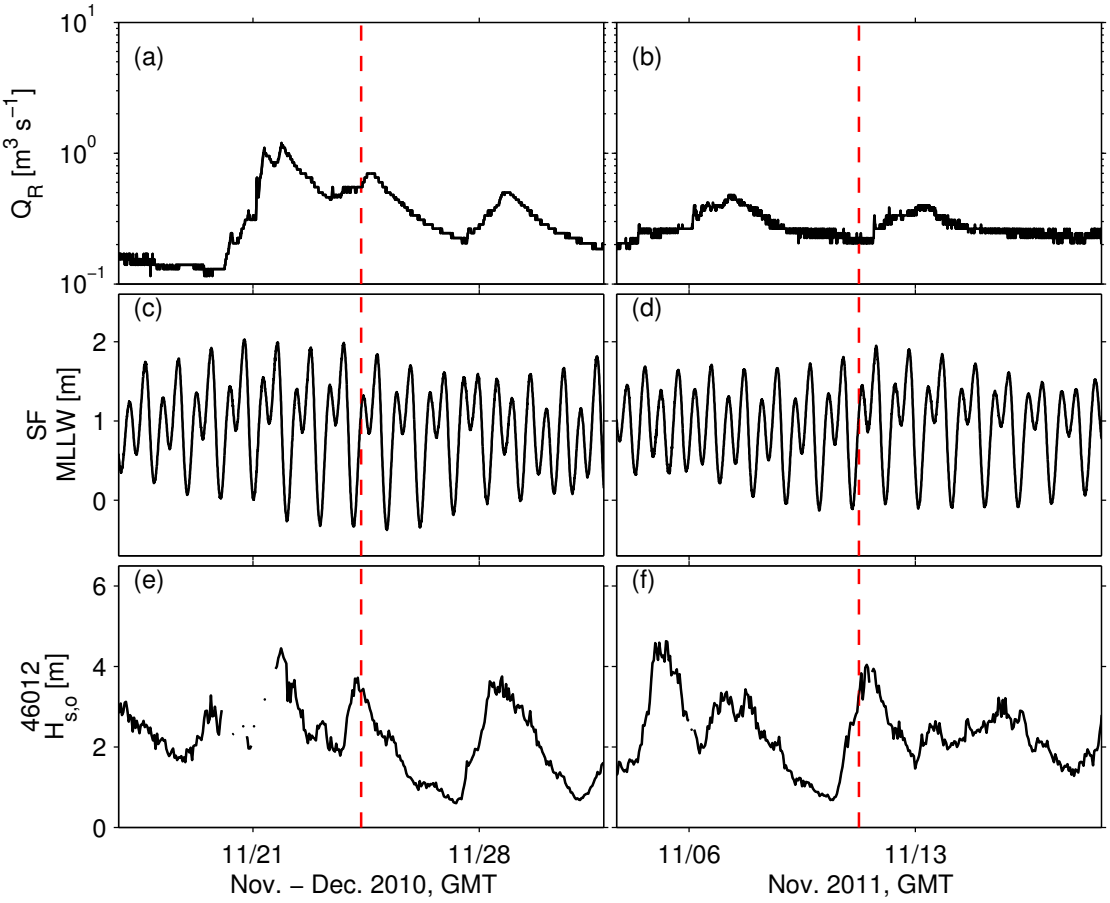

Figure 2.22: Freshwater streamflow (a,b) into the estuary, tidal conditions (c,d) and ocean wave conditions (d,f) surrounding breach events in November 2010 and November 2011. The red line gives the time of maximum water level preceding the water draw down.

depths of the estuary (Figure 2.26 and 2.27). In this case mixing does occur within the surface layer and within the stratified lower layer, but not between the two.

This discussion will look at the first type of breach event to generally understand what happens, and then point out differences in the breach events with limited mixing and hypothesize what causes these differences.

Figure 2.19 depicts east and north velocities at DS as well as salinity at DS and US during the 24 November, 2010 breach. The lagoon water level reached a maximum at 08:20 GMT on 24 November and began to fall, slowly at first, and then rapidly from 14:45 until the water level equilibrated with the incoming tide at 07:00 the next day. In this event, the estuary water surface dropped over 1.5 m. Maximum outflowing velocity magnitudes were 0.4 m s^{-1}. CTDs report that by 05:30 GMT on 25 November, 2010, the water column is

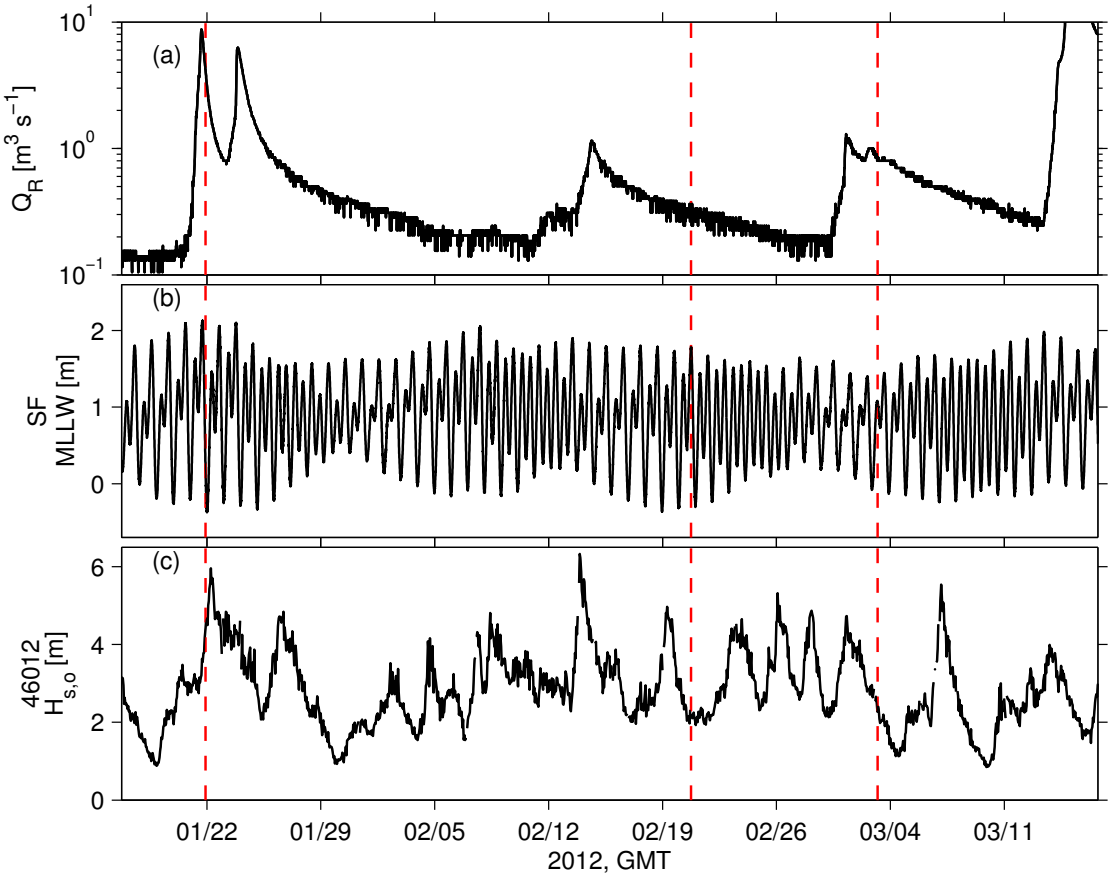

Figure 2.23: Freshwater streamflow (a) into the estuary, tidal conditions (b) and ocean wave conditions (c) surrounding breach events in January, February, and March 2012. The red line gives the time of maximum water level preceding the water draw down.

well-mixed at 8-9 PSU. This intermediate salinity suggests mixing has occurred. A uniform salinity of 3.5 PSU or less (the surface salinity pre-breach) could indicate that the lower estuary was flushed by fresher waters upstream, rather than indicate a mixing event.

The dramatic breach event is obvious when the lagoon was quickly draining, but velocity data and depth data suggest that there was a gradual lead up to the fast part of the breach. Data seem to suggest that relaxation of the wind-induced setup of the lagoon water surface instigated flow downstream which overtopped the sand bar. Comparing across other breach events sheds some light on processes involved in triggering the breach.

Inlet bar breach triggers

Streamflow measurements show an elevated freshwater discharge in conjunction with three breach events: November 2010, January 2012, and March 2012 (Figures 2.22a and 2.23). The February 2012 breach occurred in the absence of precipitation and we know that breach

to be artificial. Low streamflow in November 2011 suggests it may also have been created by human intervention (Figures 2.22b).

Within the events hypothesized to be naturally occurring, only the January 2012 inlet opening occurred with very high freshwater flows. The sand bar seems able to hold some flooding, possibly with help from wave overwash carried sand transport in conjunction with stormy conditions. A complementary mechanism is suggested by data in the case of the November 2010 and March 2012 events. In both instances, a wind transition occurred a few hours before maximum draining of the lagoon (Figures 2.19a,b and 2.27a,b). In the case of November 2010, strong winds upwelled the pycnocline and then shutoff as discussed in the previous section. In the case of March 2012, significant upwelling is not visible in CTD data measurements, but the surface sensors are temporarily slightly saltier, suggestive of movement of the stratified water masses. Similar velocity structure occurred in March 2012 with less dramatic setup and setdown followed by flow downstream of surface waters and eventually a dramatic drop in the water surface elevation as the sand bar gives way.

In both cases, the wind shifts directions and greatly slows. Wind shear high enough to upwell the pynocline will do so via a pileup of fresher waters in the lee side of the lagoon. In the case of wind blowing from the ocean, flow is driven upstream, and gravity will cause this piled up water to return downstream when the wind shuts off. Coupled with increased freshwater flows, the slosh back may instigate the natural breach of the closed estuarine inlet. If this is the case, the early breach is characterized by surface flow out, and stagnant or reverse flow in the lower water column upstream, probably bathymetrically determined, but little water level drop. Slow erosion of the sandbar at the mouth the occurs while flow accelerates to the point where the breach develops rapidly. It is in the rapid fall of the lagoon water level that the highest velocities are seen and full mixing of the isopycnals occurs.

In November 2011 and February 2012 breach events no wind setup (and setdown) preceded the breach (Figures 2.24 and 2.26). In January 2012 there was was wind-induced movement of the stratified water masses, but strong wind was from the land (Figure 2.25). Wind stress in the direction of the mouth could have aided in pushing water downstream and triggering the breach. No velocity data is available from that event to shed insight on this speculation.

Not yet mentioned is the influence of the ocean wave climate on the inlet opening (Figures 2.22e,f, and 2.23). Large ocean waves conditions may result in sand bar overtopping from the ocean side at high tide. Several of the breach events occurred in the presence of large ocean wave climates. However, storm conditions which bring precipitation also result in large waves. Whether mouth opening is aided by ocean waves is not obvious from these data.

Mixing vs. non-mixing breach events

Full mixing occurs when the lagoon drains quickly. Based on our limited number of observations, this occurs when:

- the lagoon water level is very high, and/or

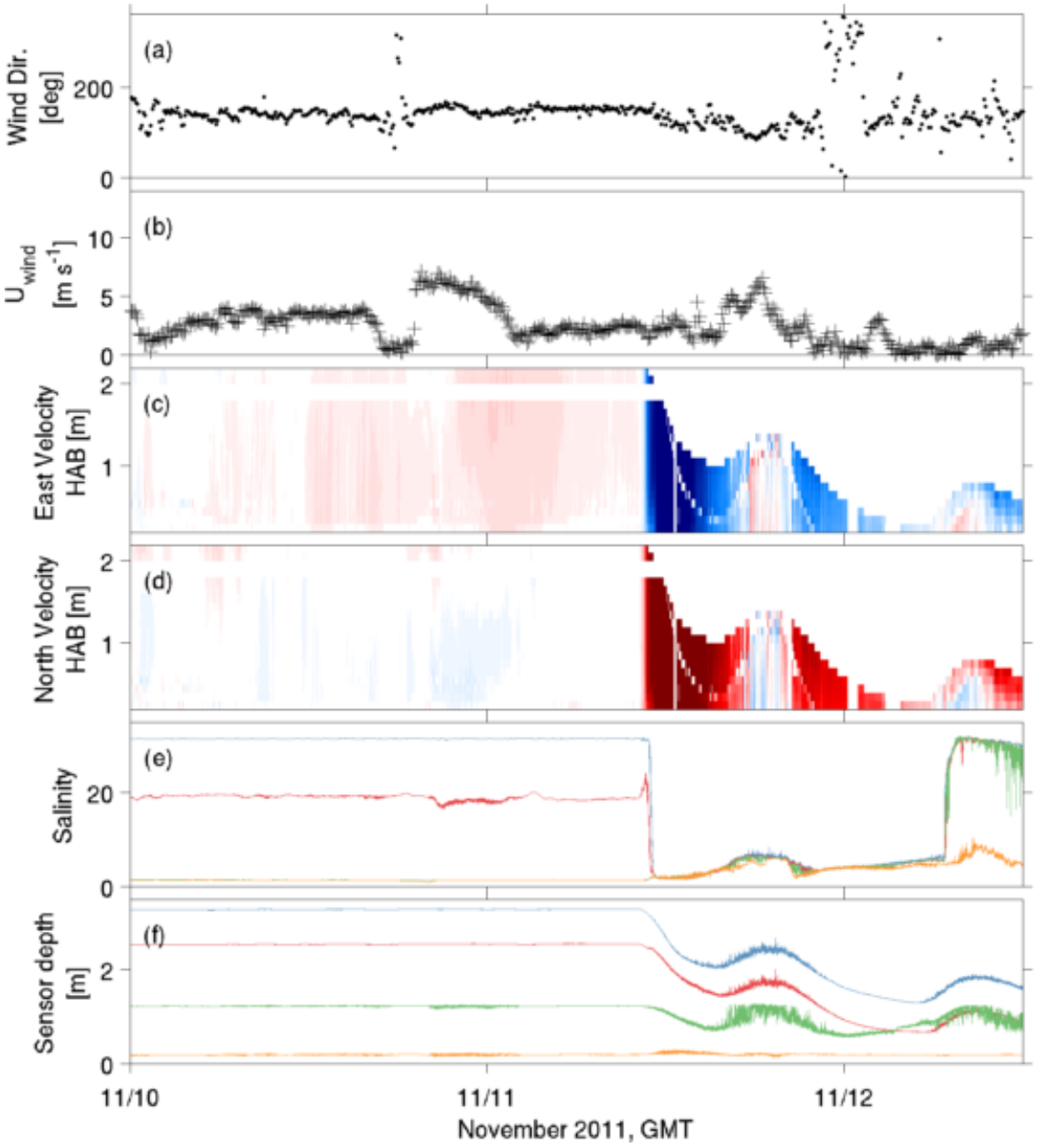

Figure 2.24: Observations of the inlet breach on 10-11 November, 2011. Plotted are wind measurements in the Pescadero marsh (a) and (b), velocity [color range ± 0.5 m s^{-1} with red positive and blue negative] (c) and (d) and the DC CTD mooring measurements (e) and (f). Solid lines in (e) and (f) represent CTDs at the DC mooring. Colors match for the salinity (e) time series and the instrument depth (f), indicating where in the water column each sensor was located. Measurements show a rapid draining of the estuary which resulted in full mixing of the water column at the DC mooring.

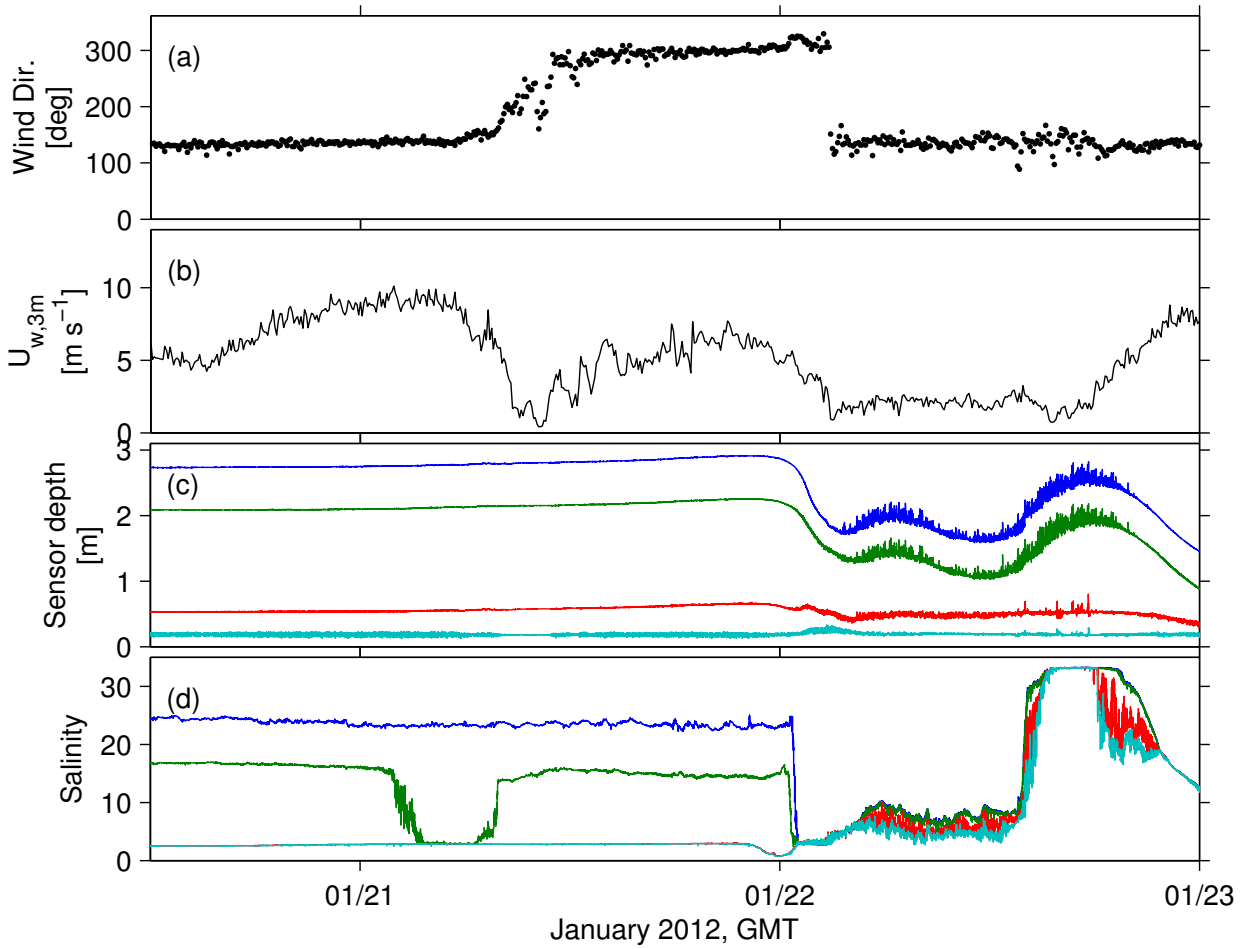

Figure 2.25: Observations of the inlet breach on 21-22 January, 2012. No velocity data is available for this event. Wind measurements in the Pescadero marsh (a) and (b) and the DC CTD mooring measurements (c) and (d) show a wind setup event early on 21 January, and a rapid draining of the estuary which resulted in full mixing of the water column at the DC mooring. Solid lines in (c) and (d) represent CTDs at the DC mooring. Colors match for the salinity (c) time series and the instrument depth (d), indicating where in the water column each sensor was located.

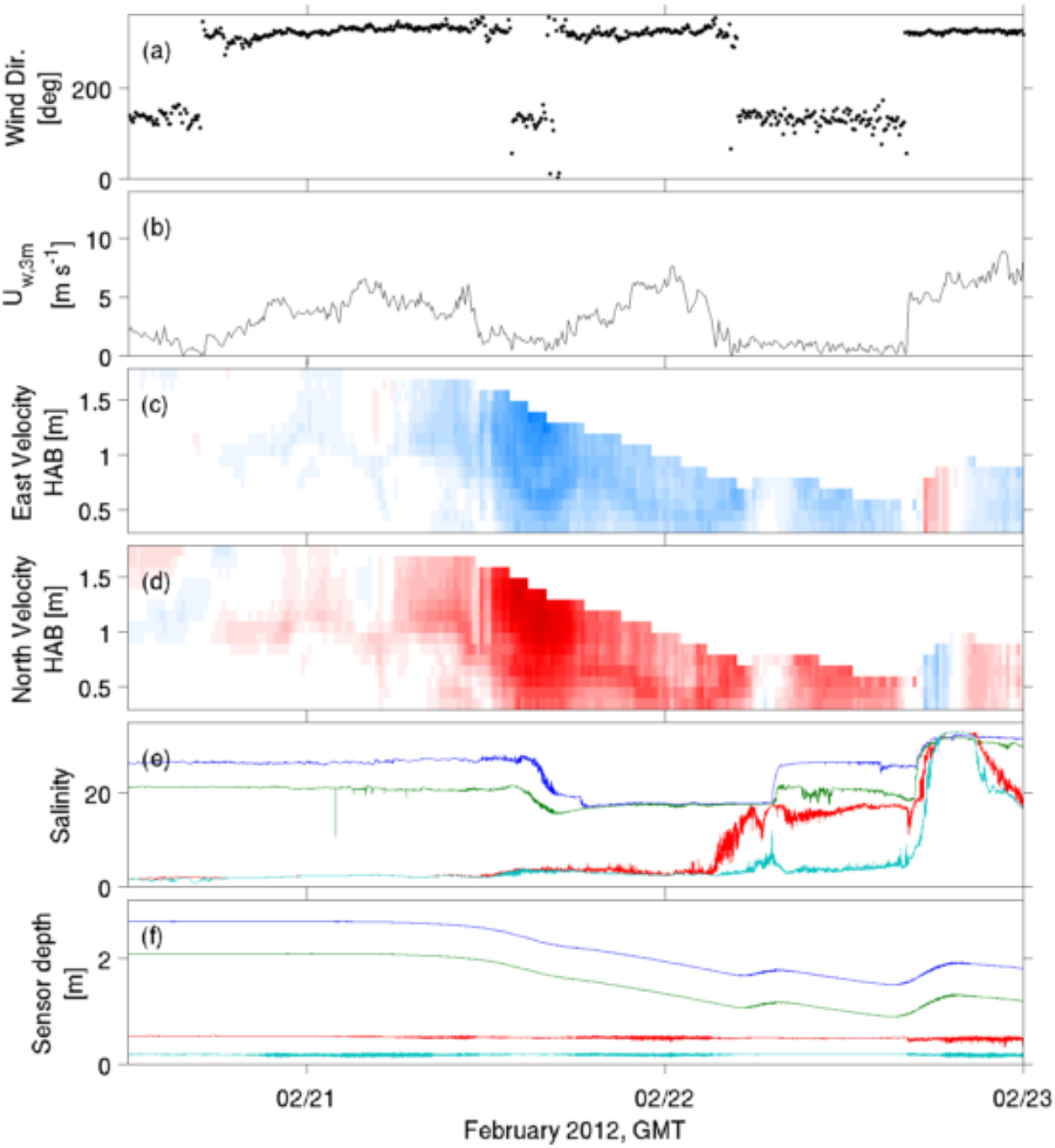

Figure 2.26: Observations of the inlet breach on 21-22 February, 2012. Plotted are wind measurements in the Pescadero marsh (a) and (b), velocity [color range ± 0.5 m s^{-1} with red positive and blue negative] (c) and (d) and the DC CTD mooring measurements (e) and (f). Solid lines in (e) and (f) represent CTDs at the DC mooring. Colors match for the salinity (e) time series and the instrument depth (f), indicating where in the water column each sensor was located. Measurements show a slow draining of the estuary occurred. Mixing in the deep water occurred, but complete vertical mixing is absent during this event.

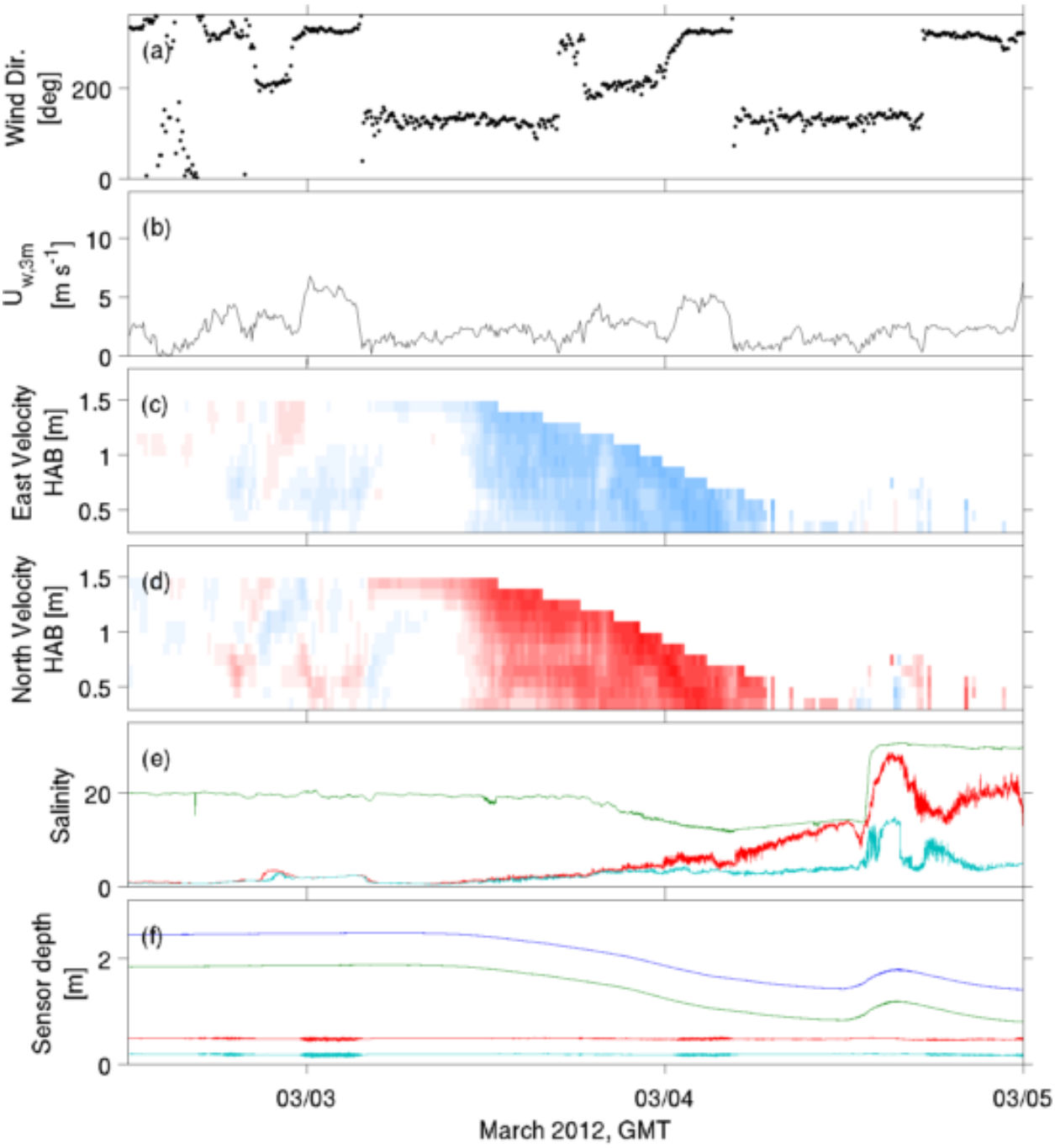

Figure 2.27: Observations of the inlet breach on 3-4 March, 2012. Plotted are wind measurements in the Pescadero marsh (a) and (b), velocity [color range ± 0.5 m s^{-1} with red positive and blue negative] (c) and (d) and the DC CTD mooring measurements (e) and (f). Observations show slow draining of the estuary. Mixing in the deep water occurred, but complete vertical mixing is absent during this event. The bed CTD conductivity cell was malfunctioning during this window and so those salinity data are not shown.

- freshwater discharge from the creeks is very high.

November breaches after several months of closed estuarine conditions are characterized by massive flooding of the marsh complex. In November 2011, the marsh between lower Butano Creek and the narrow estuary just below the confluence of the two creeks was flooded to the point that it was easy passable by canoe. January 2012 water levels were also high, and the draining outflow was aided by high creek discharge. The two slow drains in February and March 2012 occurred when water levels were not as high and/or freshwater streamflow was low.

General breach dynamics show that in some breach events surface flows across the entire lagoon start as a result of wind forcing, and as the sand bar erodes, flow out of the estuary rapidly transitions from surface flow to flow throughout the entire water column. This was the case in November 2010 and March 2012 (Figures 2.19 and 2.27). Flow structure in November 2011 seems to abruptly become nearly uniformly outflowing (Figure 2.24). With no spin up by wind, this is probably the result of manual removal of part of the sand bar. Here, flow is siphoned from the end and velocities at the ADCP (approximately 400 m upstream of the mouth) reflect flow that has developed as a drain near the mouth. Flow in the February 2012 breach is somewhat between these two cases: sudden flow starts over a large part of the upper water column, but does not penetrate to deep water (Figure 2.26).

2.4 Annual and interannual variability

The largest variability observed year to year was in the timing of mouth closure and opening in the Pescadero estuary. The estuary while open to the ocean in September 2010 was highly marine, while during the same days the following year, the mouth was closed and the character of the water column was completely different. Late summer open state conditions transform the lower estuary into an environment where marine flora and fauna have been seen and the water is very clear. Late summer closed estuary conditions produce a more turbid estuary with high vertical stratification.

Low rainfall in water year 2012 limited the freshwater outflow available to maintain an open mouth, and the mouth repeatedly closed and opened during winter 2011-2012 and spring 2012 in what was a seemingly uncharacteristic way. The drought currently occurring in California as of summer 2014 has allowed the mouth to close earlier and stay closed longer. The magnitude of freshwater flow into small California estuaries sets the length of closure of these systems (e.g. Elwany et al. 1998). A continuation of this drought may drastically alter the closure regime in the Pescadero estuary. The open or closed state of the mouth determines estuarine dynamics, so in this way the influence of changing hydrologic conditions may be multiplied in California's small estuaries by altered closure patterns.

2.5 Conclusions

The small size of the Pescadero estuary, as well as other bar-built estuaries in California allows them to respond quickly to external forcing. Closed-state dynamics in the Pescadero estuary are set by the stratifying inputs of freshwater and salt water and destratifying inputs from wind stress. This wind forcing may play a role in starting the closed mouth breach.

Wind, wave, freshwater and tidal forcing in the Pescadero estuary are all dependent on the state of the inlet. While closed, tides bring water near the top of the berm and waves allow salt water to overtop the berm, growing the sand berm and supplying a salt water source to the estuary. While open, tides contribute momentum, and move salt in and out of the estuary. Freshwater inputs in the open state are often small compared to tidal exchange (except after large storm events, which were infrequent during our study). Late-summer freshwater flow may be negligible if the inlet is open, but if the inlet is closed these inputs slowly accumulate and become a thick fresh surface layer. This layer impedes mixing by wind and limits the exchange of thermal heating and oxygen into stratified or saline bottom waters. Wind drives flow while the estuary is closed, but its effect during the open state is not necessarily noticeable in the face of dominant tidal forcing. Predictive capabilities in estuaries such as the Pescadero will not be possible without an understanding of inlet dynamics superior to our current state of knowledge. Processes at work in determining inlet conditions include the nonlinear interactions between waves, swash, tides, river flow and their influence on sediment resuspension, transport, and deposition. In return the changing morphology alters these processes, creating a dynamic and difficult interplay to understand.

Chapter 3

Tidally discontinuous estuarine hydrodynamics

3.1 Introduction[1]

California's coast is dotted with small estuaries draining the pristine, agricultural, or highly urbanized watersheds found along the state's coastline. Similar to bar-built estuaries found in Mediterranean climates on wave-dominated coasts worldwide, the inlets of these estuaries may become choked closed by sand for extended periods of time (e.g. Elwany et al. 1998; Hanes et al. 2011; Fortunato et al. 2014; Ranasinghe and Pattiaratchi 2003). Nearshore sediment transport processes compete with ebb tidal and river flow to set the open or closed state of the inlet (Behrens et al. 2013). While open, the inlets of intermittently closed estuaries remain highly constricted, altering tidally-driven hydrodynamics and salt transport in these systems.

Some studies in temporarily open/closed estuaries (TOCE) in South Africa, intermittently closed and open lakes and lagoons (ICOLLs) in Australia, and intermittently closed estuaries in California sheds some insight on the hydrodynamics in these systems. Tidal forcing is typically highly attenuated in these estuaries (e.g. Ranasinghe and Pattiaratchi 1999; Gale et al. 2007). Salt movement in the South African Palmiet estuary occurs as ocean water moves up estuary as a density current, becomes trapped in deep pools of the estuary and then is removed by shear-induced mixing from above (Largier and Taljaard 1991). Similar salt-wedge or two-layer structure has been observed in the open state of other intermittently closed estuaries (e.g. Sharples et al. 2003). Overall, hydrodynamic observations are limited.

Many of the previous observations have looked at overall circulation patterns of an estuary on seasonal scales, leaving the effects of short term processes like a changing wave climate or spring-neap cycle under described. In contrast to large estuaries with deep inlets, the

[1]This chapter has been submitted to the *Journal of Geophysical Research: Oceans* as "Tidally discontinuous ocean forcing in bar-built estuaries: the interaction of tides, infragravity motions, and frictional control" by M.E. Williams and M.T. Stacey. At time of submission of this dissertation, the manuscript was in review.

shallow mouth of open-state intermittently open estuaries alters tides and causes ocean waves to break outside the inlet. The effects of these features on estuarine hydrodynamics have not been characterized. And, though estuaries with closing inlets exist in various parts of the world, those on the west coast of North America have received little attention.

Because sparse hydrodynamic characterizations of open-state hydrodynamics of intermittently closed estuaries exist, we must look to processes important to these systems in other contexts. The mouth or inlets of these systems cross beaches with active wave environments (see Mei and Liu 1993; Battjes 1988). Wave setup observed in lagoonal estuaries (e.g. Malhadas et al. 2009) may be analogous to similar setup on coral reef lagoons (e.g. Becker et al. 2014) and wave-driven flow on these reefs (Monismith 2007) may also be important in lagoonal estuaries.

Here we present results of extensive field observations in the Pescadero estuary of Northern California aimed at characterizing hydrodynamics of small bar-built estuaries with intermittent connections to the ocean.

3.2 Experimental site and overview of conditions

As part of a longer-term study to analyze dominant drivers of hydrodynamics and salt transport in California's small estuarine systems, extensive field measurements were made in the Pescadero estuary.

3.2.1 Site description

The mouth of the Pescadero estuary sits on the California coast midway between the Golden Gate and the northern extent of Monterey Bay (Figure 3.1a). The mouth is constrained to the south by a rocky cliff. To the north, the Pescadero State Beach is the southern extent of approximately 10 km of sandy beach with three other small inlets. The inlet is approximately 100 m long, and opens into a shallow lagoonal estuary (Figure 3.1b)

The lower estuary has a maximum high tide depth of approximately 2.7 m, in the deep channel 350 m upstream from the mouth (Figure 3.1b) and maximum spring tidal range of 1.4 m. The mouth of this estuary typically closes with sand between August and October due to nearshore sediment transport and reopens with the start of the California rainy season in November. During the dry water year 2012, the mouth closed and opened several times, not remaining open for an extended period until early March 2012. Results presented here are exclusively from the open inlet state of the estuary.

The Pescadero creek arrives to the ocean through the largest wetland complex between the San Francisco Bay and Elkhorn Slough on Monterey Bay. Two creeks, the Pescadero and Butano, connect 700 m upstream of the mouth. The Butano Creek meanders through extensive salt marsh while the Pescadero creek remains more channeled and riverine up to the confluence. On the Pescadero Creek upstream of the confluence, a channel connects a shallow pond to the estuary through dilapidated culverts, installed as part of a restoration

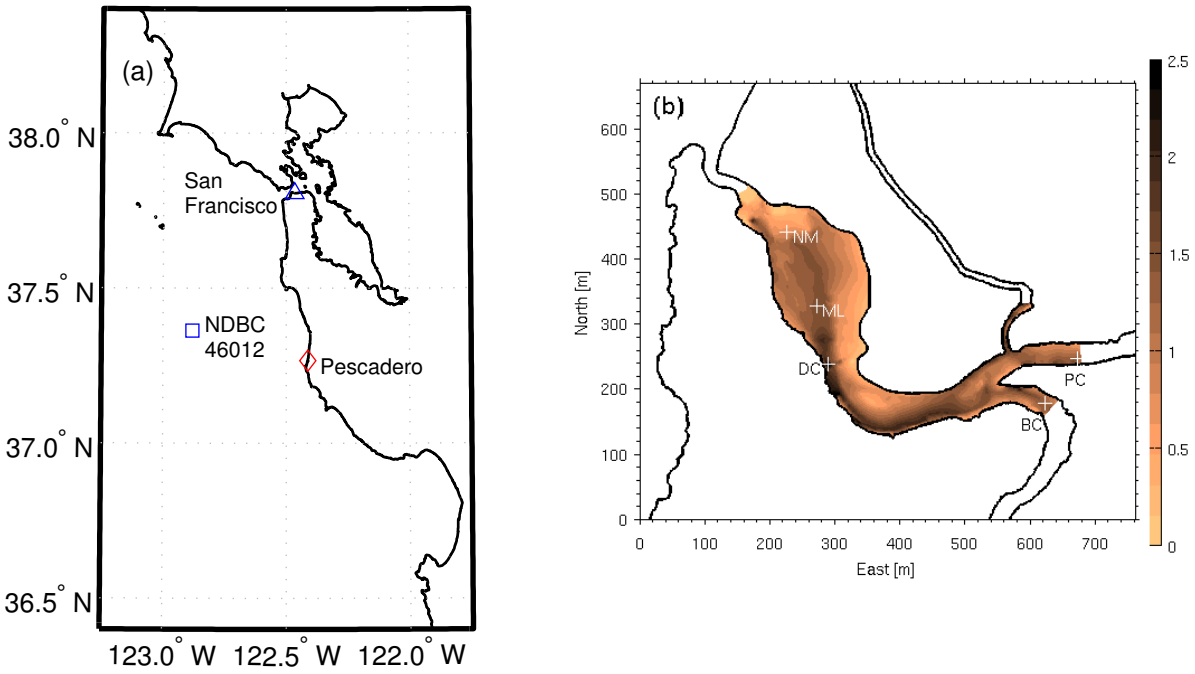

Figure 3.1: (a) The Pescadero estuary sits on the California coast between Monterey and San Francisco Bays. The location of sensors referenced for tidal and wave conditions are shown. (b) The coastline and depth at high tide in the Pescadero estuary. Pescadero Creek flows into the estuary from the northeast, and Butano Creek from the south. The narrow channel connects the estuary to a northern pond through culverts.

project. The presence of the North Pond likely influences the inlet dynamics by increasing the tidal prism, but due to very limited connectivity through small culverts, we ignore its effect on hydrodynamics.

The Pescadero watershed covers 210 km^2 in the coastal Santa Cruz mountains. A USGS gauge (11162500), 8.5 km upstream of the mouth captures captures 57 % of the watershed. Unaccounted for freshwater diversions exist due to agriculture in the watershed, but freshwater flow into the estuary, Q_R, is approximated by scaling the gauged freshwater discharge, $Q_{R,G}$, by the entire watershed area. The rainfall dominated coastal watershed is flashy during the wet winter, and dry during the summer season, reflecting the Mediterranean-climate seasonality of the region.

3.2.2 Field measurements and data processing

Measurements

Measurements were made in the lower Pescadero estuary from 17 April - 5 June, 2012 with high frequency velocity measurements limited to a shorter subset of this time. A

suite of instruments measuring temperature, salinity, pressure, and velocity were distributed longitudinally and vertically in the water column (Figure 3.1b).

An acoustic Doppler velocimeter (ADV; Nortek Vector) was installed on 18 April recording in 512 s bursts every 15 minutes at a sampling rate of 8 Hz at the near mouth (NM) station. The instrument's sampling volume was positioned 20 cm above the bed. A collocated CTD recorded salinity and pressure at a frequency of 1 Hz. The deep channel (DC) station had a bed-mounted acoustic Doppler current profiler (ADCP; RDI Workhorse Monitor 1200 kHz). The height of the ADCP plus blanking distance meant that the first depth cell was located 71 cm above the bed at DC. The bed at DC is approximately 19 cm below MLLW. Co-located with these velocity instruments were bed, surface, and mid-column CTDs. A CTD was moored upstream in the Pescadero Creek (PC) at a height of 20 cm above the bed, sampling every 30 s. Previous attempts to collect data in the mouth, even for a short duration (under 24 hours), left instruments buried in the sand, so proximity of moorings to the mouth was limited.

Tidal, freshwater, and ocean wave condition measurements were obtained from NOAA and USGS gauges (cf. 3.2.3).

Data processing

Estuarine depth measurements were made using several bed-mounted CTDs with the atmospheric pressure offset calculated from measurements made at the coastal Half Moon Bay airport (KHAF). Estuarine significant wave height, $H_{s,e}$ was calculated as $H_{s,e} = \sqrt{4m_o}$ where m_o is the variance of the a 20 min moving average signal subtracted from the depth signal to remove the tidal component. Surface oscillations due to waves and bores were recorded, but oscillations considered are of low frequency (period $>$ 30 s) so depth attenuation of the wave signal should be minimal. Some slight attenuation of the signal may occur, especially at high tide, and this would result in a slight underestimation of the estuarine significant wave height.

Velocity measurements (ADV and ADCP) were rotated in to principle coordinates (u,v) based on a linear fit of each instrument's dataset. Tidal velocities,$\overline{< u >}$, are approximated by the depth averaged 20 min moving average of ADCP velocity measurements. The moving average is intended to remove the higher frequency velocity signal. Due to the blanking distance above the bed-mounted ADCP, 'depth-averaged' velocities are missing flow at the bottom of the water column. While this missing data is likely relevant, the study was limited to available instruments commonly deployed in much deeper water.

The definition of the infragravity band varies by author, with a lower end period between 20 and 30 s and an upper end period between 4 and 8 min. Here we use the gravity wave band within a period of 1 s to 30 s and infragravity period from 30 s to 5 min, consistent with Munk (1950).

To observe general salt dynamics, CTD sensor data were interpolated onto an x-z cross section of the estuary. Vertical distribution of CTDs at DC was concentrated in the upper water column because of an instrument failure. We know that sharp gradients exist

in the vertical so to observe salinity in the water column with time (Figure 3.12a-c), the vertical profile from interpolated x-z data (Figure 3.11a-f) was used so that upstream and downstream sensors contribute to the estimated profile. Any interpolation method makes stability analysis difficult because the pycnocline may be 10 cm thick and our measurements lack the fine resolution needed to calculate an accurate Brunt–Väisälä frequency, N.

3.2.3 Overview of conditions

General conditions are based on a streamflow gauge maintained by USGS, and a tide gauge and wave buoy maintained by NOAA (Figure 3.2).

In California's Mediterranean climate, precipitation is seasonal and does not usually occur during the summer months. The last notable rainstorm of water year 2012 occurred between April 11 and 15, so freshwater was present in the Pescadero estuary during the study, but no rain was recorded (Figure 3.2a).

The California coast experiences a mixed semi-diurnal tide. The tidal range is between 1.1 m and 2.7 m at the closest NOAA gauge in San Francisco (NOAA 9414290, Figure 3.1a, Figure 3.2b). The study encompassed spring-neap variation.

A NOAA National Data Buoy Center (NDBC 46012) wave buoy in 208.8 m depth approximately 40 km WNW of the Pescadero estuary gives a proxy for the wave climate experienced at the coast. Significant wave heights offshore varied between 0.6 m and 4.8 m during the study (Figure 3.1a, 3.2c).

3.3 Analysis of hydrodynamics

Estuaries are driven by ocean tides, but lagoonal estuaries often have an attenuated tidal signal compared to the ocean coast primarily due to friction losses (e.g. Rydberg and Wickbom 1996). By comparing the tidal ocean water level with the tidal estuarine water level in the Pescadero estuary (Figures 3.4a, 3.3), a picture of tidally-varying estuarine-ocean connection emerges. Tidal attenuation in the Pescadero estuary occurs only on the large ebb of the semidiurnal mixed tide. Throughout the rest of the tidal cycle, the ocean and estuarine water levels are nearly the same.

This two-phase connection where for 16-17 hours of the 24 h tidal cycle the nearshore and estuary are connected but for 7-8 hours the bodies of water separate sets the hydrodynamic conditions and determines different forcing during these distinct phases of the tide (Figure 3.3). Here we examine processes during each phase and describe how this tidally varying connection affects estuarine dynamics.

3.3.1 Nearshore-estuarine connection

Observations show that while the estuary water level and and ocean water level are the same, the estuary and nearshore are connected and tidal forcing is accompanied by velocity

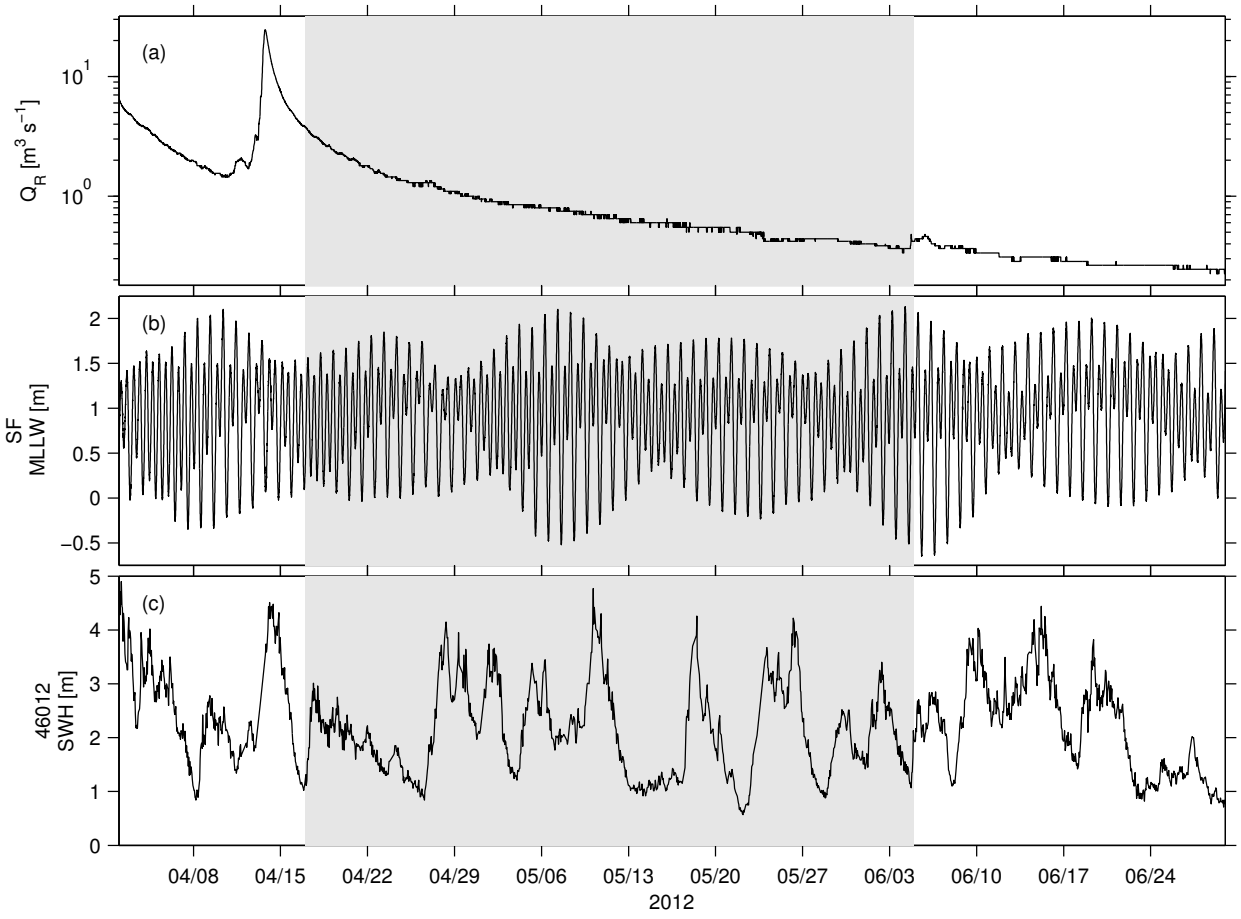

Figure 3.2: Conditions during field deployment. The freshwater streamflow into the estuary (a) is scaled up by watershed area from the USGS Pescadero gauge (11162500). San Francisco tidal water level data (b) is given by NOAA measurements at Crissy Field (9414290). The NOAA NDBC buoy (46012) gives ocean significant wave height (c) 40 km WNW of the Pescadero estuary. Gray area indicates period that sensors were collecting data. Higher frequency measurements were obtained during the first 5 days to three weeks of the experiment, but CTD and some velocity data were collected for the entire shaded period.

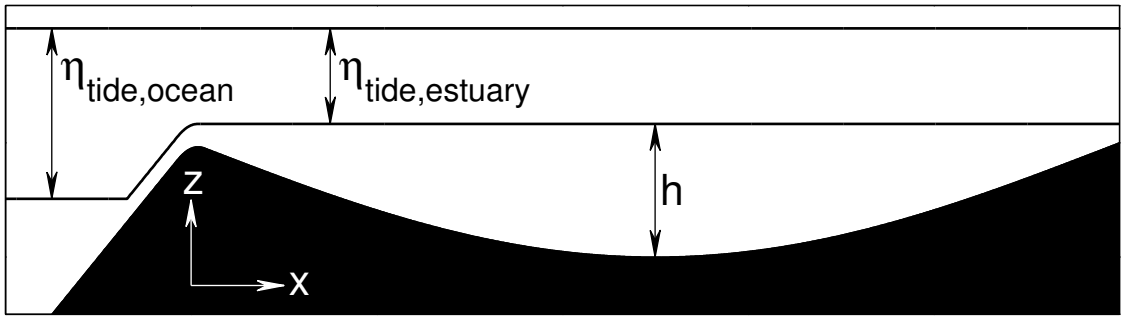

Figure 3.3: For most of the mixed semidiurnal tidal cycle, the estuary and ocean water levels are approximately the same, allowing for connection between the nearshore and estuarine environments. As the tide falls to it's daily low low state, the ocean retreats below the mouth of the perched estuary.

oscillations attributed to infragravity motions.

Tidal timescales

Looking at tidal timescales approximated by the depth average of the 20 min moving average ADCP dataset, $\overline{< u >}$, for the small spring tide conditions on 23 to 26 April, 2012, tidal velocities oscillate between -30 cm s^{-1} and +20 cm s^{-1}. Measured ebb-dominance may be influenced by the two-layer nature of the flow and missing data in the lower 71 cm of the water column where positive velocities would be observed on the flood. Maximum estuarine water level leads peak flood tidal velocities by 1-2 hours (Figure 3.4a,b).

Infragravity timescales

On top of the tidally induced velocities and changes in water level, oscillating motions are observed during the nearshore-estuarine connection phase of the tides in both velocity and as a surface expression (Figure 3.5). These oscillations in η and u are attributed to the presence of infragravity motions in the nearshore, due to their observed period within the infragravity band of 30 s to 5 min (Figure 3.6). No instrumentation was deployed in the nearshore during this field campaign, but infragravity motions are consistently present on sandy beaches (Contardo and Symonds 2013) and we expect them to be present here. By characterizing the wave-like surface oscillations as an estuarine significant wave height, $H_{s,e}$ (Figure 3.4c), we can use this as a metric for the presence of infragravity motions in the estuary and thus as a proxy for nearshore-estuarine connection. When $H_{s,e}$ is above 1 cm (Figure 3.4, black lines/points), the relationship between ocean tides and estuarine tides are nearly 1:1, and tidal velocities obey an expected sinusoidal shape in relation to tidal water level. When $H_{s,e}$ falls below this threshold, the relation between the estuarine and ocean water level diverges, and a disconnected state persists (Figure 3.4a,c).

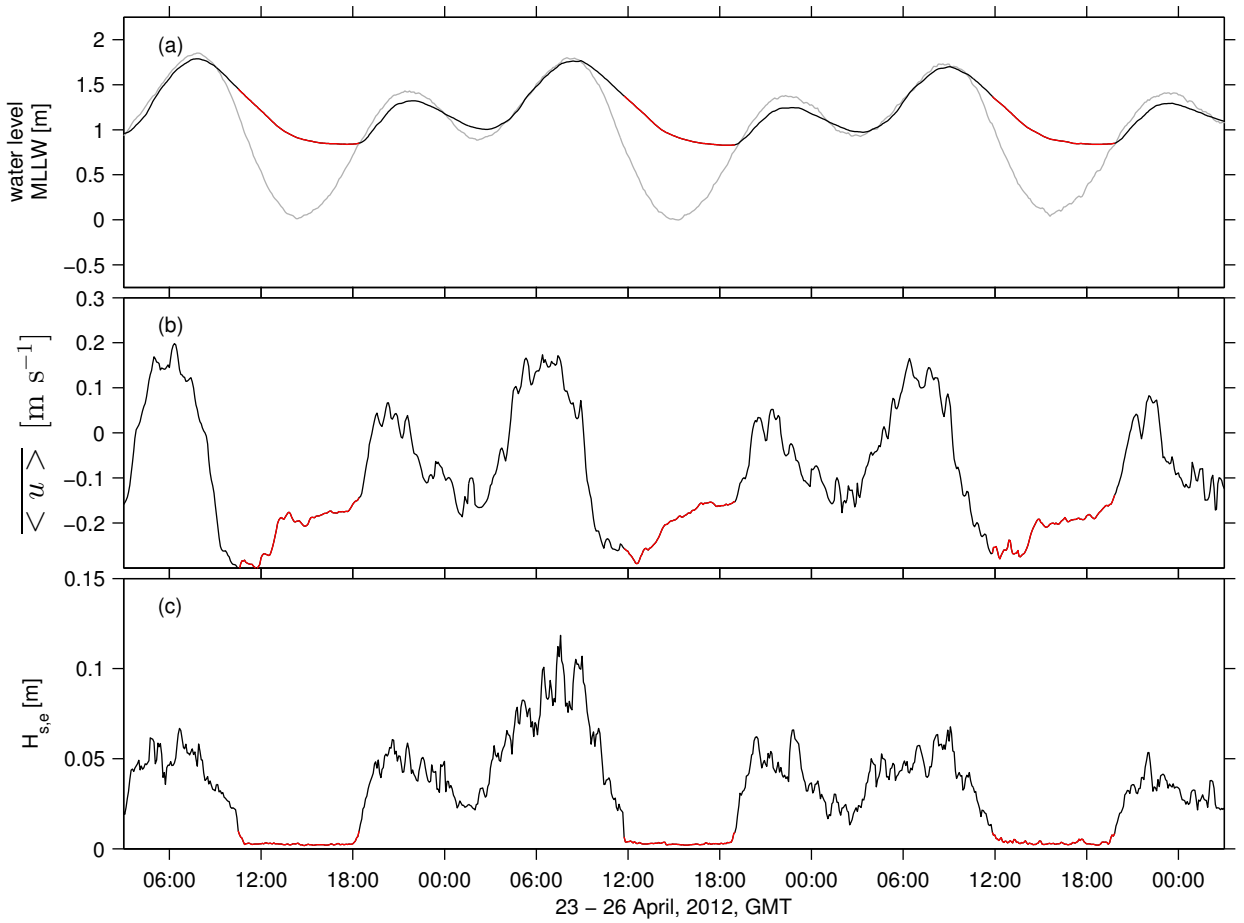

Figure 3.4: Time series of water level (a), depth-averaged velocity (b), and estuarine significant wave height (c). Ocean water level variations (a - gray line) due to tides are much greater than the estuarine water level changes (a - black and red line). Depth-averaged velocity (b) at DC shows a sinusoidal velocity and a frictionally controlled velocity during different phases of the tide. The presence of water surface oscillations is determined by an estuarine significant wave height (c). A threshold of 1 cm determines the presence of "waves" and the water level (a) and depth-averaged velocity (b) time series have been color-coded to presence of of this infragravity forcing (black - nearshore forced, red - no infragravity oscillations).

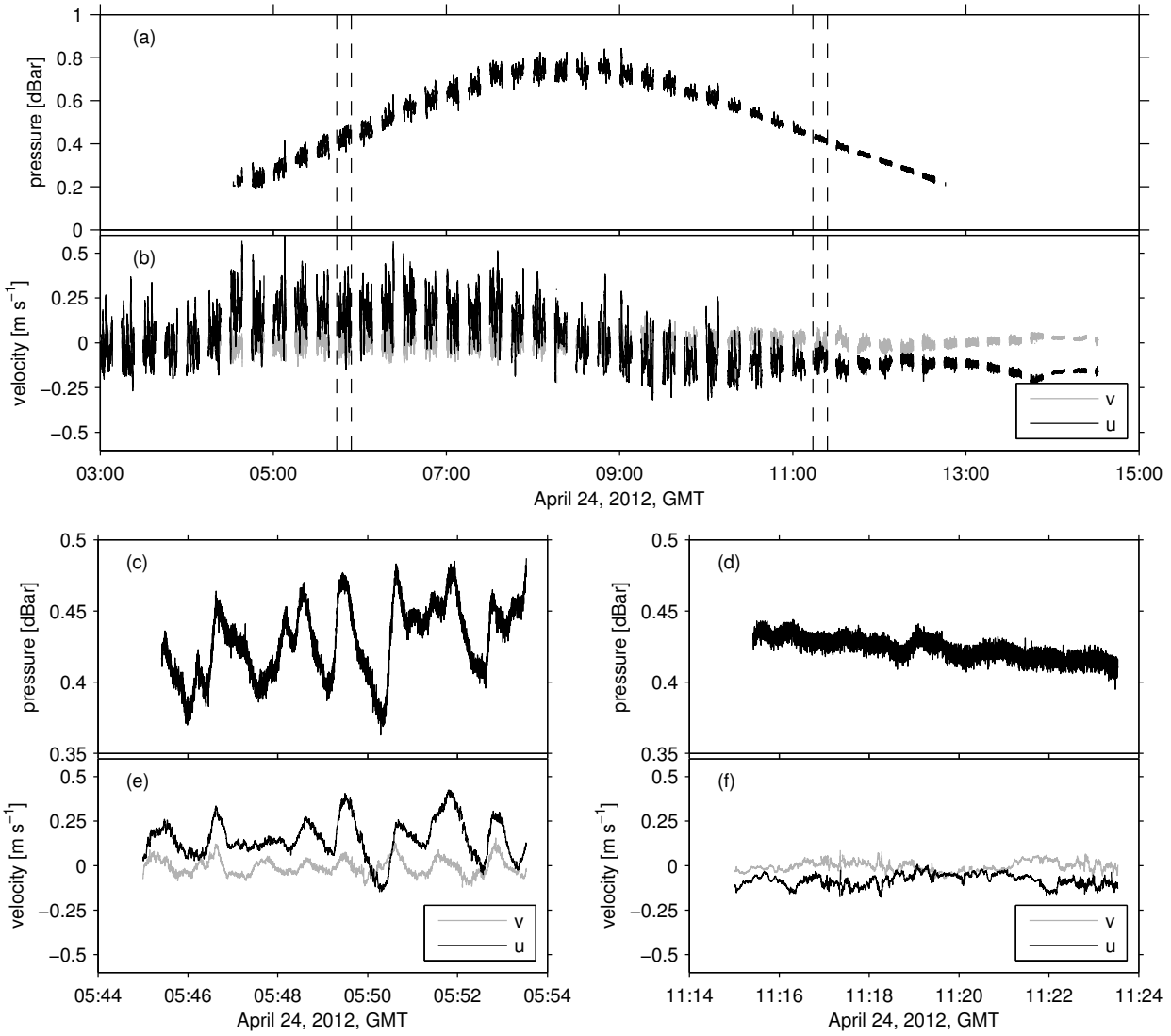

Figure 3.5: Measurements from an ADV measuring 20 cm above the bed at the NM station. (a) is the pressure record and (b) shows u and v components of velocity where u is principle flow determined by the 7.5 day dataset, and v is lateral flow orthogonal to u. The remaining plots (c-f) show two bursts when the tide was flooding (c,e) and ebbing (d,f) at approximately the same water depth. During flood large velocity oscillations occur with the surface motions. On ebb, these wave-like oscillations are cutoff in both pressure and velocity. The first 25 s of each pressure burst has been removed due to apparent aliasing.

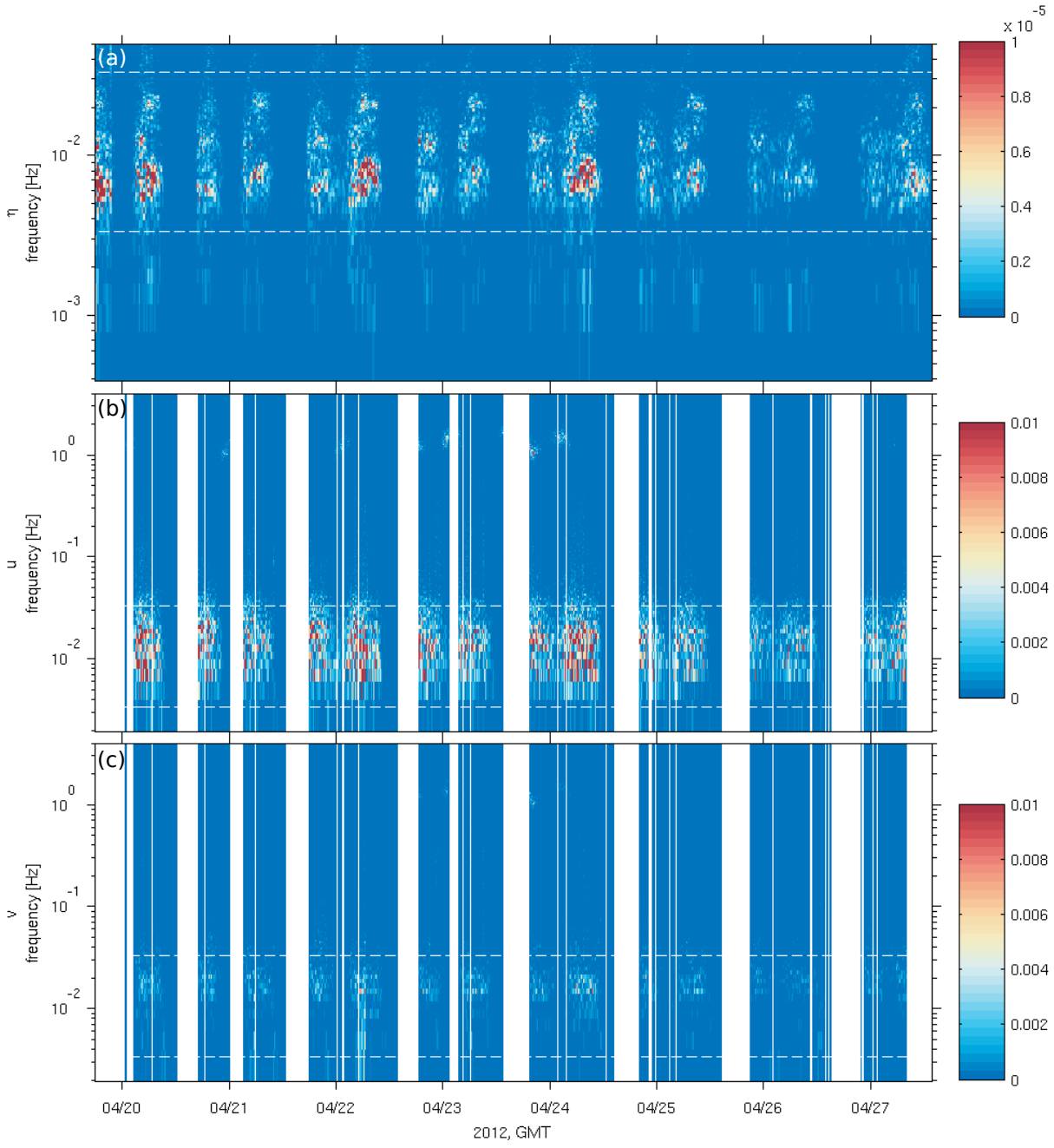

Figure 3.6: Variance preserving spectra of (a) depth (1 Hz CTD measurement), (b) u, and (c) v (8 Hz ADV measurements). Where data exists, spectra are computed on each burst. The white dashed lines indicate the infragravity frequency limits of $\frac{1}{300}$ Hz to $\frac{1}{30}$ Hz. The CTD was always submerged but the ADV came out of the water at some low tides.

Infragravity motions, aside from suggesting that the ocean and nearshore water levels are high enough to maintain a connection with the estuary through the shallow mouth, induce high velocity oscillations. On an incoming tide, infragravity motions in the nearshore cause bores to propagate into and up the estuary, and in phase with these bores are velocity oscillations larger than the tidal velocities (Figure 4c,e). These oscillations are consistent during the nearshore-estuarine connected phase of the tide, only shutting off when the nearshore water level retreats from the mouth (Figure 3.4,3.6).

Gravity waves of a period 1 s to 30 s break in the nearshore and this energy is filtered out by the perched mouth (Figure 3.6). In the small Pescadero estuary, infragravity surface motions were observed at all moorings, and the velocity signature was present at all locations where velocity was measured.

3.3.2 Estuary-nearshore disconnection and frictional control

As the ocean water level falls due to the outgoing tide, the estuarine water level also retreats, but at a much slower rate (Figure 3.4d). The shallow mouth bathymetrically constrains the flow of water out of the estuary, and infragravity motions do not cause sufficient setup in the nearshore to overcome the water level difference and infragravity motions in the estuary are shut off.

Infragravity oscillations persistent on the flood tide are not present at the same estuarine water level on the large ebb (Figure 3.5d,f). The shutdown of these motions occurs both in water level and velocity (Figure 3.6), further indication that the motions are externally forced.

In this state where the estuary is disconnected from nearshore forcing, the depth-averaged tidal velocity is no longer sinusoidal, but has a maximum ebb velocity as the infragravity motions are shutting off (cf 3.4.3) and then slows. The shape of the velocity curve, the change in the rate of estuarine water level fall, and visual observations suggest that the estuary reaches a frictionally controlled state. Similar conditions are observed on tidal flats at low tide (e.g. Ralston et al. 2013). The analytical description of frictionally controlled velocity can be arrived at starting with the incompressible Reynolds-averaged Navier-Stokes (RANS) equations:

$$\begin{aligned} \frac{\partial u_i}{\partial t} + u_j \frac{\partial u_i}{\partial x_j} &= -\frac{1}{\rho_0}\frac{\partial p}{\partial x_i} + \frac{\partial}{\partial x_j}\left(\nu_T \frac{\partial u_i}{\partial x_j}\right) - g\delta_{i3} \\ \frac{\partial u_i}{\partial x_i} &= 0 \end{aligned} \tag{3.1}$$

The x-momentum RANS equation along a bed of slope angle θ is

$$\frac{\partial u}{\partial t} + u\frac{\partial u}{\partial x} + v\frac{\partial u}{\partial y} + w\frac{\partial u}{\partial z} \qquad =$$

$$-\frac{1}{\rho_0}\frac{\partial p}{\partial x} + \frac{\partial}{\partial x}\left(\nu_{_T}\frac{\partial u}{\partial x}\right) + \frac{\partial}{\partial y}\left(\nu_{_T}\frac{\partial u}{\partial y}\right) + \frac{\partial}{\partial z}\left(\nu_{_T}\frac{\partial u}{\partial z}\right) - g\sin\theta, \tag{3.2}$$

where $\nu_{_T}$ is turbulent viscosity. In the frictionally controlled state, the flow is assumed to be fully developed, steady state, two-dimensional, and the water surface slope is assumed to be the same as the bed slope. Using these assumptions, equation 3.2 reduces to:

$$0 = \frac{\partial}{\partial z}\left(\nu_{_T}\frac{\partial u}{\partial z}\right) - g\sin\theta \tag{3.3}$$

Depth-averaging ($\overline{u} = \frac{1}{h}\int_0^h u\mathrm{d}z$) equation 3.3 with bed stress ($\nu_{_T}\frac{\partial u}{\partial z}\Big|_{z=0} = \frac{\tau_b}{\rho}$) and free surface ($\nu_{_T}\frac{\partial u}{\partial z}\Big|_{z=h} = 0$) boundary conditions where τ_b is bed stress and z is positive upward from the bed gives

$$0 = \frac{\tau_b}{h\rho} - g\sin\theta \tag{3.4}$$

Using a friction velocity (u_*) parameterization, $\tau_b = \rho u_*^2$, $u_*^2 = c_{_D}\overline{u}^2$, and the small-angle approximation of $\sin\theta \sim S$, where $c_{_D}$ is a bed drag coefficient that accounts for roughness due to bed material and bed-forms, S is the bed slope, $\overline{u}$ is a depth-averaged velocity gives

$$c_{_D}\overline{u}^2 = gSh \tag{3.5}$$

Given relatively constant values of S and $c_{_D}$, the depth-averaged velocity $\overline{u} \sim h^{\frac{1}{2}}$. This describes the shape of the velocity curve during this frictionally controlled state (Figure 3.4b, 3.8b,d).

3.3.3 Longer term variability

Within the open-mouth estuarine conditions observed during the field experiment, varying wave conditions were experienced and the spring-neap cycle was represented. The effects of this longer term variability is shown to alter the processes occurring on tidal and infragravity timescales.

Tidal timescale processes

General semidiurnal forcing within the Pescadero estuary is due to ocean tides, but even neglecting the long friction ebb, the variation in tidal amplitude within the estuary is highly non-linear and cannot be explained by ocean tidal forcing alone.

The tidal water level variation in the Pescadero estuary is shown to be an attenuated but wave-amplified version of the ocean tides. As observed in other coastal lagoons (e.g.

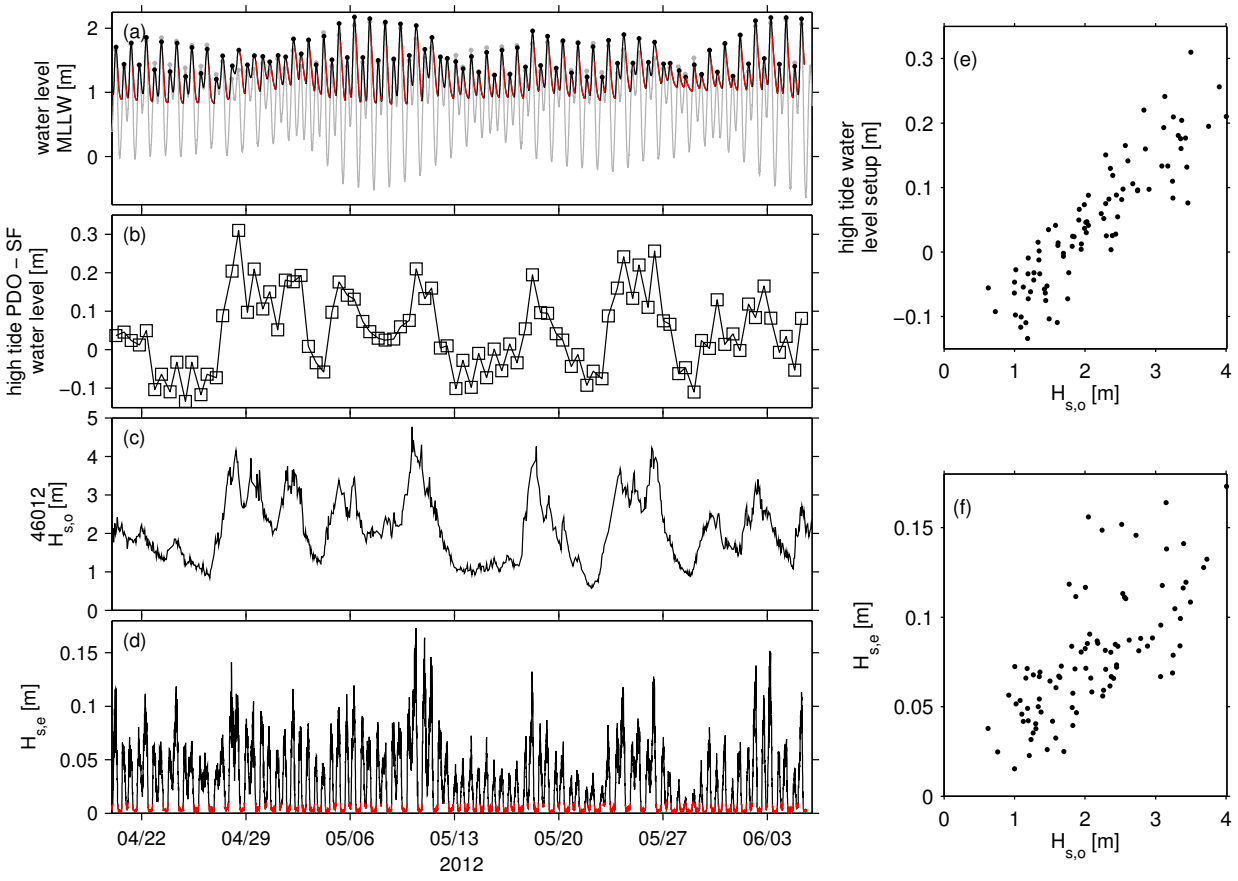

Figure 3.7: The relation between ocean water level and estuarine water level depends on ocean wave conditions for much of the tide. By subtracting the semidiurnal high tide in San Francisco (a, gray line) from the high tide water level in Pescadero (a, black/red line), the resulting setup (b) is in agreement with the size of ocean waves as given by the deep water wave buoy (c). This relationship is illustrated in (e) where figures (b) and (c) are plotted against each other on a time interpolant. An increase of 1 m in ocean waves causes a 10 cm increase in estuarine water level setup within the estuary. The amplitude of estuarine wave height also increases with larger waves (d) with an approximate 3 cm increase in the maximum estuarine wave height for every 1 m increase in ocean significant wave height (f).

Malhadas et al. 2009), larger ocean waves cause setup in the nearshore, resulting in higher tides within the estuary. Subtracting the maximum estuarine water level from the maximum tidal elevation in San Francisco to remove effects of phasing we see linear agreement between significant wave heights in the coastal ocean and increased estuarine sea level (Figure 3.7). During our field measurements, a one meter increase in significant wave height corresponded to a 0.1 m increase in tidal elevation. This relationship seems to hold while the estuary is ocean-forced.

Wave setup should also affect estuarine hydrodynamics at low low tide as the ocean water level where the nearshore and estuary disconnect would be lower. These effects are not separable from effects of erosion and accretion of the bed of the inlet without high resolution surveying data.

Larger waves in the ocean also correspond with larger waves within the estuary. As the ocean significant wave height increases, so does the tidally-modulated estuarine significant wave height (Figure 3.7d). Comparing peak $H_{s,e}$ values to the ocean significant wave height $H_{s,o}$, we see a 1 m increase in ocean waves increases the maximum estuarine significant wave height by 3 cm.

With this alteration of tidal timescale water levels by wave setup, either the duration of high tide or the tidal velocities would have to increase as the amount of water entering and leaving the water increases. Both cases seem to exist in this dataset. The tidal water level on 27 April is distorted in alignment with ocean significant wave heights of 4 m (Figure 3.8a). Here the tidal signal was transitioning into a neap, so velocities and water level should have been decreasing, but water level increased and the tidal velocity was roughly as high as the previous day. A bigger jump in wave setup on 2 May corresponded with an increase in velocities. In general, higher flood velocities occur with higher water levels whether the higher water level is attributed to the spring tides or wave setup.

Over the longer term, the spring tides induce higher tidal velocities than the neap tides (Figure 3.8). Wave shut off occurs consistently on the large ebb of the semidiurnal spring or neap tide (Figure 3.8, red lines). The shape of the depth-averaged velocity with time is consistent with our understanding of frictional control for spring tide conditions (Figure 3.8b,d). During the neap tide, the frictionally dominated velocity-water level relationship of $\overline{u} \sim h^{\frac{1}{2}}$ is not clear.

Infragravity time scale processes

On time scales representative of higher frequency infragravity motions, an increased wave climate in the ocean corresponds to an increased wave climate within the estuary (Figure 3.7d), and corresponding velocity oscillations are greater.

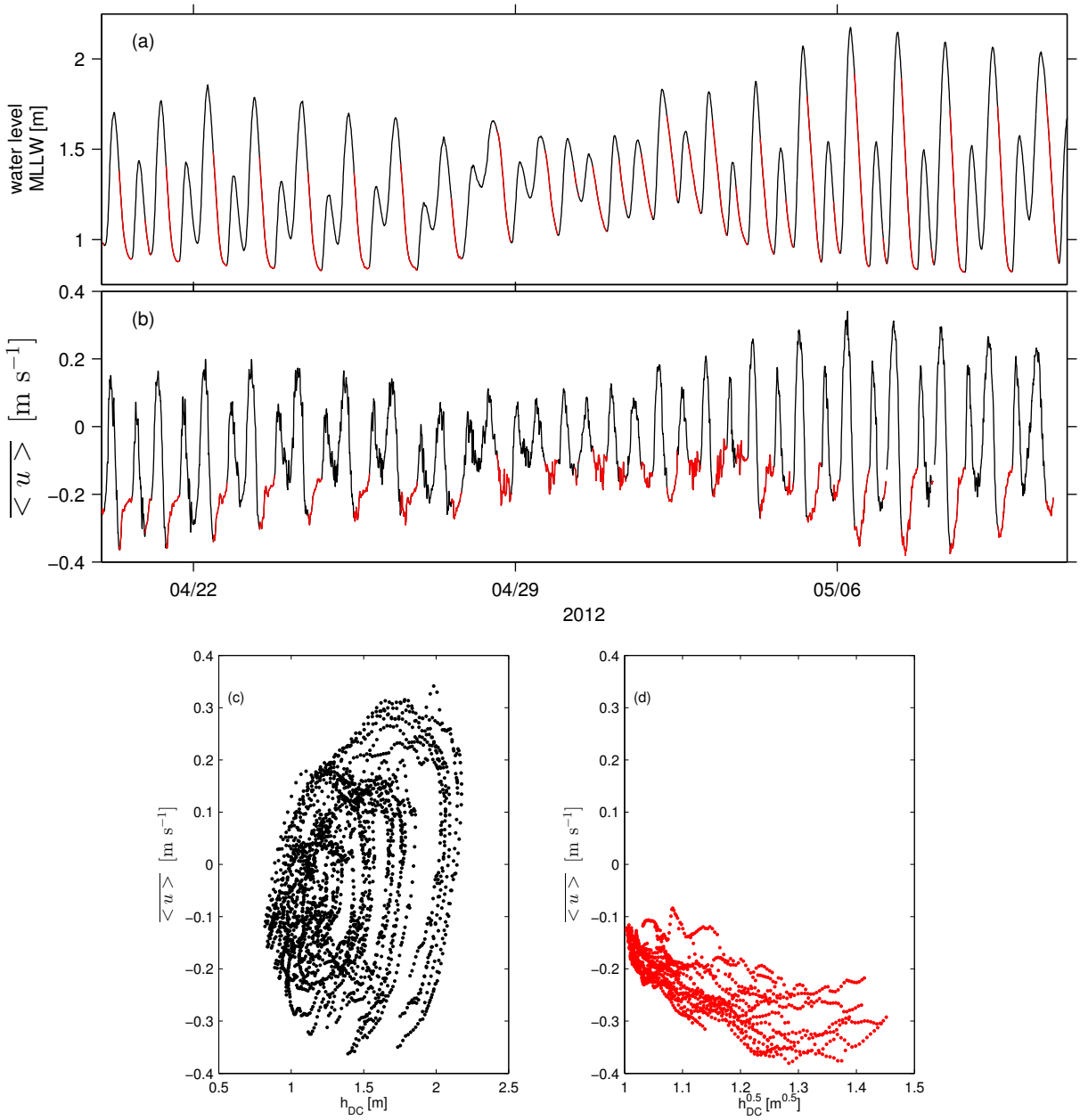

Figure 3.8: The general trend of oscillation between ocean/wave forced and non-wavy persists through the spring-neap cycle, shown by three weeks of estuarine water level (a) and depth-averaged velocity (b) data. Depth and velocity data are plotted against each other in (c) and (d) for the spring tides (28 April to 4 May is excluded). The frictionally controlled regime is clear during the spring by the shape of $\overline{u}$, plotted with $h^{\frac{1}{2}}$ in (d), but with higher low tide during the neap, the ebb may not be long or ocean water level low enough to reach a frictional state.

3.4 Discussion

3.4.1 Frictionally controlled and ocean influenced States

Tidal velocities and water levels in the estuary are driven by the tidal amplitude in the ocean for most of the semidiurnal tide, and then exhibit frictional dependence as the ocean water level retreats below the perched estuarine mouth.

This frictional control period of the tidal cycle is highlighted by the $\overline{u} \sim h^{\frac{1}{2}}$ relationship (Figure 3.8d) and accompanied by the shutoff of infragravity motions. Frictional control may exist in other parts of the shallow estuary, but is visually most pronounced at the mouth. To accurately calculate a coefficient of drag, $c_{_D}$, for the frictionally controlled state, accurate survey data and measurements in the mouth are needed. We can, however, constrain the drag coefficient with some estimations. Assuming the water surface slope matches the bed slope at the mouth and is flat across the the lower estuary and no hydraulic jumps occur between DC and the mouth (Figure 3.3), by conservation of mass at the mouth (subscript m) and DC station (subscript DC),

$$\overline{u}_m = \frac{\overline{u}_{DC} A_{DC}}{h_m A_m}, \tag{3.6}$$

where A is cross-sectional area of the channel. Taking the DC station cross section to be triangular, $A_{DC} = \frac{1}{2} b_{DC} h_{DC}$ where b is the width of the estuarine or inlet cross section, and taking the mouth to be rectangular, $A_m = b_m h_m$. The mouth accretes and erodes regularly, but is based on the depth at NM, we estimate the bed at the mouth to be $h_m = h_{DC} - 0.8$ m. Estimating the bed slope to be S as 0.001 to 0.01 to Characteristic early frictional control values of $\overline{u}_{DC} = -0.3$ m s^{-1} and $h_{DC} = 1.45$ m give a range of $c_{_D}$ from 0.014 to 0.14. Characteristic late frictional control values of $\overline{u}_{DC} = -0.2$ m s^{-1} and $h_{DC} = 1$ m give a range of $c_{_D}$ from 0.002 to 0.02.

A typical value for $c_{_D}$ of a sandy bed is 0.004 (Soulsby 1983) and this value has been observationally recorded in inlets to tidal lagoons (Rydberg and Wickbom 1996). Bedforms at the mouth of the Pescadero estuary probably increase the drag above $c_{_D} = 0.004$, but do not probably account for the very high drag suggested early in the ebb. The changing drag coefficient may be a function of several factors: (1) sediment transport at the mouth creates ripples and waves which are constantly changing, (2) early frictional control may be set by the inlet slope while later the shallow embayment of the estuary may further control the flow, (3) what appears to be frictional control early in the ebb based on the apparent $\overline{u} \sim h^{\frac{1}{2}}$ relationship may actually be a control set by the ocean water level and the water slope may not yet match the bed slope, and (4) these measurements are rough approximations. Surveying and further measurements at the mouth would provide insight into the applicability of the frictional control framework.

This tidal control contrasts with limited tidal amplitudes in other estuaries caused by tidal choking. Bed friction coupled with Bernoulli acceleration explains water level differences between the ocean and lagoon in tidally choked systems (e.g. Rydberg and Wickbom

1996; Hill 1994) based on the formulation $|h_o - h_i| = \left(1 + \frac{c_D BL}{A}\right) \frac{u^2}{2g}$ (Stigebrandt 1980). This formulation expects water surface slope above the inlet to be independent of the bed slope, a condition not observed in the Pescadero estuary on the large ebb. Furthermore, in the Pescadero estuary, a very short channel between the ocean and the estuary limits the frictional effects on the rising tide and slow velocities make the Bernoulli acceleration term very small.

The tidal oscillation between estuarine connection to the nearshore and frictional control exists on a background of wave setup. Under larger wave climates, the transition to frictional control may occur at a slightly higher estuarine water level than the ocean wave climate is smaller, and this we attribute to the influence of wave setup on the lagoon. This setup is likely tidally dependent as seen in coral reef flats (Becker et al. 2014).

3.4.2 Infragravity waves

The presence of infragravity waves in sandy inlets has been previously observed *(Schubert and Bokuniewicz 1991)*, but recently has received renewed attention. Forcing has been measured as currents up to 40 cm s^{-1} in the Ra de Santiuste in Northern Spain (Uncles et al. 2014). Work focused on wave-current interaction in the inlet to the Portuguese Albufeira lagoon noted the presence of velocities on an infragravity timescale equal to 50% of the tidal velocities (Dodet et al. 2013). Elsewhere in California, surface oscillations on an infragravity timescale were observed in the Russian River estuary at a measurement location 2.4 km from the mouth for the two days between the closed inlet opening to the reclosure in early October 2010. Observations 7.4 km from the mouth did not exhibit these oscillations (data not shown). Similar to the tidally discontinuous forcing in the Pescadero estuary, surface oscillations shut off for part of the tidal cycle. The dominant infragravity frequencies were lower in the Russian River estuary than in the Pescadero estuary, probably because the higher frequencies dissipate closer to the mouth as seen in the Pescadero estuary and inferred by the lack of an infragravity signal 7.4 km from the mouth of the Russian River. Given the expected presence of infragravity motions on beaches worldwide (Contardo and Symonds 2013) and given the observed presence of an infragravity signal in sandy inlets and bar-built estuaries, we conclude that this forcing is likely ubiquitous in this type of estuary.

Considering the kinetic energy per unit volume in the water column,

$$KE = \frac{1}{2}\rho(u^2 + v^2), \tag{3.7}$$

infragravity motions are shown to cause bursts of kinetic energy in the Pescadero estuary (calculated from the point ADV measurement, Figure 3.9). In a highly stratified estuary, such as Pescadero, this energy no doubt contributes to mixing the water column thus reducing density stratification. Work to quantify this mixing is ongoing. In small estuaries where residence time during the open state is small or wind-mixing is limited, energetic velocity bursts due to infragravity in the nearshore should be a dominant driver of buoyancy mixing.

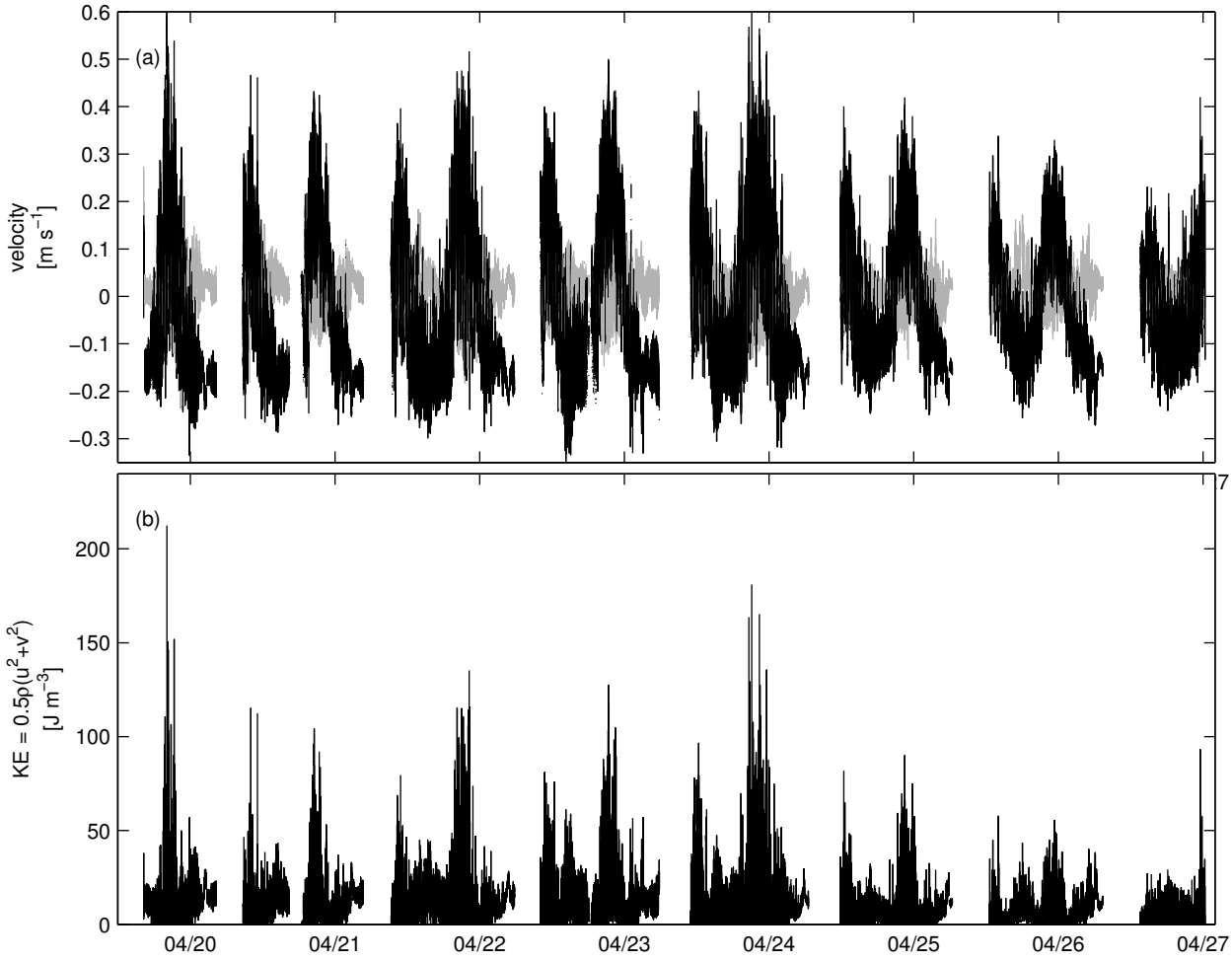

Figure 3.9: Velocity and kinetic energy measurements by the ADV at NM. Principle flow u is depicted in black and lateral flow v is gray in (a), and kinetic energy of both horizontal components of velocity is given in (b).

In larger, density stratified estuaries, such as California's Russian River estuary, these high energy events likely contribute to buoyancy mixing near the mouth, thus setting the salinity of ocean-sourced water being advected upstream where other processes may dominate mixing and transport. In largely marine systems such as the Albufeira lagoon in Portugal where freshwater inflow is low, these high velocities near the mouth will still contribute to mixing, but with no discernible density stratification influence will be limited to biological or geological relevance.

Infragravity motions are seen to be relevant for sediment transport in the surf zone, tidal inlets, and in the closed state of intermittently closed, bar-built estuaries, swash overwash is the mechanism by which the sand berm grows (Beach and Sternberg 1988; Green and MacDonald 2001; Baldock et al. 2008). In the Pescadero estuary, where in the open state velocities attributed to infragravity motions may be three times larger than the tidal velocity, we expect this flow to be responsible for resuspending sediment and dominant in geomorphological change. While the mouth of the Pescadero estuary is closed, swash overwash is observed to occur on infragravity timescales, and this overwash has been seen to raise the water level of the closed lagoon (data not shown), which must be accompanied by geomorphic change as seen in the accretion of sediments at the mouth of other estuaries (Baldock et al. 2008).

3.4.3 Transitions

The two states of nearshore-estuarine connection and frictional control where infragravity oscillations disappear dominate the majority of the tidal cycle in the tidally-discontinuous Pescadero estuary. The transitions between the two states occur rapidly.

We observe the cutting off of wave forcing near peak ebb velocity (Figures 3.4, 3.8). Using the same mass conservation approach as in section 3.4.1, using characteristic early frictional control values of $\overline{u}_{DC} = -0.3$ m s^{-1} and $h_{DC} = 1.45$ m, the estimated Froude number at the estuary mouth,

$$Fr_m = \frac{\overline{u_m}}{\sqrt{g\overline{h_m}}}, \tag{3.8}$$

is $Fr_m = 0.26$, which is subcritical. This suggests that the shut down of wave-like motions in the Pescadero estuary is not due to wave blocking. Late frictional control values of $\overline{u}_{DC} = -0.2$ m s^{-1} and $h_{DC} = 1$ m give a $Fr_m = 0.76$, which remains subcritical but is much higher than the early ebb value. Visual observations of the far ocean end of the inlet suggest that a further narrowing of the inlet at low tide may accelerate flows and create super critical flow. Sand waves also form making it difficult to distinguish hydraulic jumps from flow over a wavy bed. Rapid sediment transport at the inlet prevented us from being able to make accurate measurements there, but future work should attempt to improve our understanding of the downstream control of these estuaries.

As the nearshore environment retreats from the mouth of the estuary, flow out is constrained to a sandy channel. As the ocean water level rises and nearshore-estuarine connec-

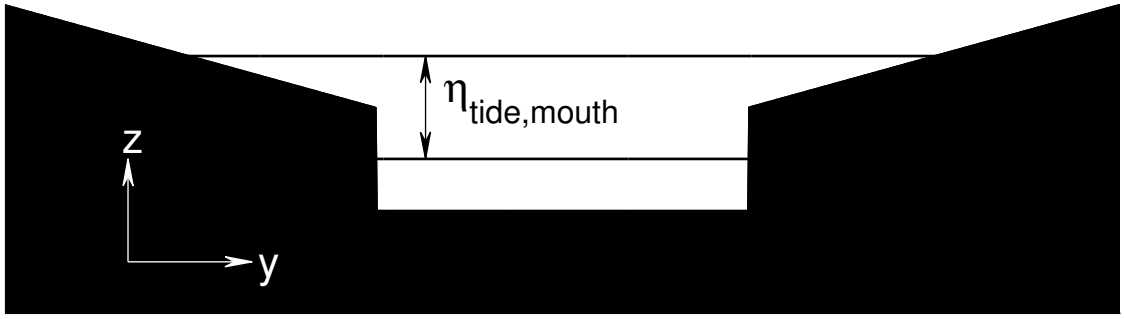

Figure 3.10: At low water, the inlet tends to be channelized and flow is laterally restricted. As the water level increases, flow across the flat beach is possible, introducing further nonlinearities to wave motions.

tion is again established, initial flow remains limited to the narrow channel. Infragravity motions then cause bores to propagate up the channel. As the tide continues to rise, the connection changes as swash spills over the beach (Figure 3.10). Initially bore height and velocity are in phase, but at higher tides more nonlinearities are introduced.

The infragravity motion-induced bores resemble tidal bores seen in some shallow estuaries on coasts with large tidal ranges. Field observations of tidal bores show that undular tidal bores do little to dissipate tidal energy (Wolanski et al. 2004) while breaking tidal bores contribute an energetic burst of turbulent kinetic energy (TKE) (Simpson et al. 2004). The bore structure in the Pescadero estuary as the tide rises is usually undular but has been observed to be breaking when the ocean wave climate is very large.

3.4.4 Salt transport

Description of salinity response in the Pescadero estuary

The salt response to the tidally disconnected forcing should depend on freshwater inflow, size, and shape of the estuary. The response of the salt field in the Pescadero estuary is described here in general terms applicable to other salt stratified bar-built estuaries.

Looking first at salt movement at several snapshots in time in an estuarine cross section, Figure 3.11 (a-f) depicts the salt field in x and z as interpolated with nine CTDs. The location of each instrument is marked with a (+), and the corresponding estuarine water level and depth-averaged velocity are shown (Figure 3.11g,h). Starting with a completely or nearly fresh estuarine basin, at the start of the flood tide ocean water moves upstream with a strong frontal or salt-wedge structure (Figure 3.11a). This salt water moves upstream and establishes strong longitudinal stratification (Figure 3.11b). With tidal flow reversal and in the presence of freshwater flow, the longitudinal stratification relaxes to vertical stratification (Figure 3.11c) and a reversal of the pycnoclines may occur (Figure 3.11d). Salt water continues to be removed from the salt trap through the rest of the ebb (Figure 3.11e).

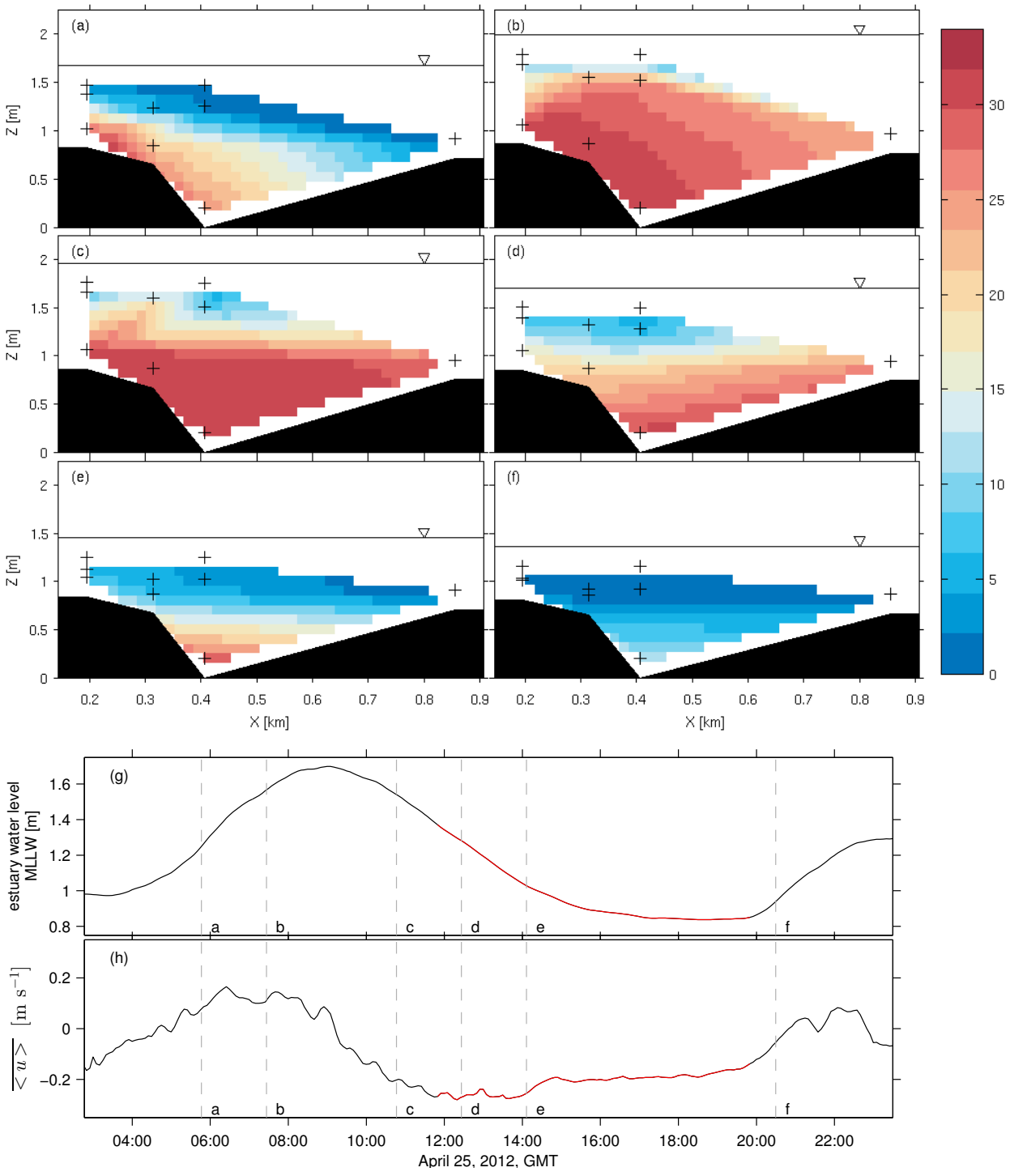

Figure 3.11: Interpolated salt cross-sections of the Pescadero estuary for six different times (a-f) on the tidal cycle, shown in (g,h). Location of CTDs used for interpolation are shown with (+), and x is positive upstream. (g,h) gives the estuarine water level and depth-averaged velocity at DC corresponding to the salt-profiles above.

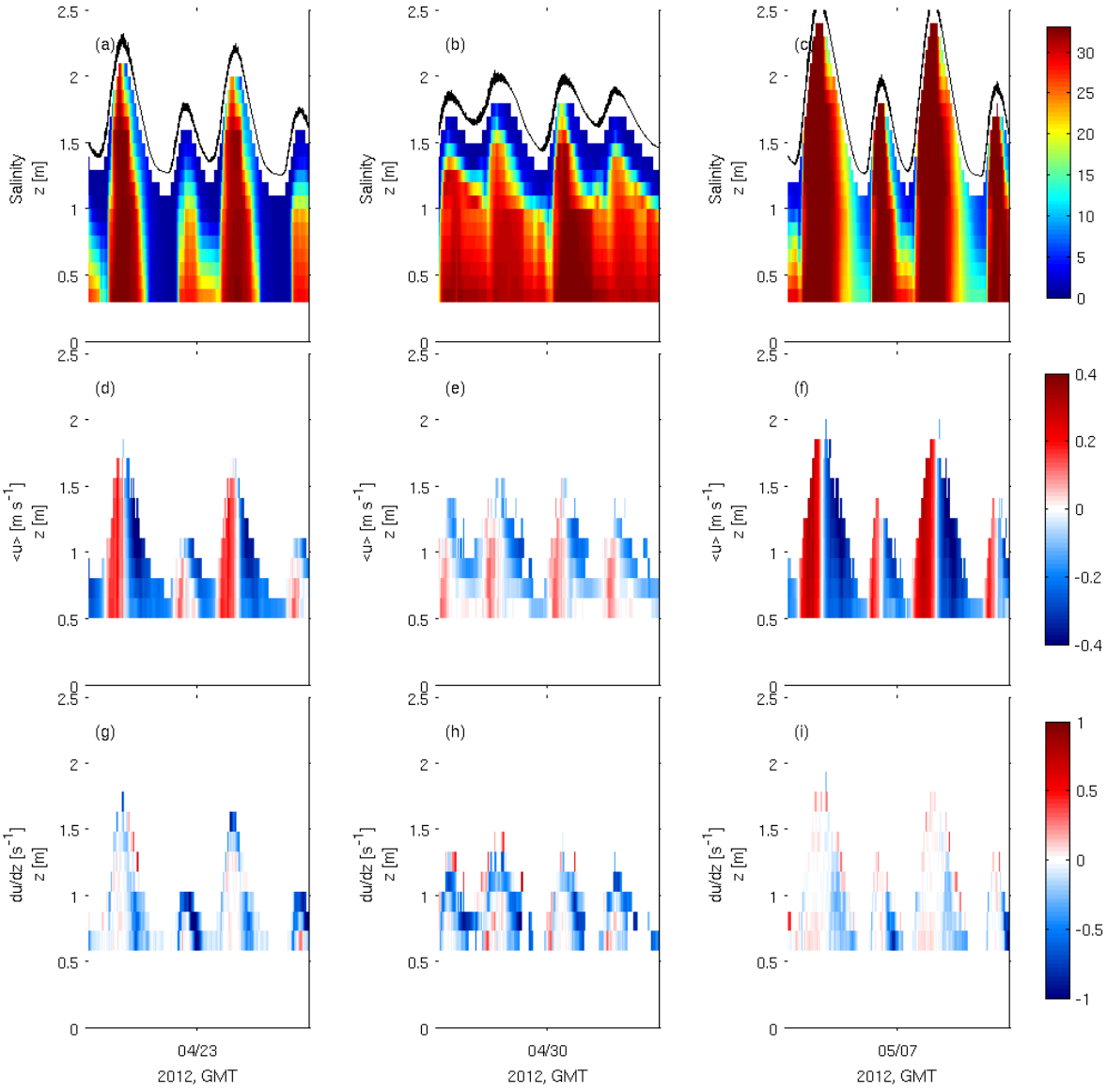

Figure 3.12: Salinity, velocity, and vertical shear with time for three conditions during the field deployment. The first column (a,c,g) shows conditions during a spring tide with higher freshwater flow. The second column (b,e,h) gives neap conditions and an intermediate freshwater flow, and the third column (c,f,i) gives spring conditions for larger spring tides than previously and with less freshwater flow into the estuary.

Figure 3.12 depicts the changing salinity and velocity structure and shear ($\frac{\partial u}{\partial z}$) with time over two tides for spring conditions with substantial freshwater inflow to the estuary (a,d,g), neap tidal conditions (b,e,h) and spring conditions with a larger tidal elevation change and less freshwater (c,f,i).

The velocities are measured in 15 cm bins, with an ADCP blanking distance of 50 cm. In this very shallow flow, dynamics are lost by not measuring the bottom of the water column, but the study was limited by available instruments. Salinity data from four instruments (three instruments in the first period) were interpolated onto a grid. CTDs were spaced unevenly and more concentrated in the upper water column (cf 3.2.2), so we expect there to be unresolved gradients. We expect to see a sharper salinity gradient than appears with our interpolation scheme. However, relevant salt dynamics still are made apparent with this method.

The general structure of salt moving in and out of the estuary follows the tidal velocities. On the large flood, salt is advected upstream. Shear in the water column is low and slightly positive, consistent with unstratified channel flow. In the presence of sufficient freshwater, surface waters at DC only momentarily become saline (Figure 3.12a). The measurement of shear suggests reduced flood velocities occurred at the surface due to outflowing freshwater. Comparatively, in the later spring tide when less freshwater was present, ocean salinity water is present at the surface for a longer duration and evidence of two-layer flow on the flood is absent (Figure 3.12c,f,i).

On the ebb, as seen in Figure 3.11, the water column vertically stratifies. Flow out of the estuary is two layer as evidenced by high negative vertical velocity shear. The mechanism by which salt appears to be removed from deep regions of the estuary is through shear-induced mixing. On the smaller of the semidiurnal ebbs, salt is sometimes retained in the lower reaches of the estuary, and very high shear is observed as the lower water column velocities approach zero.

Smaller tidal amplitudes during the neap tide reduce the tidal velocities throughout the water column. Ocean water is still advected in with a near-ocean salinity on the flood, but slower ebb velocities may prevent a complete flushing of the estuarine salt pockets. Very high shear is observed as lower water is consistently very slow moving, thus we again see the salt pocket being eroded away by shear-induced mixing.

The last time period shown depicts bigger spring tides as well as the beginning of the transition from the wet season to the dry season. Reduced vertical shear on the ebb suggests both advection and shear-induced mixing are responsible for moving salt water downstream. Less freshwater in the system probably reduced stratification, which also could have been influenced by higher mixing with the larger tidal velocities.

In general, over the tidal cycle, salt water moves upstream primarily due to advection, and then removal of salt water from the estuary is by advection and shear-induced mixing. Variation due to tidal amplitudes and freshwater flow alter the specifics of salt dynamics on tidal timescales.

Effects of two-layer flow on frictional control

Two-layer flow seen on the ebb while salt water is trapped at depth and freshwater flows out across it will allow surface waters to flow more quickly than if they were in contact with the rough bed. Given that frictional control is established long after the depth-averaged velocities have become negative (Figure 3.43.8), it is possible that the establishment of frictional control on the water column corresponds to the point at which flow at the mouth and in the shallow region of the estuary is one-layer and the only salt water retained in the system is in the deep salt traps.

Relation to salt transport in other estuaries

Estuaries with a deep inlet do not have a discontinuous connection between the dense ocean and fresh riverine boundaries of the estuary. In these estuaries, buoyancy differences between these boundaries drives gravitational circulation, a constant subtidal exchange (MacCready and Geyer 2010). In the Pescadero estuary where the mouth is set above low water level in the ocean, this continuous exchange flow cannot exist as the dense water source is disconnected daily. Salt transport is then limited to processes on tidal and supratidal timescales.

3.5 Conclusions

We have observed dominant hydrodynamic processes within one California estuary which are likely similar to those present in similar estuaries along the western coast of the Americas as well as in Australia, South Africa, and in estuaries in Mediterranean climates on the Atlantic west coast of Europe, as well as in shallow sandy inlets elsewhere.

We see that in the open state of intermittently open estuaries:

1. The mouth of the estuary may remain perched above low water in the ocean.
2. The perched mouth limits tidal velocities and does not allow ocean gravity waves to enter the estuary while permitting infragravity motions to pass through the inlet.
3. High velocities induced by these infragravity motions are energetically important.
4. On the large ebb the ocean retreats from the mouth, nearshore forcing is cut off, and frictional control describes the velocity.
5. The salt field is tidally advected upstream but disconnects from the ocean and is removed by shear.

This work has highlighted the strong dependence of hydrodynamics of small bar-built estuaries on nearshore processes. Future field observations in these estuaries should include nearshore measurements to better quantify this connection. Previous work has not described the influence of nearshore forcing on estuarine hydrodynamics, thus the oscillation between

nearshore-forced and disconnected has also not been described. Salt movement within the Pescadero estuary reflects similar transport observed elsewhere.

Chapter 4

Estuarine dispersion

4.1 Introduction

Salt transport in small, bar-built estuaries tends to be frontal. Sharp gradients exist between freshwater and salt water, both vertically and horizontally. In the open state of the Pescadero estuary, salt moves in and out as described in chapter 3. This general description treats salt water and freshwater as relatively immiscible, a character deemed untrue by decades of estuarine physics research. Here, salt mixing and dispersion characteristics in small bar-built estuaries are explored.

The common framework for understanding estuarine dispersion has been developed for larger and more well-mixed estuaries. Gravitational circulation - estuarine circulation on subtidal timescales - is driven primarily by the density gradient between ocean water and freshwater, but also includes contributions from wind, the earth's rotation, and inertial and frictional effects (Fischer 1976). This gravitational circulation is the main driver of salt transport in most large estuaries, and dispersion in this case is by vertical shear on subtidal timescales.

On shorter timescales, vertical and lateral shear flow in estuaries is created by friction at the bed or channel edges, and the effect of salinity gradients may alter the shear flow. In estuaries, lateral shear dispersion is typically the dominant dispersion mechanism on tidal timescales (Fischer et al. 1979). As described in chapter 3, the open state tidal forcing in the Pescadero estuary is discontinuous. At low low tide in the ocean, the estuary becomes a draining reservoir as the ocean water level retreats below the mouth. This feature cuts off the open boundaries necessary for density-driven exchange flow, and thus we expect no subtidal currents to exist and the focus must be on tidal timescale processes.

In estuaries with peripheral channels or margins, tidal trapping increases longitudinal dispersion processes. The balance between momentum and friction differs in the main channel of an estuary compared to side channels and embayments and allows for trapping. Okubo (1973) modeled this as a diffusive process where the presence of traps increases dispersion via Fickian diffusion. The approach is intended to be valid over many tidal cycles. Missing

from Okubo's analysis is the possibility that the changing friction/momentum balance in channels with branches and shallow periphery could be an advective process. MacVean and Stacey (2011) addressed this limitation with a new formulation of dispersion due to tidal trapping where the periphery is allowed to empty and fill on tidal timescales.

Salt is a conservative tracer, making transport and mixing of salinity a quantifiable term, and the tracer a popular one in understanding estuarine dynamics. Monismith et al. (2002) examined the salinity structure with time in Northern San Francisco Bay to understand the intrusion of salinity in relation to freshwater flow important to the Sacramento-San Joaquin delta ecosystem and the municipal drinking water supply. They found the longitudinal dispersion, K_x, to be dependent on freshwater flow rate and location in the estuary, and varying from under 10^1 m^2 s^{-1} to over 10^3 m^2 s^{-1}. Lerczak et al. (2006) examined salinity dispersion in the Hudson River, and found it to be driven by vertical shear dispersion induced by gravitation circulation, with values of K_x up to 2500 m^2 s^{-1}. Implications of salinity transport and mixing can help to characterize similar effects on other terms such as nutrients, temperature, plankton, or suspended sediment.

Here, we will transform the complexities of the Pescadero estuary into a one-dimensional system in order to calculate dispersion of salt to understand mixing and dispersion characteristics of the estuary. This framework allows comparison to other estuaries.

4.2 Methods

4.2.1 One-dimensional advection-diffusion equation

We start with the one-dimensional depth-averaged advection-diffusion of salinity,

$$\frac{\partial S}{\partial t} + U\frac{\partial S}{\partial x} = K_x \frac{\partial^2 S}{\partial x^2} \tag{4.1}$$

where S is salinity, U is depth-averaged velocity, and K_x is the longitudinal dispersion coefficient. The K_x in this form is independent of space ($K_x \neq f(x)$). In an estuary, the salt structure is advected upstream and downstream with the tides. By moving the frame of reference along with these tides, the velocity term drops out (U=0) equation 4.1 becomes

$$\frac{\partial S}{\partial t} = K_x \frac{\partial^2 S}{\partial x^2} \tag{4.2}$$

Assuming salinity follows a step function at time $t = 0$ and that the boundaries of the system remain at ocean salinity, $S = S_0$ and freshwater salinity $S = 0$, an analytical solution to equation 4.2 can be obtained,

$$S(x,t) = \frac{S_0}{2}\left(1 - erf\left(\frac{x - x_c}{\sqrt{4K_x t}}\right)\right) \tag{4.3}$$

where x_c is the center of the salt front. This solution describes the relaxation of the salt field to be a function of time and dispersion, and predicts a form shown in figure 4.1. Using

observations of the salinity field, the value of K_x can be obtained from this analytical solution. Here the spatially independent K_x is also assumed to be invariant in time ($K_x \neq f(x,t)$).

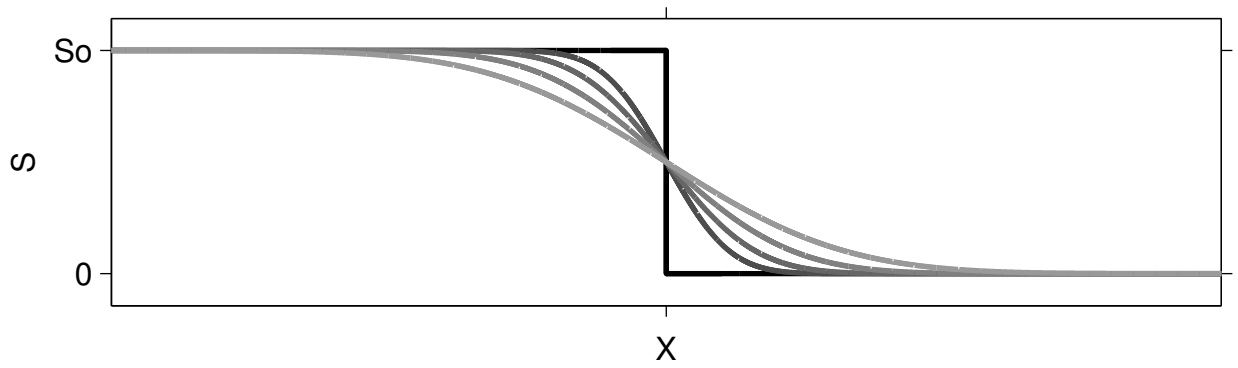

Figure 4.1: Equation 4.3 starts from a step function and smooths over time. In this graphic, the line grows lighter with increasing time.

Ralston and Stacey (2005) applied a similar one-dimensional framework to observations of frontal mixing of salt within the intertidal zone of mudflats in Northern San Francisco Bay. There they found $K_x = 10$ m^2 s^{-1} due to the combination of vertical shear dispersion on stratified ebbs and lateral shear dispersion from the interaction of flow over shallow mudflats and a deeper channel.

4.2.2 Using observations in an analytical framework

To solve for K_x in equation 4.3, the salinity structure in time and space within an estuary must be known. Salinity measurements were made in the Pescadero estuary with good temporal resolution and some longitudinal distribution during an April - June 2012 field campaign. However, longitudinal salinity gradients in the Pescadero estuary as well as in other small bar-built estuaries are very sharp, so locating instruments close enough to each other to directly measure the longitudinal gradient and getting spatial coverage to understand dynamics of a whole system would be nearly impossible. Therefore, we resort to recreating the salinity structure in time using measurements from a collocated ADV and CTD.

The sensors give a time series of salinity and velocity (0.3 m above the bed at NM, figure 4.2). Velocity is the rate of change of distance with time,

$$U = \frac{dx}{dt} \tag{4.4}$$

$$\tag{4.5}$$

so integrating velocity,

$$\int U dt = \int dx = X \tag{4.6}$$

transforms the time series of point measurements of velocity and salinity (Figure 4.2) into a spatial representation of salinity ($S(x)$, Figure 4.3). This transformation assumes pure advection past the sensors.

4.2.3 Data processing

To make this dataset, velocity measurements were burst-averaged (the instruments collected data for 512 s out of every 900 s) and an 800 s moving average was applied to the CTD measurements. Averaging was intended to remove the infragravity oscillation component of velocity and salinity measurements to focus on tidal processes. Velocity measurements in earth coordinates (East velocity, North velocity) were then rotated into the direction of principle flow (or maximum variance).

To get K_x from the recreated *S(x)*, equation 4.3 is rearranged into the linear form:

$$erf^{-1}\left(1-\frac{2S}{S_0}\right)=\frac{x-x_c}{\sqrt{4K_xt}} \tag{4.7}$$

and a linear fit ($y = ax + b$ where a $= \frac{1}{\sqrt{4K_xt}}$ and b $= \frac{-x_c}{\sqrt{4K_xt}}$) is applied. Given a linear regression fit value for a, to solve for K_x, a value of t must be determined. In this case it is appropriate to use the time between when the front floods past the sensors and subsequent ebb of said front following an isopycnal ($t_{isopycnal}$). This method assumes an infinitely sharp front at time t_0 (Figure 4.1). Setting t_0 as the time at which the front floods past the sensors will overestimate K_x. Thus, an estimation on the initial time from a sharp front to the flood front is made. By setting a step function at the mouth, and approximating advection velocities U = 0.1 m s^{-1} and a length from the ocean to NM of 100 m, initial time, t$_0$ is 1000 s. This time is then added to the time between a selected isopycnal passing by the sensor, $t = t_{isopycnal} + t_0$. Specific considerations in selecting the isopycnal to follow, and influence of t_0 will be discussed in section 4.6. A value for S_0 is also necessary, and here we have used S_0=33.5.

4.3 Observations

Time series of collocated velocity and salinity measurements at NM are shown in figure 4.2. Gaps in measured data occur when the water level is very low and sensors were out of the water. In response to coastal California's mixed semidiurnal tide, the time series shows that salt water does not remain in the system on the low high tide as long as it does on the high high tide suggesting limited tidal excursion of the salt field. Here we focus only on the tidal cycle associated with high high water level, referred to in this test as the "large tide."

The time series plots of salinity and velocity (Figure 4.2) show that the transition from fresh to ocean salinity water occurs rapidly on the flood and the return to fresh water on ebb is a longer duration process. Also, the ebb salinity field passes the sensors in two distinct segments with a transition on each apparent on each large ebb between 10 and 15 PSU.

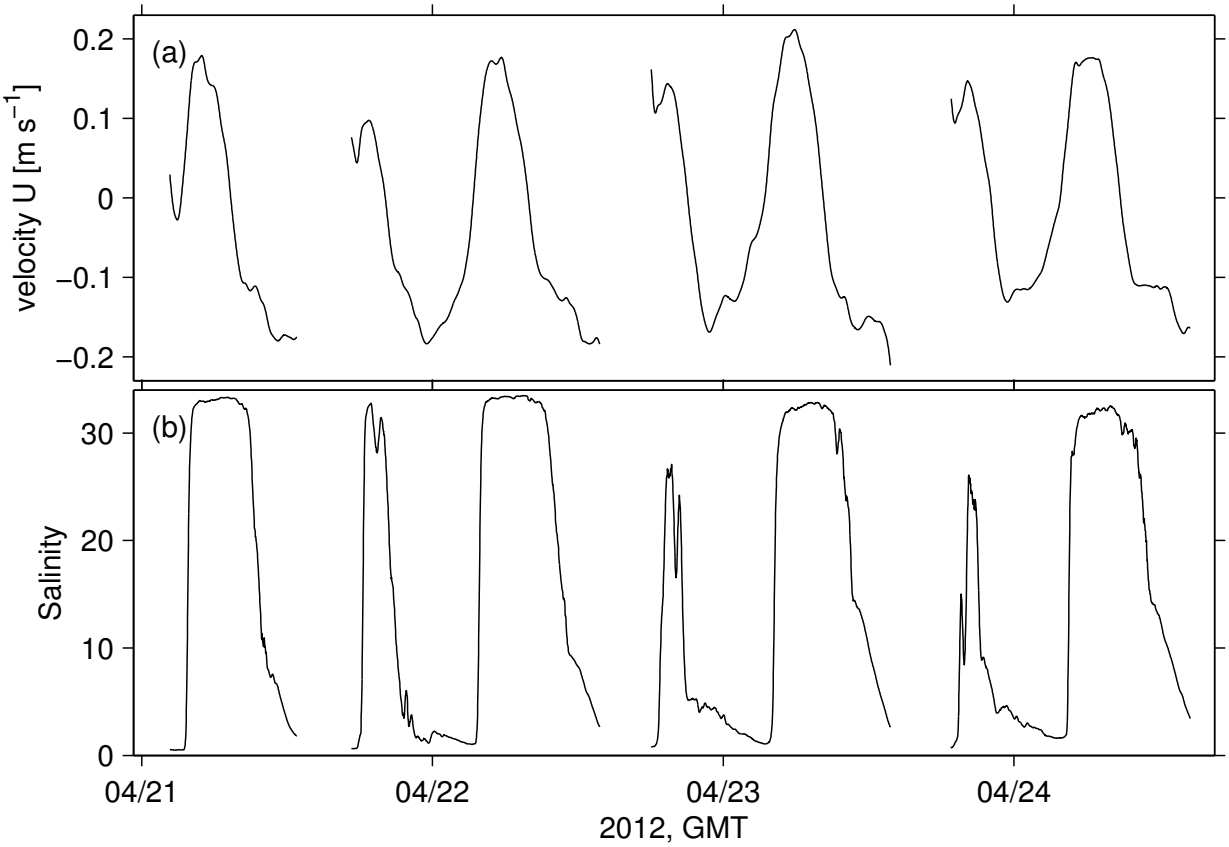

Figure 4.2: Velocity (a) and salinity (b) records 30 cm above the bed at station NM. Velocity measurements have been averaged across their 512 s burst and rotated into the direction of principle flow. An 800 s moving average has been applied to salinity measurements. Averaging was done to remove higher frequency oscillations.

The flood salinities do not exhibit this feature. To investigate whether this observation is an actual transition in salinity and not just a reduction in water velocity, as well as to approach a quantification of K_x, the time series is transformed into a spatial record as described in section 4.2.

Figure 4.3 shows the salt front on flood (a) and on ebb (b) for the four large tides on 21 - 25 April, 2012. Spatial mapping of the salinity field shows that the estuary transforms the salinity front from a smooth, sharp structure on flood to a two-part relaxed structure on ebb, where $S(x)$ is much more relaxed among lower salinities than among higher salinities. This mirrors the time series salinity and implies that there is a physical change in the salt field between flood and ebb. This non uniform structure requires the calculation of two different values of K_x for the higher and lower salinities.

By fitting the error function curve to the two ebb salinity fields determined by the salinity of the transition point (S_T), values of K_x are thus calculated for the higher ($K_{x,S_T \to S_0}$) and

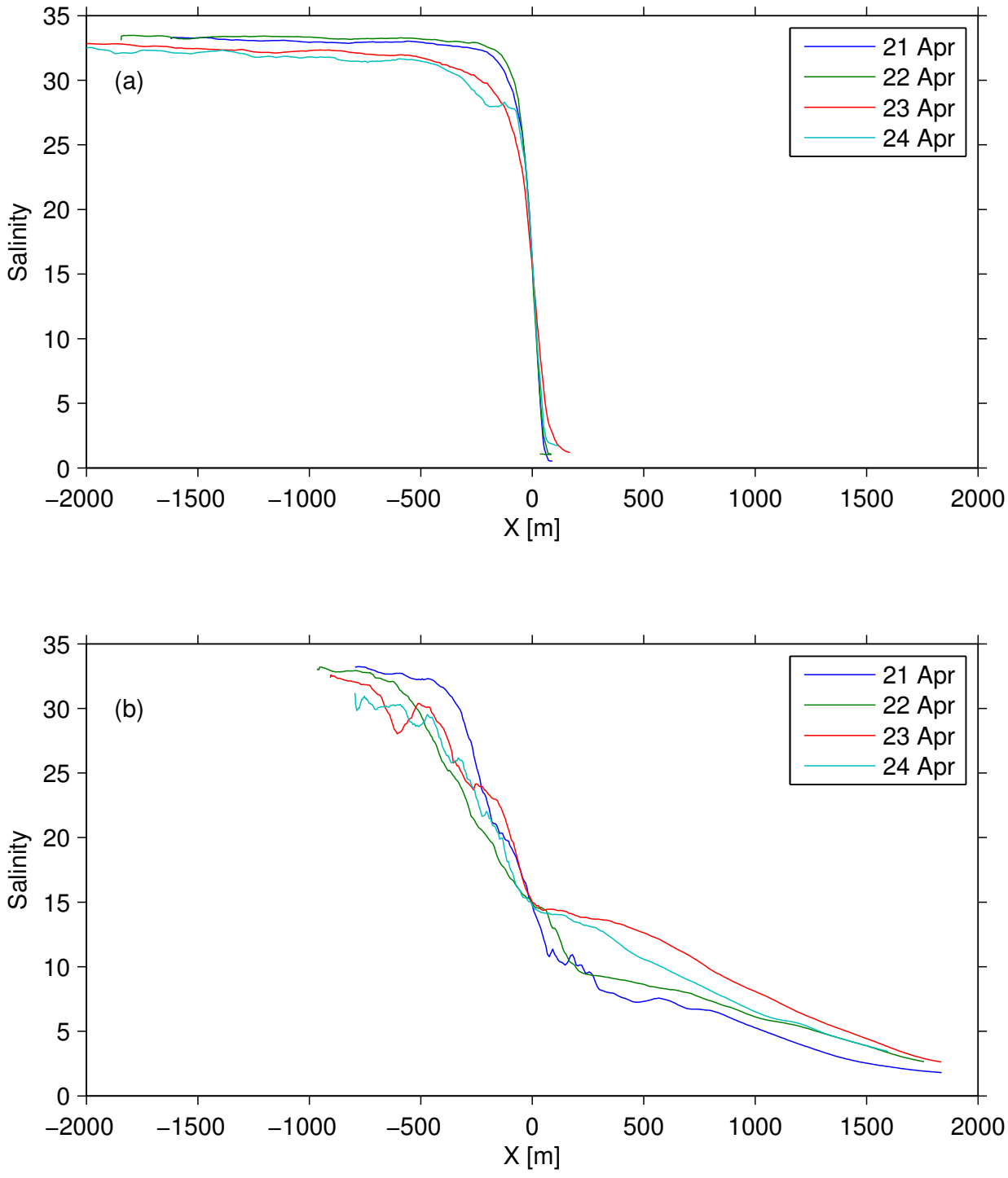

Figure 4.3: The spatially reconstructed salinity field, S(x), for four floods (a) and four ebbs (b) at NM, 30 cm above the bed. In both figures, the profiles are centered (x=0) around the S = 15 PSU pycnocline.

lower salinities ($K_{x,0\rightarrow S_T}$) in the four tidal cycles (Table 4.1 and Figures 4.4- 4.7). Averaged across the four days, $K_x = 4.1$ m^{2}s^{-1} at higher salinity and $K_x = 45.4$ m^{2}s^{-1} at lower salinity. Values of t for K_x calculations are taken to be the time between when the 8 PSU and 20 PSU isopycnals flood and ebb past the sensor for lower and higher salinity K_x values, respectively.

Dispersion is shown to be much greater at lower salinities than at higher salinities in the Pescadero estuary which is reflected in the more relaxed $S(x)$ curves from $S = 0 to S_T$. Values of K_x are an order of magnitude higher in lower salinities than in higher salinities. Dispersion coefficients in lower salinity water ($K_{x,S=0\rightarrow S_T}$), are higher in the first two days than in the last two. Dispersion coefficients in higher salinity water ($K_{x,S=S_T\rightarrow S_0}$) are lower in the first two days than in the second two days.

Date	S_T	$K_{x,S=0\rightarrow S_T}$	$K_{x,S=S_T\rightarrow S_0}$	$t_{S=0\rightarrow S_T}$	$t_{S=S_T\rightarrow S_0}$
21 Apr	11.5	44.9 m^{2}s^{-1}	2.2 m^{2}s^{-1}	2.1×10^4 s	2.5×10^4 s
22 Apr	10.5	55.6 m^{2}s^{-1}	2.9 m^{2}s^{-1}	2.4×10^4 s	3.1×10^4 s
23 Apr	14.4	28.3 m^{2}s^{-1}	5.0 m^{2}s^{-1}	2.3×10^4 s	3.1×10^4 s
24 Apr	14.1	28.7 m^{2}s^{-1}	5.7 m^{2}s^{-1}	2.4×10^4 s	3.2×10^4 s

Table 4.1: Values of K_x for the large flood and ebb on four days in April 2012, and corresponding salinity transition (S_T), and time used for the calculation (t).

Comparison to theory, hypothesized mechanisms of dispersion, reasons for the two-phase structure of *S(x)*, and changes with physical forcing are discussed below.

4.4 Comparison to theoretical estimations of K_x

Longitudinal dispersion caused by vertical shear in an unstratified open channel was found by Elder (1959) to be

$$K_x = 5.93 h u_* \tag{4.8}$$

where h is the height of the water column and u_* is the shear velocity defined by $u_* = \sqrt{\tau_0/\rho}$, τ_0 is a bed stress and ρ is water density. The friction velocity is parameterized by a bed drag coefficient, $c_{_D}$, as $u_* = c_{_D}^{1/2} U$. In the Pescadero estuary, h ranges from 0.2 m to 2.7 m depending on location in the estuary and tidal conditions, U can be $\pm$ 0.4 m s^{-1} with spring tides, and surges due to infragravity motions may result in positive velocities of 0.6 m s^{-1}. Estimating c_D as 0.01, the largest K_x by this formulation would be $K_x = 0.96$ m^2 s^{-1} using the maximum value of h and the infragravity velocity of $U = 0.6$ m s^{-1}. Values appropriate to this dataset of $h = 1m$ and $U = 0.2$ m s^{-1} result an estimated $K_x = 0.12$ m^2 s^{-1}. In either case, this value of K_x is well below observations, suggesting dispersion by vertical shear is a small contributor to dynamics of salt in the estuary.

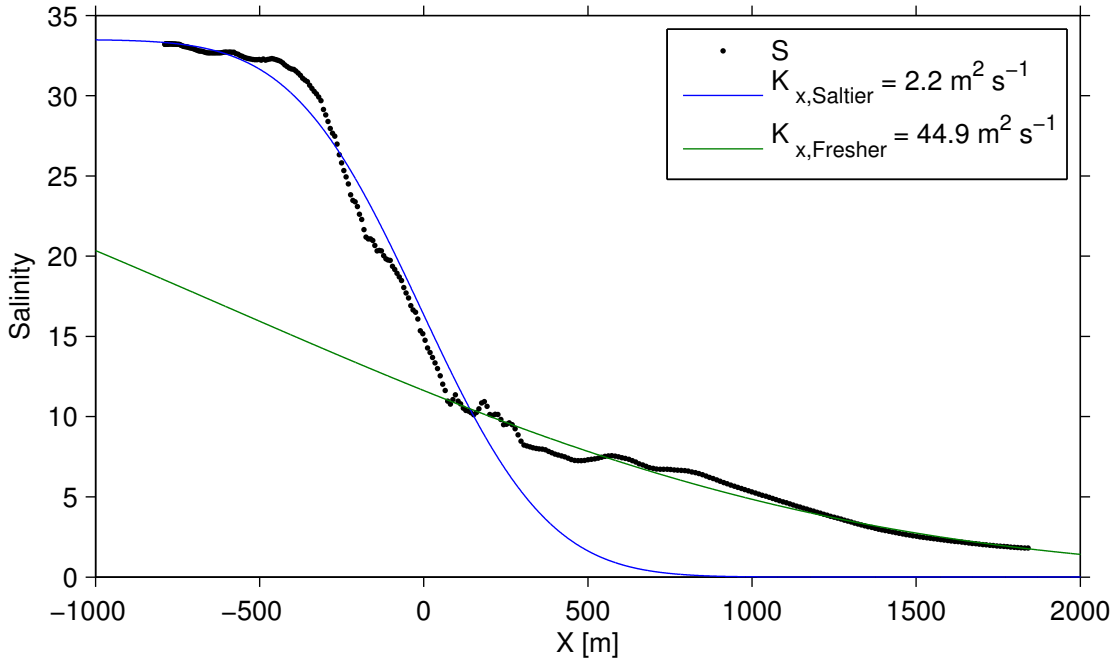

Figure 4.4: Spatially reconstructed salinity field, $S(x)$, and K_x values for the large tidal cycle on 21 April, 2012.

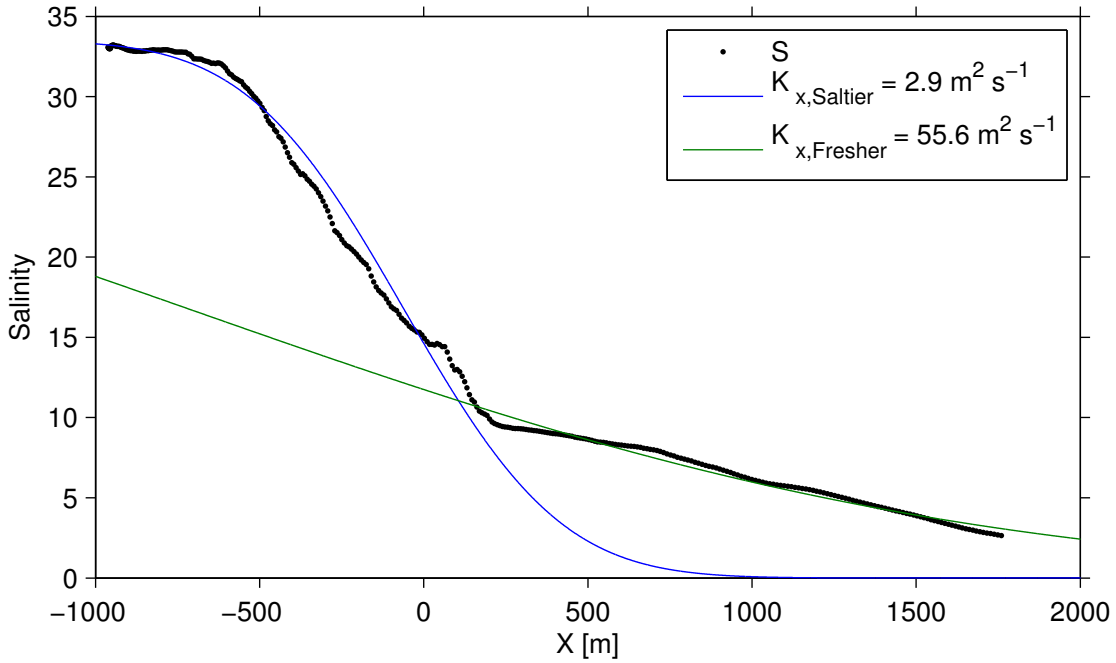

Figure 4.5: Spatially reconstructed salinity field, $S(x)$, and K_x values for the large tidal cycle on 22 April, 2012.

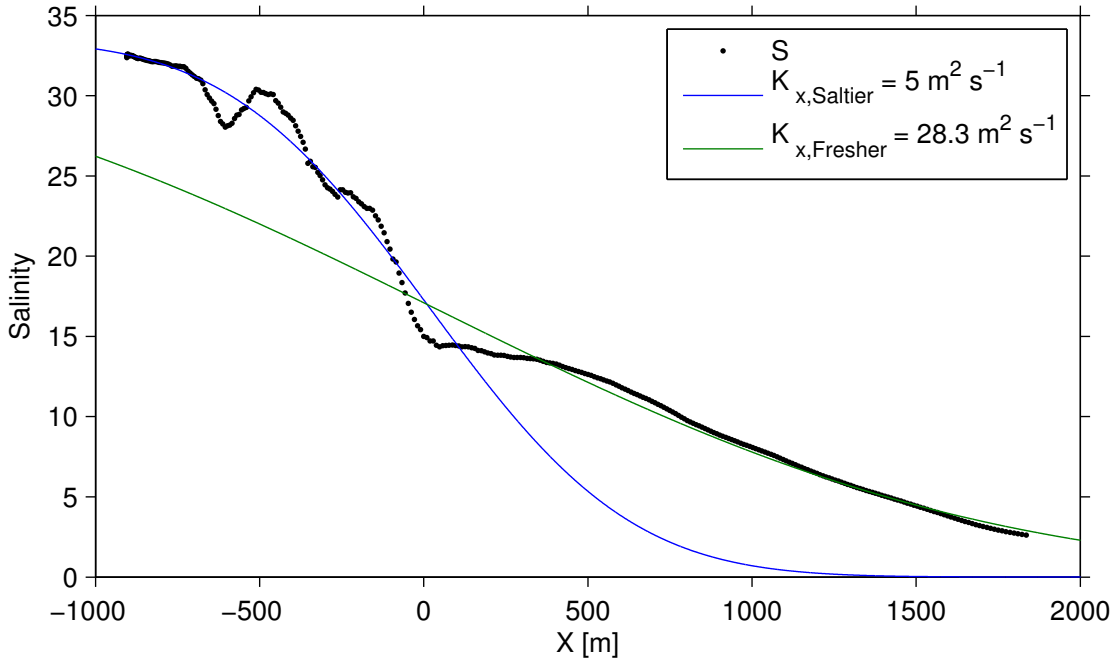

Figure 4.6: Spatially reconstructed salinity field, $S(x)$, and K_x values for the large tidal cycle on 23 April, 2012.

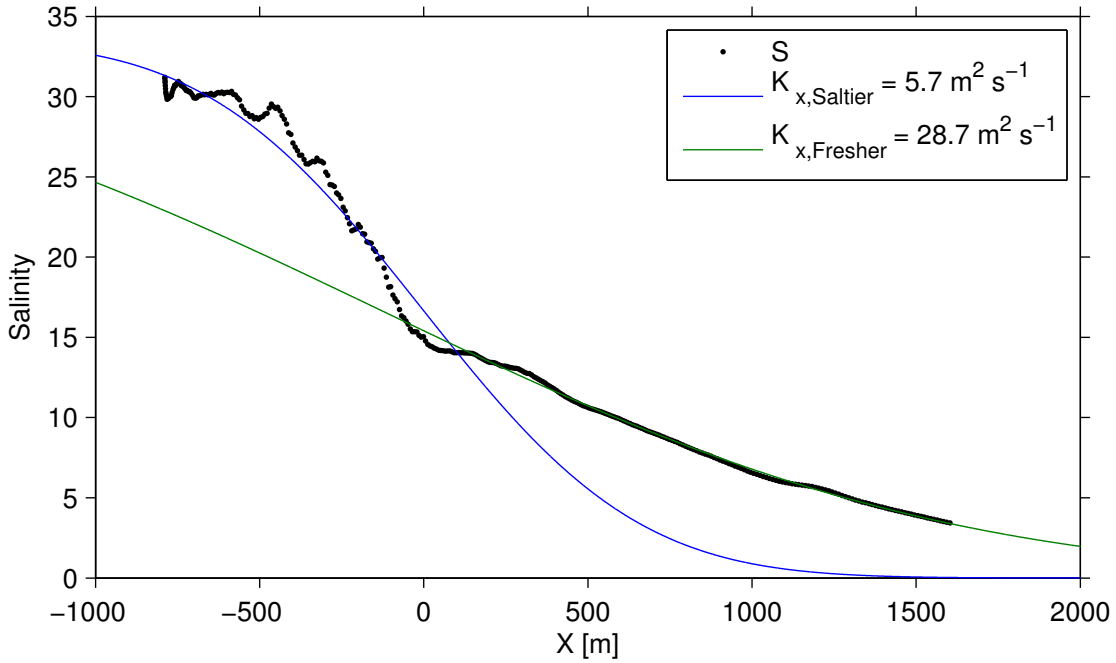

Figure 4.7: Spatially reconstructed salinity field, $S(x)$, and K_x values for the large tidal cycle on 24 April, 2012.

Lateral shear dispersion tends to dominate over vertical shear dispersion in most estuaries that are not very very wide. In rivers, lateral shear is time invariant, but in estuaries the oscillatory flow may partially reverse the dispersion. Whether this is the case depends on a timescale of lateral mixing. Fischer et al. (1979) gives longitudinal dispersion by lateral shear to be

$$K_x = 0.1\overline{u'^2}T\left[\frac{1}{T'}f(T')\right] \tag{4.9}$$

where T is the tidal period, u' is the velocity deviation from a cross-sectional average, parameterized as $\overline{u'^2} = 0.2U^2$, and $T' = T/T_c$, a ratio of the tidal period to time for complete lateral mixing, T_c. Following the method described by Fischer et al., the timescale for cross-sectional mixing is a scaling of the estuary width, W by the lateral dispersion term, K_y,

$$T_c = W^2/K_y \tag{4.10}$$

and the lateral dispersion is scaled as $K_y = 0.6u_*h$. The quantity, $\left[\frac{1}{T'}f(T')\right]$ scales with T' up to a maximum of 0.8 (see Fischer et al. 1979, section 7.2).

Using the values of U, h from the vertical shear dispersion estimate above, an approximate estuary width of $W = 60$m, and setting T equal to $t_{isopycnal}$, the value $\left[\frac{1}{T'}f(T')\right]$ is found to be between 0.18 and 0.23 because the lateral mixing time is an order of magnitude higher that the time that salt is retained in the Pescadero estuary for one tidal cycle. Characteristic times, $t_{isopycnal} = 2 \times 10^4$s to 3×10^4s (Table 4.1) give a range of lateral shear dispersion coefficients of 2.9m^2 s^{-1} for higher salinity water to 5.2 m^2 s^{-1} for lower salinity water which spends more time in the estuary.

Though these calculations of longitudinal dispersion by lateral shear rely on a lot of approximations, they do suggest two things: (1) at lower salinities, lateral shear dispersion alone cannot cause the dispersion observed, and (2) at high salinities, lateral shear dispersion may account for dispersion observed. Though a difference in the longitudinal dispersion coefficient between higher and lower salinities is calculated, this difference is based on time and should steadily increase moving from low salinity to high salinity. The jump in dispersion coefficients observed in our data must be due to another mechanism.

Looking for mechanisms which disperse low salinity water, and by the assumption that the low salinity water is either near the surface or at the upstream edge of the estuary, we look to other dispersion processes that may be active in those regions. The marsh and branching channels of the upper Pescadero estuary should induce dispersion via tidal trapping. Okubo (1973) solved for the dispersive effects of tidal trapping by considering it to be a diffusive flux, having the form in oscillatory tidal flow of

$$K_x = \frac{K'}{1+r} + \frac{ru_0^2}{2k(1+r)^2(1+r+\omega/k)} \tag{4.11}$$

as reported in Fischer et al. (1979). K' is the longitudinal dispersion coefficient in the main channel, r is the volume ratio of traps to channel, $\omega = 2\pi/T$, and k^{-1} is a characteristic

time for exchange between the traps and the main volume. Approximating $r = 0.5$, $u_0 = U$, using $T = t_{0\to S_T} \approx 3 \times 10^4$ s, and $k^{-1} \approx 2 \times 10^4$ s (an estimation based on tidal height above a threshold),

$$K_x = \frac{2}{3}K' + 15.6\mathrm{m}^2\mathrm{s}^{-1} \tag{4.12}$$

showing that tidal trapping can greatly increase longitudinal dispersion, and is the likely mechanism for the high dispersion coefficient calculated for lower salinity waters in the Pescadero estuary. Roughly speaking, the second term on the right in equation 4.11 is the increase of dispersion due to tidal trapping.

This equation is somewhat problematic for use in the Pescadero estuary because tidal trapping as a diffusive term should be over many tides, and we observe the system to reset on tidal timescales. What it does imply, however, is that tidal trapping can greatly increase longitudinal dispersion within an estuary. A more appropriate calculation may be that provided in MacVean and Stacey (2011). Their formulation still quantifies dispersion over many tides, but as an advective process. A better understanding of where advective trapping occurs and measurements that do not exist for this dataset would be required to apply their method to this system.

4.5 Discussion

Spatial mapping of the salinity field from time series of velocity relies on the assumption of pure advection ($X = \int U dt$). This allows a simple parametrization of salinity mixing for the entire estuary. This method lacks the ability to inform where mixing is occurring, whether it is a continuous process or controlled by a bathymetric feature elsewhere in the estuary. An informed understanding of the Pescadero estuary and measurements elsewhere in the estuary help to shed light on the likely mechanisms of salinity dispersion.

4.5.1 Why this two-part structure?

Calculation of K_x shows that at higher salinities (S_T to S_0) dispersion is an order of magnitude less than dispersion in lower salinities (0 to S_T). There are two ways to think of salinity dependent mixing: as a longitudinal or a vertical process. In most larger estuaries, net salt transport occurs on subtidal timescales. In small bar-built estuaries, tidally discontinuous ocean forcing (cf chapter 3) and short residence times allow the estuary to reset as fresh on a tidal or daily timescale, thus eliminating subtidal gravitational circulation. This is the case in the Pescadero estuary.

In a well mixed estuary (Figure 4.8), fresh water is found on the upstream side of the estuary, salt water on the ocean end, and isopycnals (which are also isohalines in the case of salinity dependent density) are vertical. In this case, the lowest salinity water is located the farthest upstream.

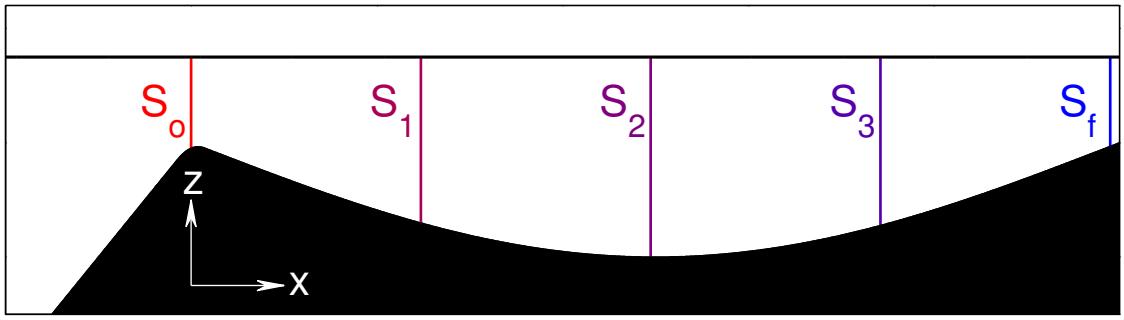

Figure 4.8: A well-mixed estuary is characterized by vertical isopycnals, represented here by isohalines because density in estuaries is usually salinity dependent.

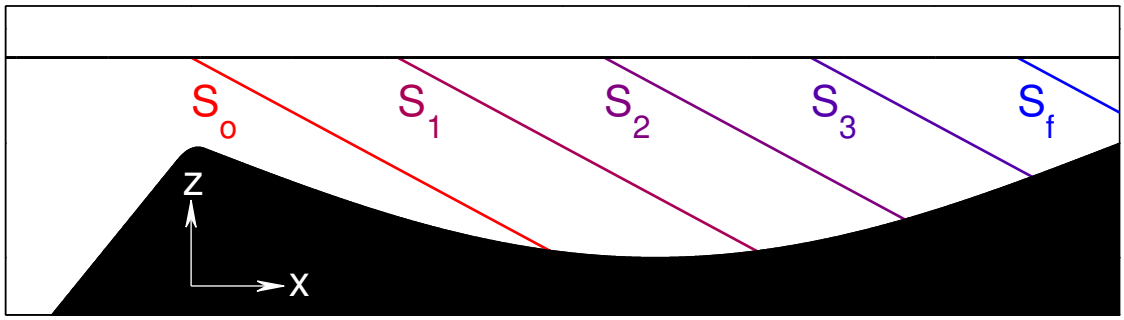

Figure 4.9: Highly stratified estuaries, have both longitudinal and vertical stratification, and isopycnals are slanted.

In a salt-wedge estuary (Figure 4.9), isopycnals are slanted. The lowest salinity water is still the farthest upstream in an estuary, and in an estuary that freshens tidally, the lowest salinity water will also travel farther than saltier water. Additionally, density effects mean that in vertically stratified estuaries, even if salt water intrudes far up estuary, fresher water will still be on the surface. In an idealized homogeneous channel estuary, whether water reaches farther upstream or has access to the surface does not matter. But, natural estuaries are not spatially homogeneous. In the Pescadero estuary, the upstream ends of the estuary are in two creeks, and probably more importantly, the estuary sits amid a marsh complex. Given the salt-wedge type salinity structure, fresher water is given access to shallow wetlands which the saltier water cannot access.

Knowing that the Pescadero estuary is nearly always vertically stratified, we begin to look at vertical differences and processes to explain the differences in dispersion among high and low salinities. The short residence time of salt water in the open estuary also means that lower salinity water is usually retained for longer time within the estuary (the exception being when high salinity water becomes bathymetrically trapped in deep regions of the estuary), so dispersive processes generally have longer time to act on fresher water.

4.5.2 Vertical processes

To understand the vastly different values of K_x in higher and lower salinities, we look to time series of salinities at different depths in the estuary. Figure 4.10 shows data from three CTDs vertically distributed in the water column at the upstream DC station, approximately 200 m upstream from the NM station (location shown on maps in chapters 2 and 3). The first subplot (a) shows the depth of each sensor. The bed sensor was fixed 20 cm above the bed and the surface sensor was floating on a buoy approximately 20 cm below the surface. The middle sensor was hanging from a buoy such that at most times its line was slack, but at high enough water levels the line went taught and the sensor was pulled down. The second subplot (b) gives salinity at these sensors.

Some features of vertical salinity differences are apparent in this plot. The bed sensor (blue lines on figure 4.10) shows that during this period of time salt completely leaves the estuary daily on the large ebb, but does not freshen completely on the small ebb. (Figure 4.2 confirms salt advects out, but as described in chapter 3, salt can become trapped in the deep region where the DC mooring is located). The mid-column sensor (blue lines on figure 4.10) in (b) shows a similar structure to the CTD collocated with the ADV at NM (Figure 4.2). The surface salinity at DC on the diurnal high high tide has two peaks (Figure 4.10b, green line). The first peak is attributed to advection of the salt field upstream with the flood tide, and the fast drop should be the movement of saline surface waters back downstream with the coupled effect of the ebbing tide and buoyancy-driven restratification of the flow. A second peak in surface salinity occurs as the high salinity at depth begins to lower. We hypothesize that this peak represents water that had been trapped upstream now moving past the lower estuary sensors.

At these sensors, the two-phase salinity time series of the middle sensor may be induced by vertical mixing in the upper water column between the second pulse of salty water and the mid-column water (green and red lines on figure 4.10). High vertical shear is observed on ebb tides (cf Chapter 3), suggesting conditions exist for vertical mixing. As the second pulse of salty water advects downstream (e.g. 07:00 on 23 April, figure 4.10), the mid-column salinity structure transitions to the more relaxed salinity gradient structure. This more relaxed salinity structure could be evidence that turbulent processes in the upper water column have mixed the second pulse of salty water. There may be also be an effect of the mid-column sensor moving up and down in space and sampling a different part of the water column.

The structure seen at the NM collocated ADV and CTD is thus evidence of mixing in the upper water column between this second pulse of salty surface water and salinities at upper and middle depth.

4.5.3 Variation in transition salinity with spring-neap cycle

There is a marked difference in the transition salinity (S_T) of ebb tides on 21 & 22 April compared to those on 23 & 24 April (Table 4.1 and figures 4.4- 4.7), with $S_T \approx 11$ on the

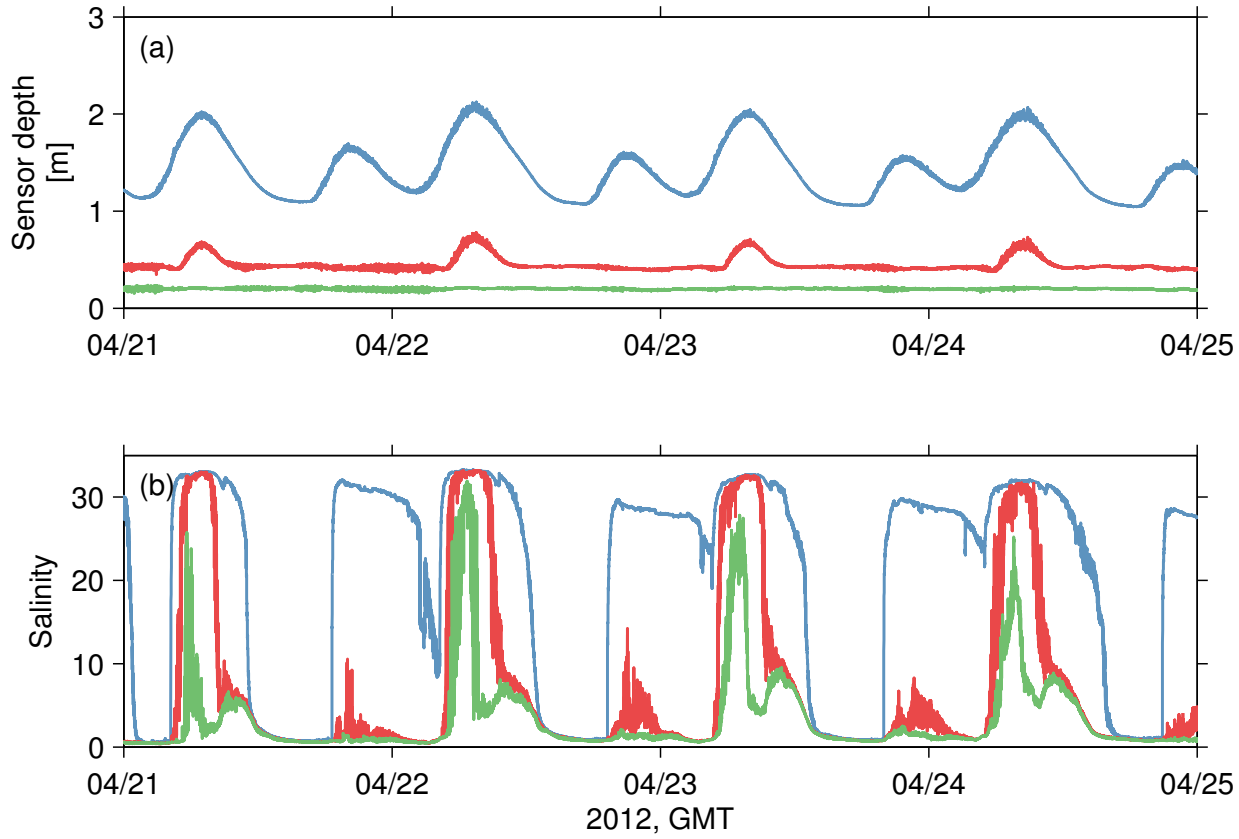

Figure 4.10: Sensor depth (a) and salinity measurements (b) at DC for the four days where K_x is computed by sensors at NM. The midcolumn sensor (red) has a similar structure to that seen at the CTD collocated with the ADV, and the surface sensor (green) suggests that this structure is an effect of mixing a second pulse of saline water on ebb.

first two days and $S_T \approx 14$ on the second two. Having concluded that $S(x)$ at low salinities is determined by surface salinity processes, such processes should also explain this variation. Figure 4.11 shows a longer time series of surface salinity at DC (shown also by the green line in figure 4.10b). On the first seven days, high salinity water did not reach the DC surface on the small flood. The large peak on these days is the salt field advecting upstream past the sensor. Immediately after the high salinity water retreats, a small pulse of saltier water passes the sensors. This pattern is easily apparent in the early days on this figure, but also exists between 4 May and 11 May when both the large and small flood tide moved salt water past the NM surface sensor, but only the large flood resulted in a second pulse of salty water. Between 26 Apil and 2 May, high salinity water did not often reach the NM station surface at all, and when it did, no second pulse of salt water followed its retreat.

The variation in salinity here follows a spring-neap cycle. The early part and late part of the time series correspond with spring tide conditions, and the middle period with neap

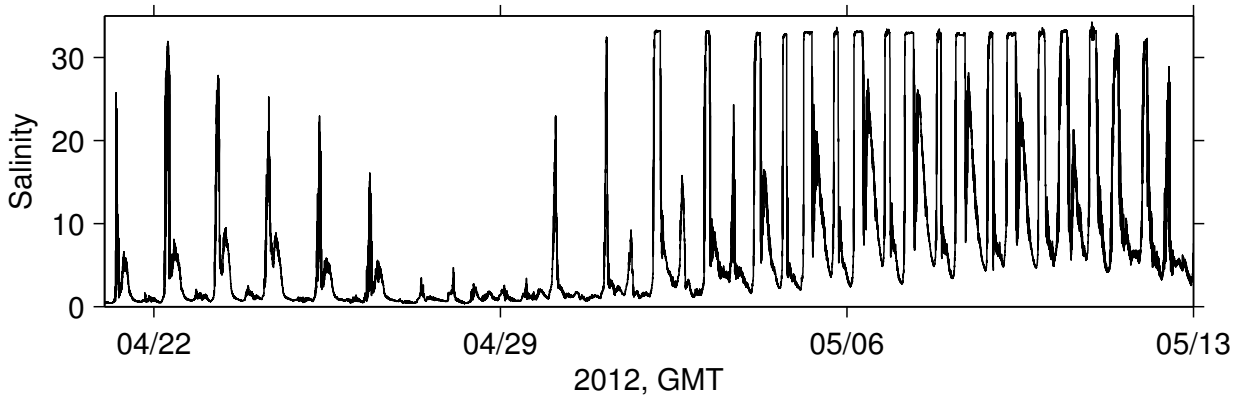

Figure 4.11: A longer record of the the surface salinity sensor at DC (green line in figure 4.10). The magnitude of the second pulse of saltier water on the ebb at the surface follows the spring-neap cycle.

tide conditions (Figure 3.2). These data continue to suggest that a bathymetric control only accessible to the upper water column traps and releases water. With the lower tidal amplitudes characteristic of neap tides, salt water cannot access these traps (if it even arrives nearby).

Furthermore, the salinity of the second pulse of water increases and decreases going into and out of the spring tide. The second spring tide saw higher salinities than the first. The difference in these two spring tides was twofold: (1) higher freshwater flow was present during the earlier dataset, and (2) the amplitude of the tides on the second spring was higher.

The spring-neap variation of the salinity of lagged pulses is shown to influence the transition salinity such that a wider range of salinities exhibit high dispersion when the salinity of this pulse is higher. Perhaps more importantly, the absence of a second pulse of surface salinity during the neap tides likely shuts down the low-salinity dispersion mechanism.

4.5.4 Longitudinal processes

Several mechanisms may allow the trapping and release of water at shallow depths that induces the second phase of salinity mixing. Surface salinity trapping probably occurs in the shallower upper reaches of the estuary. Sensors were located primarily in the lower estuary, and no surface sensor measurements were made upstream of DC, so an exact location or mechanism of trapping is not verifiable using our data. At least three features of the Pescadero estuary could contribute to the bimodal surface salinity spike seen in conjunction with the ebbing high high tide:

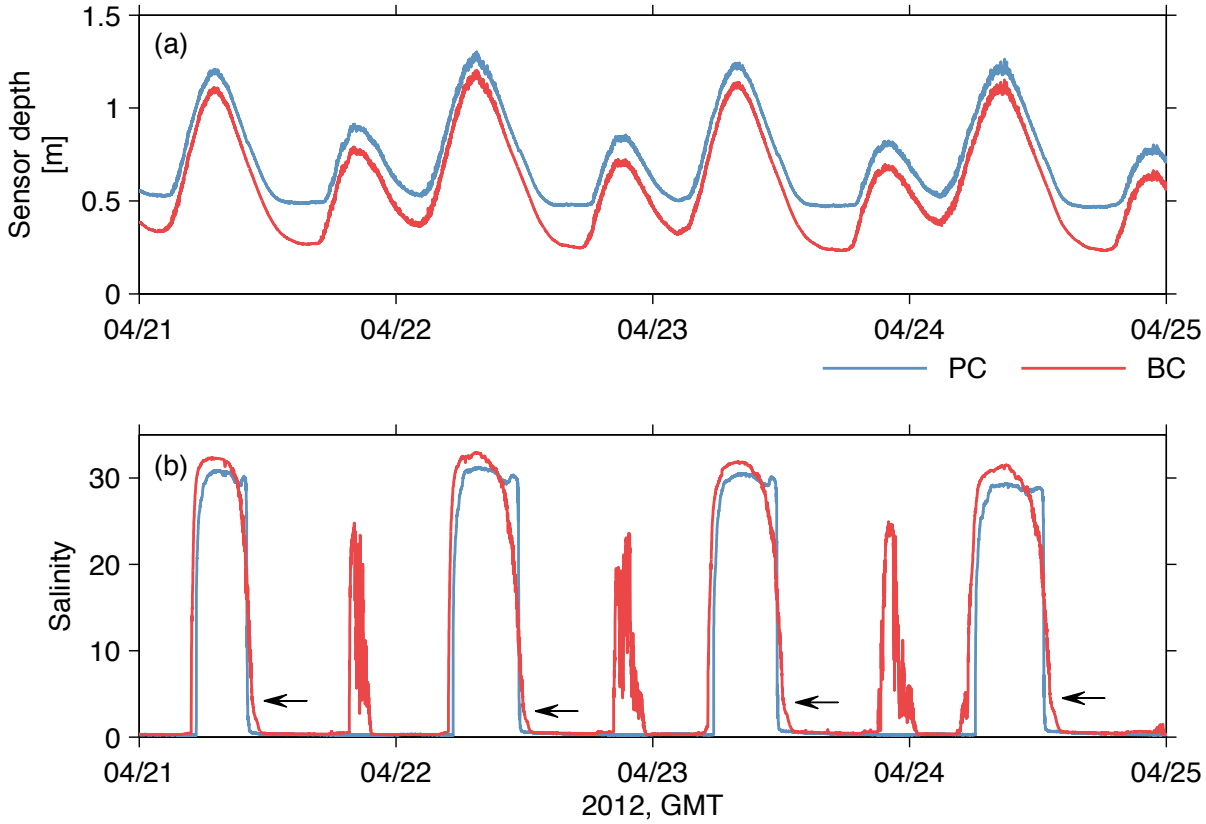

Figure 4.12: Bed CTD sensor measurements in the Pescadero (PC - blue line) and Butano (BC - red line) creeks for the four dacs of collocated ADV and CTD measurements at NM. (a) gives the sensor depth and (b) gives the salinity. The salt structure appears to be more relaxed in Butano Creek than in Pescadero Creek, both on flood and ebb. The truncated depth at low tide at PC suggests salt water does not reach the Pescadero Creek sensor on the small flood tide because of bathymetric controls. Higher freshwater streamflow may also play a role in limiting salt intrusion in the Pescadero Creek. Arrows indicate the slight transition to a two-phase structure in the measured BC salinity.

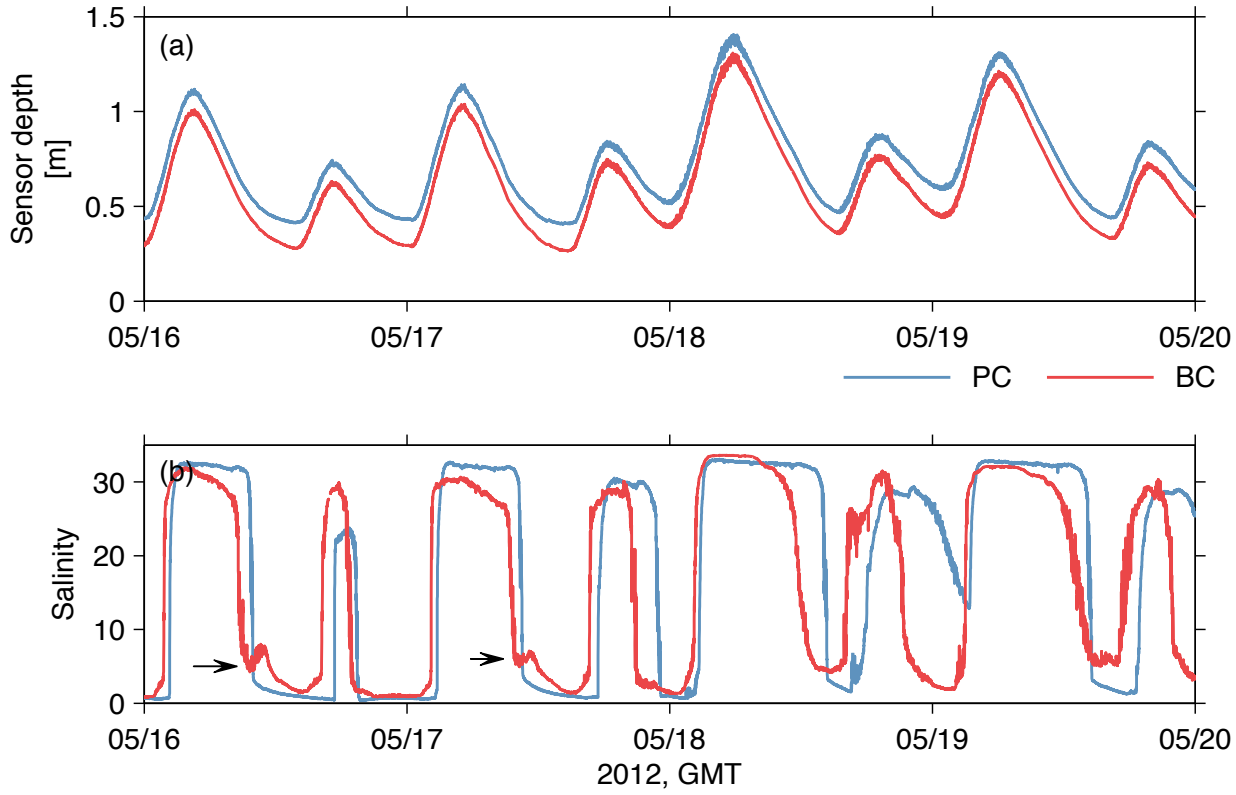

Figure 4.13: Bed CTD sensor measurements in the Pescadero (PC - blue line) and Butano (BC - red line) creeks 25 days after the measurements in figure 4.12. (a) gives the sensor depth and (b) gives the salinity. Here, the bed sensor in Butano creek measures two pulses of more saline water as well as an altered dS/dt similar to downstream sensors - suggesting the mechanism for bifurcated K_x calculations near the mouth occurs upstream of the Butano sensor. The less truncated behavior of the PC depth record compared to figure 4.12 could be from bed movement or movement of the mooring. Arrows indicate the marked transition to a two-phase structure in the measured BC salinity.

Figure 4.14: Satellite image of the Pesacadero estuary and marsh showing the confluence of the Butano and Pescadero creeks, salt marsh, branching structure of the Butano creek, and shallow channels at low tide on 19 May, 2012. Image: Google Earth.

Confluence of two creeks

Approximately 750 m upstream from the mouth of the Pescadero estuary, two creeks form a confluence (Figure 4.14). Salt water carried by the flood tide may move either up the Pescadero Creek or up the Butano Creek. (In a third process described below, it may also move through culverts into a channel to the shallow North Pond). Water that flows up perfectly equal branching channels should ebb down these channels so that two parcels of water split by the branch arrive back together. Variation in natural channels may cause divergence of these hypothetical parcels as the balance of momentum and friction in each channel differs. Phasing of tidal flow into these channels may cause interactions which set up a delayed pulse of salt water downstream, as has been observed in other branching tidal systems (MacVean and Stacey 2011).

Bed sensors in each creek were approximately 100 m upstream of the confluence. Data at these sensors (Figure 4.12) confirm that these are not completely uniform channels. Less salt water moves up Pescadero Creek than Butano Creek. This could be due to higher freshwater flow from the Pescadero Creek, which has a larger watershed. The Pescadero sensor may have been approximately 50 m farther upstream from the confluence than the Butano Creek sensor (the mooring was dragged from it's initial location), and so it is possible that this difference played a big role in whether salt reached the mooring. Further differences between the two creek channels are discussed below.

Butano marsh

The Pescadero Creek flows into the lower estuary through a relatively constricted, channelized creek bed. Meanwhile, the Butano Creek flow through an extensive salt marsh. This

marsh floods significantly with a closed mouth (cf Chapter 2), but as is the nature of salt marshes, some flooding occurs tidally. The marsh has various sloughs, and the historic Butano Creek bed has undergone massive accretion with sediments from the logged watershed (Figure 4.14), and the main channel has shifted, adding further complexity to Butano marsh and creek flow paths.

Bed salinity measurements in the Pescadero and Butano Creeks suggest that within the Pescadero Creek (upstream of the confluence of both the Butano and the culverts to the North Pond) do not demonstrate the same structure seen downstream of these controls. The time series of salinity is very sharp and mostly uniform on flood and ebb (Figures 4.12 and 4.13). Bed salinity measurements in the Butano Creek show a slightly more relaxed flood salinity structure, and hint at a two-phase ebb salinity structure. The later time series (Figure 4.13) actually shows two pulses of salty water on the ebb, similar to surface measurements downstream. These measurements seem to implicate marsh processes in setting the two-phase salinity structure.

Trapping of water which creates the later pulse of salty water downstream is likely an advective process due to interaction of sloughs and shallow channels with the main channel, but may also contain a significant diffusive component due to flow interaction with shallow marshes and vegetation. The tidal timescale suggests that perhaps the trapping mechanism is more akin to increased shear dispersion among shallow waters in the vegetated, wide upper estuary than traditional tidal trapping which requires many tides for its dispersive effects.

Figure 4.15: Photographs of culverts to North Pond, left photo 23 March, 2010, right photo 29 November, 2010. There has been further deterioration of the culverts since these photographs were taken.

Culverts and flow to North Pond

The North Pond in the Pescadero marsh is connected to the Pescadero creek through a channel and dilapidated culverts (Figures 4.16 and 4.15). The culverts through a levee were

Figure 4.16: Satellite image of the Pescadero estuary and marsh on 8 February, 2008 showing the channel from the Pescadero creek to the North Pond. Image: Google Earth.

designed to be able to regulate flow to the North Pond, but the control gates and culverts have since rusted and fallen into disrepair and culverts remain perennially open, allowing slow flooding and draining of the shallow North Pond. Flow into and out of the culverts is bathymetrically controlled because water levels below the bottom of the culverts cannot pass. The constricted flow could trap and release salt water either in accordance with the momentum-friction imbalance previous described, or by the physical barrier transforming a section of the estuary from open-channel flow to pipe flow and back.

4.6 Sensitivity to inputs and assumptions

Values of K_x in saltier and fresher salinities remain an order of magnitude apart, but are sensitive to assumptions made in the analysis. Much of the variation described below stems from the fitting of a one-dimensional equation that does not account for vertical variability.

4.6.1 Time dependence

Using equation 4.3 to get K_x values required providing a value of time t. The time used in this calculation was $t = t_0 + t_{isopycnal}$, where $t_{isopycnal}$ was the time between the flooding and ebbing of each isopycnal past the ADV and CTD at NM. Different K_x values were calculated from higher and lower salinities. The 20 PSU and 8 PSU isopycnals were selected as representative of the two separate water masses, and time between the passage of these isopycnals is given in table 4.1. The advantage to this method is its ability to include some

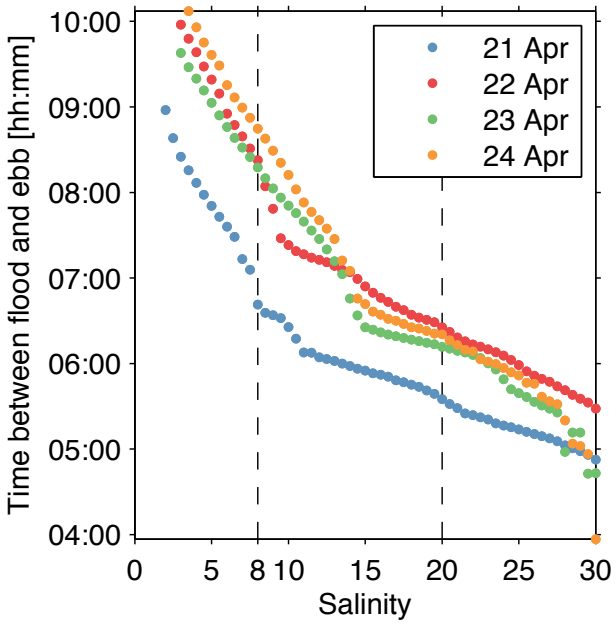

Figure 4.17: Time t used to compute K_x for the two-phase salinity structure. Time at salinity = 20 was used for the higher salinity calculation and time at salinity = 10 was used for the lower salinity calculation.

time dependence in the K_x value. The disadvantage is that K_x varies with the decision of which isohaline to follow (and thus what value of t).

Figure 4.17 gives the time between each isopycnal for the four tides. Time is not constant, so selecting a value introduces bias to the K_x calculation. Figure 4.18 shows the K_x for higher and lower salinities based on a range of $t_{isopycnal}$. Values of $t_{isopycnal}$ in the higher salinities (a) represent 15-29 PSU isohalines and values of $t_{isopycnal}$ in the fresher salinities (b) represent the 3-15 PSU isohalines. As seen in figure 4.17, lower salinities correspond with longer time t, so on each subfigure of figure 4.18, the upper range of salinities corresponds with higher K_x and shorter time, while the lower range of salinities corresponds with lower K_x and longer time. The 20 and 8 PSU isohalines are marked with a square for reference.

The variation in high salinity values of K_x is between 0.4 m^2 s^{-1} and 1.7 m^2 s^{-1} for different tides, or approximately 20-30% variation from the value obtained with $t_{isopycnal} = t_{S=20}$. The K_x values of high salinities remain very small, so this time dependence does not alter the perceived physics. The variation in low salinity values of K_x represented approximately 30-40% variation from the value obtained with $t_{isopycnal} = t_{S=8}$. Within this spread, $K_{x,fresher}$ remained an order of magnitude higher than $K_{x,saltier}$. The low salinity range may be skewed high by our calculation of $t_{isopycnal}$ through S = 15 when there is a clear transition on two of the tides at 11.5 and 10.5 PSU, well below the 15 PSU value.

Time t_0, the time from an infinitely sharp interface to the flood *S(x)* structure was estimated to be 1000 s based on physical parameters within the estuary (cf section 4.2.3).

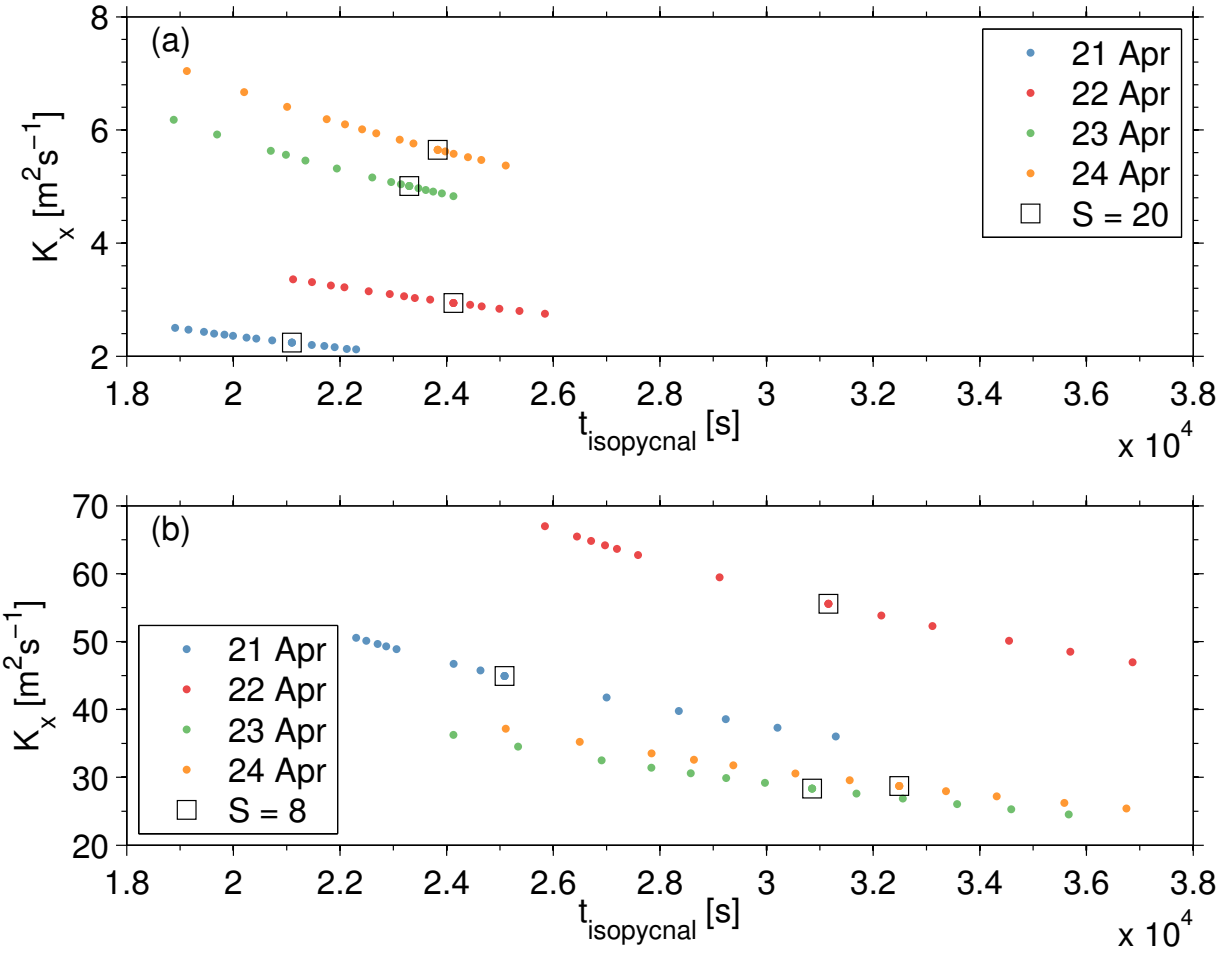

Figure 4.18: A range of K_x computed using t from different isopycnals (Figure 4.17).

K_x values are also sensitive to this value. Similar to above, smaller t_0 decreases the overall t and increases K_x, and larger t_0 increases the overall t and decreases K_x. Due to the small size of the estuary, and low river flow at the time of measurements (so a river plume advecting back in is not a concern), variation in K_x due to t_0 selection is likely to be much smaller than variation due to the selection of $t_{isopycnal}$ because both magnitude and range of $t_{isopycnal}$ values is much larger than the magnitude and range we estimate in t_0.

This analysis demonstrates the time dependence of K_x, but the range of values remains reasonable. Within the range of appropriate time values, the lower salinity $K_{x,S=0\rightarrow S_T}$ is much greater than the higher salinity $K_{x,S=S_T\rightarrow S_0}$.

4.6.2 Influence of water retained in deep pools of the estuary

Near the mouth, the water column was seen to freshen on the semidiurnal tide (Figure 4.2) but in the deep channel upstream, freshening sometimes only occurred on the large ebb (red line, figure 4.10). The K_x calculation assumed t based on the passage of the salt front past the collocated ADV and CTD at NM, a time of less than one tidal cycle. However, some of the high salinity water passing the NM sensors on the large ebb has been retained for two tidal cycles. Recalculating $t_{isopycnal}$ using the passage of the 20 PSU isopycnal from the flood tide which initially brought salt water into the estuary (which is the previous flood on the 23 and 24 April large ebbs), the value of K_x drops to 2.1 m^2 s^{-1} and 2.5 m^2 s^{-1}, bringing the values in line with the previous two tides. Retention time in the salt pocket seems to explain the higher dispersion coefficient derived with a shorter time than physically realistic.

4.6.3 Bias from S_0 value

The value of $S_0 = 33.5$ was used to calculate K_x at high and low salinities because it was representative of the salt field seen to flood past the NM collocated ADV and CTD. Figure 4.10 shows that the surface salinity at DC only reached the value of the bed salinity on 22 April, and fell short on the other days (green line salinity < red line salinity). If the flood is also treated as having a two-part structure, calculating K_x for lower salinities with $S_0 < 33.5$ reduces the dispersion coefficient. Setting $S_0 = 25$ reduces K_x to 20 - 45 m^2 s^{-1}. Again, this bias is due to a one-dimensional assumption in a non one-dimensional estuary, but the overall conclusions remain the same.

4.7 Conclusions

Mixing and dispersion of the salt field in the Pescadero estuary has been approached via application of the one-dimensional advection-diffusion equation to the salinity field in the estuary. By recreating the longitudinal salt structure in the estuary, it became apparent that the estuary was dispersing higher salinity water much less than low salinity water, and through calculation of the longitudinal dispersion coefficient, K_x, this difference was quantified to be an order of magnitude higher among lower salinities than higher salinities. Looking at the vertical structure of salinity revealed that on the large ebb tide, high surface salinities rapidly relaxed, and a second pulse of salty water followed the relaxation. This pulse may have induced vertical mixing in the water column, and certainly influenced the more dispersed salinity structure at lower salinities. The one-dimensional framework simplifies some complexities of the system yet captures dispersion by different physical processes.

Upstream processes are implicated in trapping which causes this second pulse of salty water. The exact location or mechanism of trapping is not distinguishable by our dataset, but it is probably within the Butano marsh. As the salinity of the second pulse becomes higher during spring tides, it appears that there is a bathymetric effect only accessible to surface waters. With spring tides, the water level becomes higher and higher salinity water

which is lower in the water column due to density effects has access to the tidal trap(s). This effect should then feed back into the range of salinities which experiences high dispersion.

In this way, we have been able to capture and interpret vertical and longitudinal processes within a one-dimensional equation analysis. Findings, though location-specific in detail, should be relevant to highly stratified estuaries in general. The small dispersion coefficient among high salinities is expected for an estuary that remains highly stratified, though dispersion coefficient calculations are rare in this type of estuary. The higher dispersion coefficient among lower salinity water seems to emphasize the role of shallow traps in setting dispersion characteristics and may be comparable to dispersion in more well mixed estuaries with different mechanisms of mixing and dispersion.

Chapter 5

Bar-built estuarine response to tsunami forcing

5.1 Introduction

The 9.0 Mw Tohokū earthquake hit Japan at 05:46 GMT on March 11, 2011, triggering a devastating tsunami that would propagate across the Pacific Ocean, reaching as far as Chile (Mori et al. 2011; Lagos and Haro 2011). On the California coast, the first waves arrived at low tide, but despite the timing and small amplitude of the tsunami in the Eastern Pacific, extensive damage occurred to harbors in Santa Cruz and Crescent City both with the initial arrival of waves and later when the high high tide and tsunami combined to create strong currents (Wilson et al. 2012).

Coastal California is dotted with bar-built estuaries where rivers and streams arrive to the ocean through small estuaries set behind sandy beaches (Figure 5.1a). Combined nearshore sediment transport and low seasonal streamflow choke the mouths of many of these estuaries closed with sand, limiting or completely cutting off the tidal exchange. Even in the open states of these estuaries, the mouth is shallow and narrow, attenuating tidal amplitudes and currents, and at times cutting off ocean connection during the low low tide (cf Chapter 3). This limited forcing allows these shallow estuaries to remain strongly salt-stratified. Tidally, salt water advects upstream as a salt-wedge on the flood and may become trapped in deeper pools of the estuary on the slow ebb (e.g. Largier and Taljaard 1991; Ranasinghe and Pattiaratchi 1999), transitioning these small estuaries into vertically salt-stratified lakes. Except for when low low tide in the ocean lowers the surf and swash zones below the level of the perched mouth, infragravity motions in the nearshore induce fast water velocities in these estuaries (cf Chapter 3).

Our analysis of the Pescadero estuary in Northern California (Figure 5.1b) has established that nearshore processes with timescales of 30 seconds to three minutes modulated by the semidiurnal tide dominate the dynamics of these systems (cf Chapter 3). Here, we examine a perturbation of the system by the arrival of the Tohokū tsunami, including the impacts on

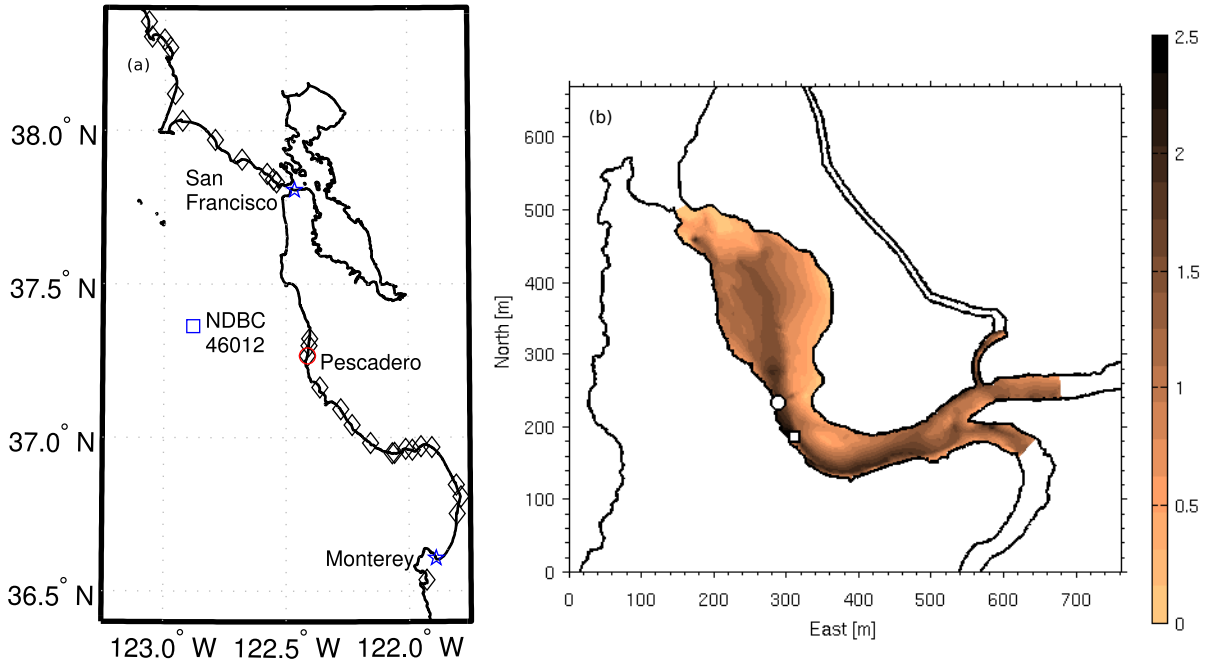

Figure 5.1: Northern California (a) and Pescadero (b) coastlines. The California coastline map (a) shows locations of other inlets and bar-built estuaries plotted as black diamonds, the Pescadero estuary plotted within the red circle, the Monterey and San Francisco NOAA tide gauges as blue stars and the NDBC Buoy 46012 as a blue square. Bathymetry on the Pescadero map (b) is given in meters. Bathymetry data were collected during an extended mouth closure, so the highly variable depth at the sandy mouth was not recorded. The downstream (DS) mooring with an ADCP and CTDs is at the circle and the upstream (US) CTD mooring is at the square.

estuarine salinity and mixing.

5.2 Field Setup and Conditions

Two moorings were deployed in the Pescadero estuary during the March 2011 tsunami (Figure 5.1b). Installed on March 10, 2011, downstream station DS consisted of one upward-looking ADCP (RDI 1200kHz Workhorse Monitor) burst sampling at 2 Hz for ten minutes of every fifteen. Co-located with the ADCP were four vertically distributed CTDs (RBR XR-420) sampling once per minute. A surface CTD at this location was not replaced until March 15, 2011 so no surface salinity record exists before that date. Upstream station US was in place from January 27, 2011 and contained one bed and one mid-column subsurface CTD sampling at the same rate as other CTDs. The ADCP deployed was always submerged, but did not successfully compute water velocities when the estuary depth was very shallow

or when velocities were too high or too low.

The Northern California coast experiences mixed semi-diurnal tides. During the days immediately prior to and during the tsunami, tides in the nearshore had a neap-tide range of just under 1.5 m (Figure 5.3b). Large waves picked up on March 11, peaking at 4 m significant wave height offshore (NOAA NDBC 46012), with significant wave heights between 2 and 5 m for the subsequent days. Freshwater streamflow into the estuary was estimated to be between 1.3 and 2.1 m^3 s^{-1} during the days surrounding the tsunami, based on measurements by the USGS Pescadero gauge (11162500) located five miles upstream of the estuary. The creek discharge was sufficient to freshen the small estuary tidally.

Nearshore tsunami conditions are inferred from NOAA tsunami-capable tide stations in Monterey (9413450) and San Francisco (9414290) (Figure 5.1a). Records indicate that the arriving tsunami propagated generally North to South but waves reached the more southern Monterey before San Francisco due to the effect of the deep Monterey Canyon on tsunami celerity, consistent with previous tsunami observations (González et al. 1995).

5.3 Pre-tsunami conditions

Observations made immediately prior to the tsunami offer a framework for understanding non-tsunami conditions in bar-built estuaries (Figure 5.2a, c, e). The estuarine sea level is modulated by ocean tides, but the constricted, shallow mouth limits tidal amplitudes within the estuary. Tidal range the day prior to the tsunami was approximately 75 cm within the Pescadero estuary compared to twice that in the nearshore (Figure 5.3b,d). Limited tidal elevation change is coupled with limited tidal velocities in the estuary. Depth-averaged tidal velocities 400 m upstream from the mouth were measured as limited to ± 20 cm s^{-1}. On tidal timescales, the system behaves as a salt-wedge estuary, where salt water is slowly advected upstream by flooding water. Despite the shallow nature of this estuary, in the presence of limited velocities, ocean water and freshwater in the system retain their salt character due to limited mixing. Between 14:00 and 16:00 GMT on March 11 the range of ebbing salinities at the DS sensor was 3 to 29 PSU between 50 cm and 200 cm depth (Figure 5.2c). Completely fresh water was likely present at the surface above the recording sensors.

Unique to bar-built estuaries on wave-dominated coasts, ocean waves significantly affect estuarine hydrodynamics. The tidal ranges in choked lagoons are modulated by the magnitude of ocean waves [e.g. Malhadas et al. 2009]. We see evidence of an elevated lagoon level due to large waves (Figure 5.3d) in the pre-tsunami state of the Pescadero estuary. Most relevant to the dynamics of these systems, oscillations corresponding to surf beat frequencies are visible in pressure and velocity measurements in this system. When the estuary and nearshore are sufficiently connected, depending on tidal stage, mouth elevation, and ebb velocities, 30 s to 3 min oscillations are observed, notably changing the estuarine sea level (Figure 5.2e) and inducing velocity oscillations around the tidal velocities (Figure 5.2a). Velocity oscillations between -10 cm s^{-1} and 50 cm s^{-1} were observed during the pre-tsunami high high tide.

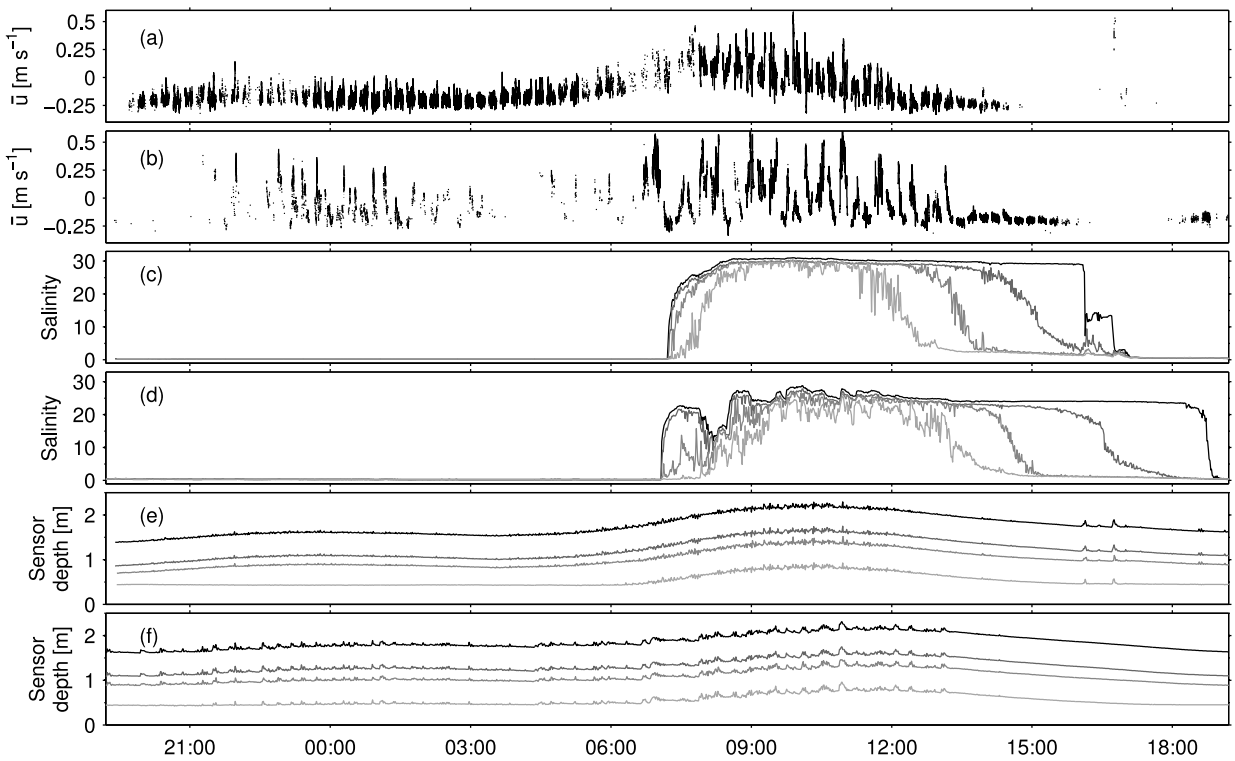

Figure 5.2: Depth-average velocity (a, b), CTD salinity (c, d) and CTD sensor depth (e, f) at the DS mooring for the tidal cycles corresponding mostly to pre-tsunami (a, c, e) and tsunami (b, d, f) conditions in the Pescadero estuary from March 10 - 12, 2011. The first waves arrive at 16:05 on March 11 (a, c, e). The deepest CTD sensor was mounted 20 cm above the bed.

Although the estuary remains salt stratified even in the presence of high velocities induced by infragravity motions, wave forcing likely affects the salinity structure in several ways: Oscillations in the mid-column CTD salinity data result from the oscillatory flow advecting the salt field upstream and downstream, and shearing and straining of this salt field must induce some mixing. When wave forcing cuts off on the ebb tide, the estuary appears to relax from a longitudinally stratified system to a largely vertically stratified system. On the ebb following the pre-tsunami high high tide, salt water remains trapped in the deep pool due to low water velocities and bathymetric constraints (after 12:00, Figure 5.2c). Typically, this water is flushed from the salt trap low frequency pulses of water begin to enter the estuary on the next flood tide, pushing downstream-sourced fresh water into the salt pocket.

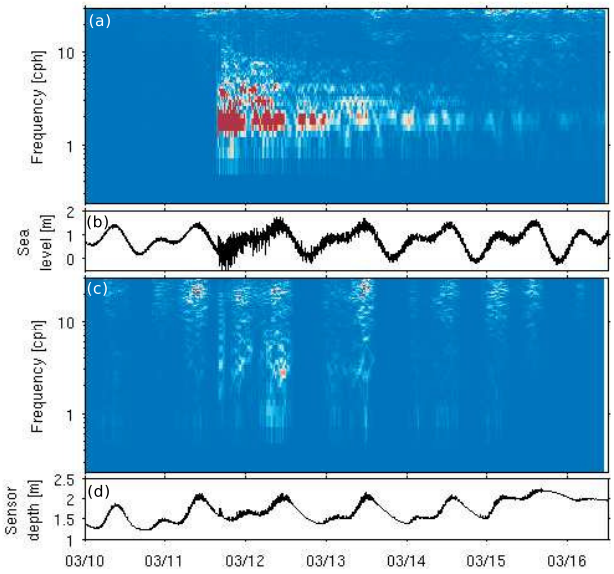

Figure 5.3: Variance preserving spectra calculated from the NOAA Monterey (9413450) tide gauge (a), (b) and from the US station in the Pescadero estuary (c), (d). The logarithmic color scale is one order of magnitude larger on the NOAA data than on the Pescadero data.

5.4 Tsunami forcing on estuary

The first waves from the Tohokū tsunami arrived to the pressure sensors in the Pescadero estuary at 16:05 GMT on March 11, preceding arrival of waves to San Francisco. Two twenty centimeter bore-shaped waves are visible at 16:05 and 16:45 in the pressure record (Figure 5.2e), but only slightly increase the depth of the shallow ebbing estuary. The salinity record indicates that these two waves freshened the depths of the estuary (Figure 5.2c), probably as fresher downstream water is forced into the deep salt traps. Overall, the low tide stage of the estuary and nearshore ocean restricted the estuarine response to the early tsunami.

As the tide rose following the onset of the tsunami, connection between the estuary and the ocean was reestablished, and tsunami-frequency motions begin to appear in the depth record (Figure 5.3c,d). The low high tide on March 11-12 was characterized by larger depth oscillations than common at this stage of the tide (Figure 5.2f). Velocity measurements, though sparse, indicate a similar trend (Figure 5.2b). Given freshwater inflow and tidal stage, salt water was not present at the moorings during this period.

Starting at 07:00 GMT on March 12, fast velocities are observed as the flood tide couples with tsunami forcing. Maximum observed velocities of 60 cm s^{-1} are comparable to the previous day's maximum velocities, but occur much more frequently. The oscillation between positive and negative velocities are also much stronger, and a tidal velocity is not obvious, but present. The salt-wedge is advected upstream, past the DS sensors, but also undergoes periods of intense vertical mixing, eventually resulting in a reduced bed salinity of 24, compared to 29 on the previous day (Figure 5.2d).

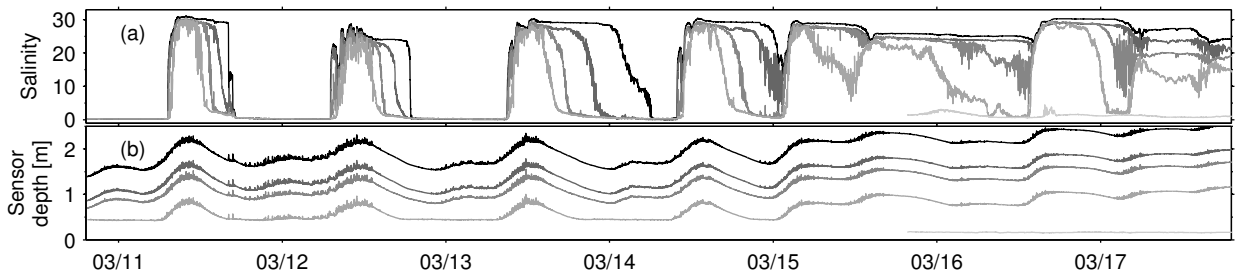

Figure 5.4: CTD salinity (a) and CTD sensor depth (b) at the DS mooring.

As the tide recedes, the ocean and estuary become disconnected and tsunami and surf beat forcing are immediately cut off around 13:15 GMT. At this point, the salt field begins to relax and be advected downstream. Tsunami frequencies in the estuary are observed on the following high tide, ultimately persisting for about two days (Figure 5.3c), much less time than the duration of tsunami frequencies at the Monterey tide gauge of over five days (Figure 5.3a). Some of this limit on tsunami forcing within the estuary is likely due to geomorphic changes at the mouth. Depth data show clearly that the mouth becomes nearly choked closed with sand on March 15 as the lagoon depth remains high (Figure 5.4a). This leads us to expect some geomorphic changes also occurred on days prior to the near-closure. The unusually timed mouth closure allowed the estuary to be converted into a salt-stratified lake with highly limited tidal forcing (Figure 5.4). Rainfall would force open the mouth on March 19, flushing all salt from the system and ending the temporary alteration of the natural estuarine state by the Tohokū tsunami.

5.5 Altered estuarine dynamics

During the tsunami, kinetic energy was raised in the estuary as flood and ebb conditions occurred with higher than normal frequency, and associated velocities were elevated (Figure 5.5). We estimate kinetic energy associated with the large flood was raised between 20% and 40% as compared with the previous tide, which already existed in an elevated energy state due to large ocean waves. Vertical mixing was shown to increase due to turbulence associated with these elevated velocities (Figure 5.2b,d). Over the tidal timescale, we expect that this increase in mixing resulted in an overall decrease of salt intrusion into the estuary. Salt intrusion occurs by a combination of advection and shear dispersion, but in the presence of vertical mixing shear dispersion is reduced. Expecting little difference in advection when pre-tsunami and tsunami high water levels are similar, we attribute the expected overall reduction in salt intrusion to reduced longitudinal dispersion caused by reduced shear dispersion.

The high velocities attributed to tsunami forcing were not much greater than the fastest velocities commonly observed in the Pescadero estuary, but tsunami velocities are persistent while during a normal tide these high velocities are seen as relatively uncommon pulses. The constrained, frictional mouth of California bar-built estuaries which normally limits

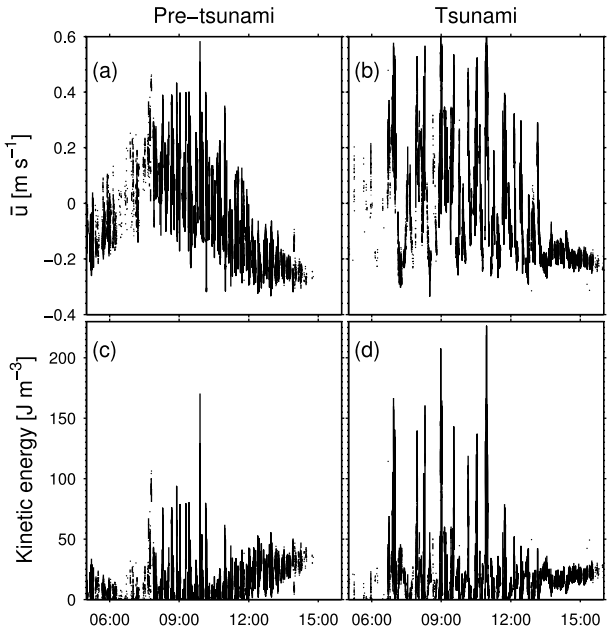

Figure 5.5: A comparison of kinetic energy based on depth-averaged velocity for a normal tidal cycle (a, c) and for tsunami conditions (b, d).

tidal velocities but allows infragravity wave-induced pulses allows the energetic tsunami to increase the kinetic energy of the high tide (Figure 5.5c,d), while completely cutting of tsunami forcing on the ebb.

Observations in the Pescadero estuary during the March 2011 Tohokū tsunami elucidate some effects of a small amplitude tsunami on a highly stratified bar-built estuary. Similar forcing likely occurred in the more than 200 small California inlets and estuaries as well as in similar systems all along the Eastern Pacific coast of the Americas.

Chapter 6

Conclusion

Through the lens of the Pescadero estuary in Northern California, this work has investigated hydrodynamics and salt transport in small, shallow bar-built estuaries, particularly those that are intermittently connected to the ocean.

Observations and analysis of the Pescadero estuary in particular showed that while closed, this estuary remains salt-stratified and limited mixing is wind induced. With this background stratification, the transition from the closed to the open state either occurs rapidly with full mixing of the water column, or more slowly with incomplete mixing between fresher surface and saltier lower waters. Future work should better quantify mixing in the closed and breaching state, and ample similarities between deep temperature-stratified lakes and these shallow salt-stratifed lagoons suggest a framework for these calculations already exists.

While open to tidal influence, California's bar built estuaries are highly influenced by the nearshore wave environment. Like traditional estuaries, the water level within the estuary follows tidal ocean forcing. Unlike estuaries with deep inlets, the shallow mouth cuts off part of the low tide as the ocean retreats below the mouth. This perched mouth limits tidal velocities and does not allow ocean gravity waves to enter the estuary while permitting infragravity motions to pass through the inlet. High velocities induced by these infragravity motions are seen to be energetically important. On the large ebb the ocean retreats from the mouth, and nearshore wave forcing is cut off. Tidally, the salt field is advected upstream but disconnects from the ocean and is removed primarily through shear entrainment with fresher water during spring tides. During neap tides, salt water may remain trapped in deep pools of the estuary for several tidal cycles.

Calculating salt dispersion is a quantifiable way of estimating mixing and transport within estuaries. For the Pescadero estuary, salinity dispersion calculations reveal that in the highly stratified flow, a very different dispersion regime exists at low salinities than at high. Data suggest that processes in the Butano marsh contribute to the salinity-dependent dispersion as low salinity water farther upstream or higher in the water column can access marsh features that increase dispersion among these waters through trapping and vertical mixing. Higher salinity water deeper in the water column (or downstream) is bathymetrically restricted access to these features, and mixes very little. While impossible to conclusively point a

finger at the process driving increased low-salinity dispersion, anthropogenic influence on the bar-built estuaries of North America has probably altered these dispersion regimes. Massive wetland loss in the state of California, where many bar-built estuaries sit amidst highly developed areas would eliminate a vegetative cause of dispersion. Logging and mining that has increased sedimentation of rivers, creeks, and estuaries, may alter dispersive processes as estuaries become shallower or channels migrate or infill on scales faster than naturally likely.

In the face of dynamic estuarine changes by tides, freshwater, wind, sand transport, and human intervention, observations revealed that small amplitude tsunami forcing also has a dramatic effect on an ever-changing estuary. The ocean wide tsunami generated by the 2011 Tohokū earthquake induced high velocity flow in the Pescadero estuary that mixed the water column much more than is typically seen. Access of the tsunami to the estuary was modulated by tides, and high velocities were on an infragravity timescale and modulated by the tsunami. This interesting cascading effect of variable frequency forcing suggests that the tsunami event can be framed as an energetic insertion of a forcing between usual infragravity and tidal periods.

Observations within the Pescadero estuary point to the large influence of the nearshore wave climate on bar-built estuarine dynamics. Future field measurements in intermittently closed estuaries should include observations in the nearshore ocean to better understand this relationship.

Moving forward in time, the future of bar-built estuaries on the west coast of North America is imperiled by a host of anthropogenic threats. Sea level rise, limited freshwater, pollution, and land-use changes will likely jeopardize the existence and health of small estuaries. These threats raise substantially more questions, and point to the need for better understanding and improved conservation practices to protect our coastal resources.

Bibliography

Baldock, T. E., F. Weir, and M. G. Hughes (2008). "Morphodynamic evolution of a coastal lagoon entrance during swash overwash". *Geomorphology* 95(3-4), pp. 398–411. DOI: 10.1016/j.geomorph.2007.07.001.

Battjes, J. A. (1988). "Surf-zone dynamics". *Annual Review of Fluid Mechanics* 20(1), pp. 257–291. DOI: 10.1146/annurev.fl.20.010188.001353.

Beach, R. A. and R. W. Sternberg (1988). "Suspended sediment transport in the surf zone: Response to cross-shore infragravity motion". *Marine Geology* 80(1–2), pp. 61–79. DOI: 10.1016/0025-3227(88)90072-2.

Becker, A., L. J. Laurenson, and K. Bishop (2009). "Artificial mouth opening fosters anoxic conditions that kill small estuarine fish". *Estuarine, Coastal and Shelf Science* 82(4), pp. 566–572. DOI: 10.1016/j.ecss.2009.02.016.

Becker, J. M., M. A. Merrifield, and M. Ford (2014). "Water level effects on breaking wave setup for Pacific Island fringing reefs". *Journal of Geophysical Research: Oceans* 119(2), pp. 914–932. DOI: 10.1002/2013JC009373.

Behrens, D. K. (2012). "The Russian River Estuary: Inlet Morphology, Management, and Estuarine Scalar Field Response". PhD thesis. University of California, Davis.

Behrens, D. K., F. A. Bombardelli, J. L. Largier, and E. Twohy (2013). "Episodic closure of the tidal inlet at the mouth of the Russian River — A small bar-built estuary in California". *Geomorphology* 189, pp. 66–80. DOI: 10.1016/j.geomorph.2013.01.017.

Bond, M. H., S. A. Hayes, C. V. Hanson, and R. B. MacFarlane (2008). "Marine survival of steelhead (Oncorhynchus mykiss) enhanced by a seasonally closed estuary". *Canadian Journal of Fisheries and Aquatic Sciences* 65(10), pp. 2242–2252. DOI: 10.1139/F08-131.

Contardo, S. and G. Symonds (2013). "Infragravity response to variable wave forcing in the nearshore". *Journal of Geophysical Research: Oceans* 118(12), pp. 7095–7106. DOI: 10.1002/2013JC009430.

Cousins, M., M. T. Stacey, and J. L. Drake (2010). "Effects of seasonal stratification on turbulent mixing in a hypereutrophic coastal lagoon". *Limnology and Oceanography* 55(1), pp. 172–186.

Dodet, G., X. Bertin, N. Bruneau, A. B. Fortunato, A. Nahon, and A. Roland (2013). "Wave-current interactions in a wave-dominated tidal inlet". *Journal of Geophysical Research: Oceans* 118, pp. 1–19. DOI: 10.1002/jgrc.20146.

Dussaillant, A., P. Galdames, and C.-L. Sun (2009). "Water level fluctuations in a coastal lagoon: El Yali Ramsar wetland, Chile". *Desalination* 246(1–3), pp. 202–214. DOI: 10.1016/j.desal.2008.03.053.

Elder, J. W. (1959). "The dispersion of marked fluid in turbulent shear flow". *Journal of Fluid Mechanics* 5(04), pp. 544–560. DOI: 10.1017/S0022112059000374.

Elwany, M. H. S., R. E. Flick, and S. Aijaz (1998). "Opening and Closure of a Marginal Southern California Lagoon Inlet". *Estuaries* 21(2), pp. 246–254.

ESA (2004). *Pescadero-Butano watershed assessment*. Tech. rep. Environmental Science Associates.

Fischer, H. B. (1976). "Mixing and dispersion in estuaries". *Annual Review of Fluid Mechanics* 8(1), pp. 107–133. DOI: 10.1146/annurev.fl.08.010176.000543.

Fischer, H. B., E. J. List, R. C. Koh, J. Imberger, and N. H. Brooks (1979). *Mixing in Inland and Coastal Waters*. Academic Press.

Fortunato, A. B., A. Nahon, G. Dodet, A. Rita Pires, M. Conceição Freitas, N. Bruneau, A. Azevedo, X. Bertin, P. Benevides, C. Andrade, and A. Oliveira (2014). "Morphological evolution of an ephemeral tidal inlet from opening to closure: The Albufeira inlet, Portugal". *Continental Shelf Research* 73, pp. 49–63. DOI: 10.1016/j.csr.2013.11.005.

Gale, E., C. Pattiaratchi, and R. Ranasinghe (2007). "Processes driving circulation, exchange and flushing within intermittently closing and opening lakes and lagoons". *Marine and Freshwater Research* 58(8), p. 709. DOI: 10.1071/MF06121.

González, F. I., K. Satake, E. F. Boss, and H. O. Mofjeld (1995). "Edge wave and non-trapped modes of the 25 April 1992 Cape Mendocino tsunami". *Pure and Applied Geophysics* 144(3-4), pp. 409–426. DOI: 10.1007/BF00874375.

Green, M. O. and I. T. MacDonald (2001). "Processes driving estuary infilling by marine sands on an embayed coast". *Marine Geology* 178(1–4), pp. 11–37. DOI: 10.1016/S0025-3227(01)00188-8.

Hanes, D. M., K. Ward, and L. H. Erikson (2011). "Waves and tides responsible for the intermittent closure of the entrance of a small, sheltered tidal wetland at San Francisco, CA". *Continental Shelf Research* 31(16), pp. 1682–1687. DOI: 10.1016/j.csr.2011.07.004.

Hayes, S. A., M. H. Bond, C. V. Hanson, E. V. Freund, J. J. Smith, E. C. Anderson, A. J. Ammann, and R. B. MacFarlane (2008). "Steelhead growth in a small Central California watershed: Upstream and estuarine rearing patterns". *Transactions of the American Fisheries Society* 137(1), pp. 114–128. DOI: 10.1577/T07-043.1.

Hill, A. (1994). "Fortnightly Tides in a Lagoon With Variable Choking". *Estuarine, Coastal and Shelf Science* 38(4), pp. 423–434. DOI: 10.1006/ecss.1994.1029.

Lagos, M. and J. Haro (2011). "Magnitude and impact from the 2011 Tohoku Tsunami in the coast of Chile". *AGU Fall Meeting Abstracts* -1, p. 1348.

Largier, J. L. and S. Taljaard (1991). "The dynamics of tidal intrusion, retention, and removal of seawater in a bar-built estuary". *Estuarine, Coastal and Shelf Science* 33(4), pp. 325–338.

Largier, J. L., J. Slinger, and S. Taljaard (1992). "The stratified hydrodynamics of the Palmiet - a prototypical bar-built estuary". *Dynamics and Exchanges in Estuaries and the Coastal Zone*. Ed. by D. Prandle. Washington D.C.: AGU, pp. 135–153.

Lerczak, J. A., W. R. Geyer, and R. J. Chant (2006). "Mechanisms driving the time-dependent salt flux in a partially stratified estuary". *Journal of Physical Oceanography* 36(12), pp. 2296–2311. DOI: 10.1175/JPO2959.1.

MacCready, P. and W. R. Geyer (2010). "Advances in Estuarine Physics". *Annual Review of Marine Science* 2(1), pp. 35–58. DOI: 10.1146/annurev-marine-120308-081015.

MacVean, L. J. and M. T. Stacey (2011). "Estuarine dispersion from tidal trapping: A new analytical framework". *Estuaries and Coasts* 34(1), pp. 45–59. DOI: 10.1007/s12237-010-9298-x.

Malhadas, M. S., P. C. Leitão, A. Silva, and R. Neves (2009). "Effect of coastal waves on sea level in Óbidos Lagoon, Portugal". *Continental Shelf Research* 29(9), pp. 1240–1250. DOI: 10.1016/j.csr.2009.02.007.

Mei, C. C. and P. L. Liu (1993). "Surface Waves and Coastal Dynamics". *Annual Review of Fluid Mechanics* 25(1), pp. 215–240. DOI: 10.1146/annurev.fl.25.010193.001243.

Monismith, S. G. (2007). "Hydrodynamics of Coral Reefs". *Annual Review of Fluid Mechanics* 39(1), pp. 37–55. DOI: 10.1146/annurev.fluid.38.050304.092125.

Monismith, S. G., W. Kimmerer, J. R. Burau, and M. T. Stacey (2002). "Structure and flow-Induced variability of the subtidal salinity field in northern San Francisco Bay". *Journal of Physical Oceanography* 32(11), pp. 3003–3019. DOI: 10.1175/1520-0485(2002)032⟨3003:SAFIVO⟩2.0.CO;2.

Moreno, I. M., A. Ávila, and M. Á. Losada (2010). "Morphodynamics of intermittent coastal lagoons in Southern Spain: Zahara de los Atunes". *Geomorphology* 121(3-4), pp. 305–316. DOI: 10.1016/j.geomorph.2010.04.028.

Mori, N., T. Takahashi, T. Yasuda, and H. Yanagisawa (2011). "Survey of 2011 Tohoku earthquake tsunami inundation and run-up". *Geophysical Research Letters* 38(7), L00G14. DOI: 10.1029/2011GL049210.

Munk, W. H. (1950). "Origin and generation of waves". *Proceedings of the 1st International Conference on Coastal Engineering ASCE, Long Beach, California*, pp. 1–4. DOI: 10.9753/icce.v1.1.

Nielsen, P. (2009). *Coastal and Estuarine Processes*. Vol. 29. Advanced Series on Ocean Engineering. WORLD SCIENTIFIC.

Okubo, A. (1973). "Effect of shoreline irregularities on streamwise dispersion in estuaries and other embayments". *Netherlands Journal of Sea Research* 6(1–2), pp. 213–224. DOI: 10.1016/0077-7579(73)90014-8.

Parkinson, M. and D. Stretch (2007). "Breaching timescales and peak outflows for perched, temporary open estuaries". *Coastal Engineering Journal* 49(03), pp. 267–290. DOI: 10.1142/S0578563407001605.

Ralston, D. K. and M. T. Stacey (2005). "Longitudinal dispersion and lateral circulation in the intertidal zone". *Journal of Geophysical Research: Oceans* 110, p. C07015. DOI: 10.1029/2005JC002888.

Ralston, D. K., W. R. Geyer, P. A. Traykovski, and N. J. Nidzieko (2013). "Effects of estuarine and fluvial processes on sediment transport over deltaic tidal flats". *Continental Shelf Research* 60, Supplement, S40–S57. DOI: 10.1016/j.csr.2012.02.004.

Ranasinghe, R. and C. Pattiaratchi (1999). "Circulation and mixing characteristics of a seasonally open tidal inlet: a field study". *Marine and Freshwater Research* 50(4), pp. 281–290.

— (2003). "The Seasonal Closure of Tidal Inlets: Causes and Effects". *Coastal Engineering Journal* 45(4), pp. 601–627. DOI: 10.1142/S0578563403000919.

Rich, A. and E. A. Keller (2013). "A hydrologic and geomorphic model of estuary breaching and closure". *Geomorphology* 191, pp. 64–74. DOI: 10.1016/j.geomorph.2013.03.003.

Rydberg, L. and L. Wickbom (1996). "Tidal choking and bed friction in Negombo Lagoon, Sri Lanka". *Estuaries* 19(3), pp. 540–547. DOI: 10.2307/1352516.

Schallenberg, M., S. T. Larned, S. Hayward, and C. Arbuckle (2010). "Contrasting effects of managed opening regimes on water quality in two intermittently closed and open coastal lakes". *Estuarine, Coastal and Shelf Science* 86(4), pp. 587–597. DOI: 10.1016/j.ecss.2009.11.001.

Scheck, J. (2012). "Tiny town Is awash in water woes". *Wall Street Journal*.

Schubert, C. E. and H. J. Bokuniewicz (1991). "Infragravity wave motion in a tidal inlet". *Coastal Sediments '91: proceedings of a Specialty Conference on Quantitative Approaches to Coastal Processes: Seattle, Washington, June 25-27, 1991*. Vol. 2. Seattle, WA: ASCE, pp. 1434–1446.

Seymour, R. J., R. R. Strange, D. R. Cayan, and R. A. Nathan (1984). "Influence of El Niños on California's wave climate". *Coastal Engineering Proceedings* 1(19). DOI: 10.9753/icce.v19..

Sharples, J., M. J. Coates, and J. E. Sherwood (2003). "Quantifying turbulent mixing and oxygen fluxes in a Mediterranean-type, microtidal estuary". *Ocean Dynamics* 53(3), pp. 126–136. DOI: 10.1007/s10236-003-0037-8.

Simpson, J., N. Fisher, and P Wiles (2004). "Reynolds stress and TKE production in an estuary with a tidal bore". *Estuarine, Coastal and Shelf Science* 60(4), pp. 619–627. DOI: 10.1016/j.ecss.2004.03.006.

Sloan, R. (2006). "Ecological investigations of a fish kill in Pescadero Lagoon, California". MA thesis. San Jose State University.

Smith, K. (2009). "Inorganic chemical oxygen demand of re-suspended sediments in a bar-built lagoon". MA thesis. San Jose State University.

Soulsby, R. L. (1983). "The bottom boundary layer of shelf seas". *Physical Oceanography of Coastal and Shelf Seas Elsevier Oceanography Series*. Ed. by B. Johns. Vol. 35. Physical Oceanography of Coastal and Shelf Seas. Elsevier, pp. 189–266.

Stigebrandt, A. (1980). "Some aspects of tidal interaction with fjord constrictions". *Estuarine and Coastal Marine Science* 11(2), pp. 151–166. DOI: 10.1016/S0302-3524(80)80038-7.

Stretch, D. and M. Parkinson (2006). "The breaching of sand barriers at perched, temporary open/closed estuaries — a model study". *Coastal Engineering Journal* 48(01), pp. 13–30. DOI: 10.1142/S0578563406001295.

Suzuki, M., A. Ovalle, and E. Pereira (1998). "Effects of sand bar openings on some limnological variables in a hypertrophic tropical coastal lagoon of Brazil". *Hydrobiologia* 368, pp. 111–122. DOI: 10.1023/A:1003277512032.

Uncles, R. J., J. A. Stephens, and C. Harris (2014). "Infragravity currents in a small ría: Estuary-amplified coastal edge waves?" *Estuarine, Coastal and Shelf Science*. DOI: 10.1016/j.ecss.2014.04.019.

Viollis, F. S. (1979). "The evolution of Pescadero Marsh". MA thesis. San Francisco State University.

Weir, F. M., M. G. Hughes, and T. E. Baldock (2006). "Beach face and berm morphodynamics fronting a coastal lagoon". *Geomorphology* 82(3–4), pp. 331–346. DOI: 10.1016/j.geomorph.2006.05.015.

Wilson, R. I., A. R. Admire, J. C. Borrero, L. A. Dengler, M. R. Legg, P. Lynett, T. P. McCrink, K. M. Miller, A. Ritchie, K. Sterling, and P. M. Whitmore (2012). "Observations and impacts from the 2010 Chilean and 2011 Japanese tsunamis in California (USA)". *Pure and Applied Geophysics*. DOI: 10.1007/s00024-012-0527-z.

Wolanski, E., D. Williams, S. Spagnol, and H. Chanson (2004). "Undular tidal bore dynamics in the Daly Estuary, Northern Australia". *Estuarine, Coastal and Shelf Science* 60(4), pp. 629–636. DOI: doi:10.1016/j.ecss.2004.03.001.

Young, D. F. (2004). *A Brief Introduction to Fluid Mechanics*. 3 edition. Hoboken, NJ?: Wiley.